

15. TEPHRA EVENT STRATIGRAPHY AND EMPLACEMENT OF VOLCANICLASTIC SEDIMENTS, MOGÁN AND FATAGA STRATIGRAPHIC INTERVALS, PART I: MINERAL AND CHEMICAL STRATIGRAPHY OF VOLCANICLASTIC UNITS AND CORRELATION TO THE SUBAERIAL RECORD¹

Mari Sumita² and Hans-Ulrich Schmincke²

ABSTRACT

During Leg 157, middle to late Miocene (14–9 Ma) stratigraphic intervals in the clastic apron of Gran Canaria were drilled at Sites 953, 955, and 956. Several hundred volcaniclastic layers composed of silt to sand-sized volcanic material, chiefly glass shards, pumice, and crystals, are interlayered with foraminifer nannofossil ooze. These intervals are 452 m thick at Hole 953C, 193 m thick at Hole 955A, and 194 m thick at Hole 956B, and were subdivided into three (Hole 953C) and two (Holes 955A and 956B) lithologic subunits. The lowermost of these subunits at all three holes correlates with the fallout tephra layers and ignimbrite cooling units of the Mogán Group on Gran Canaria (14–13.3 Ma), whereas the volcaniclastic layers of the 1–2 upper subunits correlate with the volcanic units of the Fataga Group (13.3 to ~9 Ma).

We have subdivided the cores into ~100 volcaniclastic units at each hole based on a more detailed study of the cores in the core repository. Most of the major volcaniclastic layers in the time interval between 14 and 12 Ma have been examined by petrographic analysis of 276 polished thin sections, electron microprobe (EMP) analysis of 3000 glass shards, and more than 4500 analyses of the main phenocryst minerals (feldspar, pyroxene, amphibole, and phlogopite). These data are combined with X-ray fluorescence (XRF) analyses of 40 bulk tuff samples, and reanalysis of rock powders made on board, 50 new XRF and EMP analyses of glassy vitrophyres from 12 selected ignimbrites, and microprobe analyses of feldspar phenocrysts from 23 ignimbrites to provide detailed data sets for both the subaerial and submarine tephra stratigraphies to facilitate their correlation. Nearly unique mineral phases or assemblages and compositions of glass, feldspar, amphibole, and clinopyroxene, and bulk rocks provide robust compositional criteria for unequivocally correlating formations and groups. Major changes in mineral compositions, for example, occur at equivalent stratigraphic levels on land and in the submarine sections, such as the disappearance of sodic anorthoclase, calcic amphibole, abundant hypersthene, and zircon at the boundary between the Lower and Middle Mogán Group or the appearance of abundant phlogopite at the boundary between the Mogán and Fataga Groups. We have also correlated many volcaniclastic layers in the interval between 14 and 12 Ma among the three holes and were able to identify at least 7 of the ~15 individual ignimbrite members (cooling units) of the Mogán Group present on land, notably ignimbrites P1, VI, P2, X, O, A, and D, in all three drill holes.

The high-resolution correlations of several syn-ignimbritic volcaniclastic units with well-dated anorthoclase-bearing ignimbrites on the island allow more precise sedimentation rates to be calculated. Between 14 and 13.3 Ma, sedimentation rates were 97 to 142 m/m.y. at Hole 953C, 54 to 93 m/m.y. at Hole 956B, and 43 to 72 m/m.y. at Hole 955A. The high precision correlations also help to calibrate the biomagnostratigraphic time scale, for example, during the time interval of ~12–13 Ma, where our lithological correlations suggest that the biostratigraphic ages suggested on board are significantly too high.

INTRODUCTION

Gran Canaria (28°00'N, 15°35'W), one of the two main islands of the Canarian archipelago in the central, eastern Atlantic has been volcanically active intermittently throughout the past 15–16 m.y. The island, some 200 km off the northwestern African passive continental margin, has experienced several stages of extreme magma differentiation, unique among volcanic islands. Very large volumes of silica-oversaturated trachytes and peralkaline rhyolites of the Mogán Group were erupted between 14 and 13.3 Ma and trachyphonolites of the Fataga Group between 13.3 and 8.5 Ma. These frequent explosive eruptions generated widespread rhyolitic, trachytic, and phonolitic fallout ashes as well as numerous ash flow deposits, many of which represent excellent marker beds on land.

At three sites north, southeast, and southwest of Gran Canaria, up to ~450 m of biogenic and volcaniclastic sediments were drilled during Leg 157 that represent the Mogán and Fataga stratigraphic intervals (Fig. 1). The influx of coarse volcaniclastic material to the sub-

marine volcanic apron has played a fundamental role in controlling the lithostratigraphy.

One of the scientific highlights of Leg 157 was the identification aboard ship of several volcaniclastic layers, chiefly in the Mogán stratigraphic interval, that could be correlated with specific ignimbrites on land. Our basic premise was that all of the 15 well characterized ignimbrite cooling units of the Mogán Group went into the ocean around the periphery of the island. The successful correlations between the drill holes and with subaerial pyroclastic deposits have now verified this idea.

We have studied more than 100 volcaniclastic layers of all three holes in detail and have established a catalogue of what we call volcaniclastic units (also discussed in a companion paper by Schmincke and Sumita, Chap. 16, this volume). More than 100 polished sections of major units were studied petrographically. Glass and mineral compositions were analyzed by electron microprobe (EMP) in many of these units to construct a high-resolution stratigraphic correlation between the drill holes and the subaerial record. We have now begun correlating about one third of the ~100 main volcanicastic layers so far identified in three drill holes into the volcanicastic apron of Gran Canaria, both among holes and to the source rocks on the island.

This stratigraphic framework forms the basis for several major applications. Firstly, it enables us to refine the time boundaries for biostratigraphic and magnetostratigraphic zones. Secondly, our discuss-

¹Weaver, P.P.E., Schmincke, H.-U., Firth, J.V., and Duffield, W. (Eds.), 1998. *Proc. ODP, Sci. Results*, 157: College Station, TX (Ocean Drilling Program).

²GEOMAR Forschungszentrum, Wischhofstrasse 1-3, D-24148 Kiel, Federal Republic of Germany. hschmincke@geomar.de

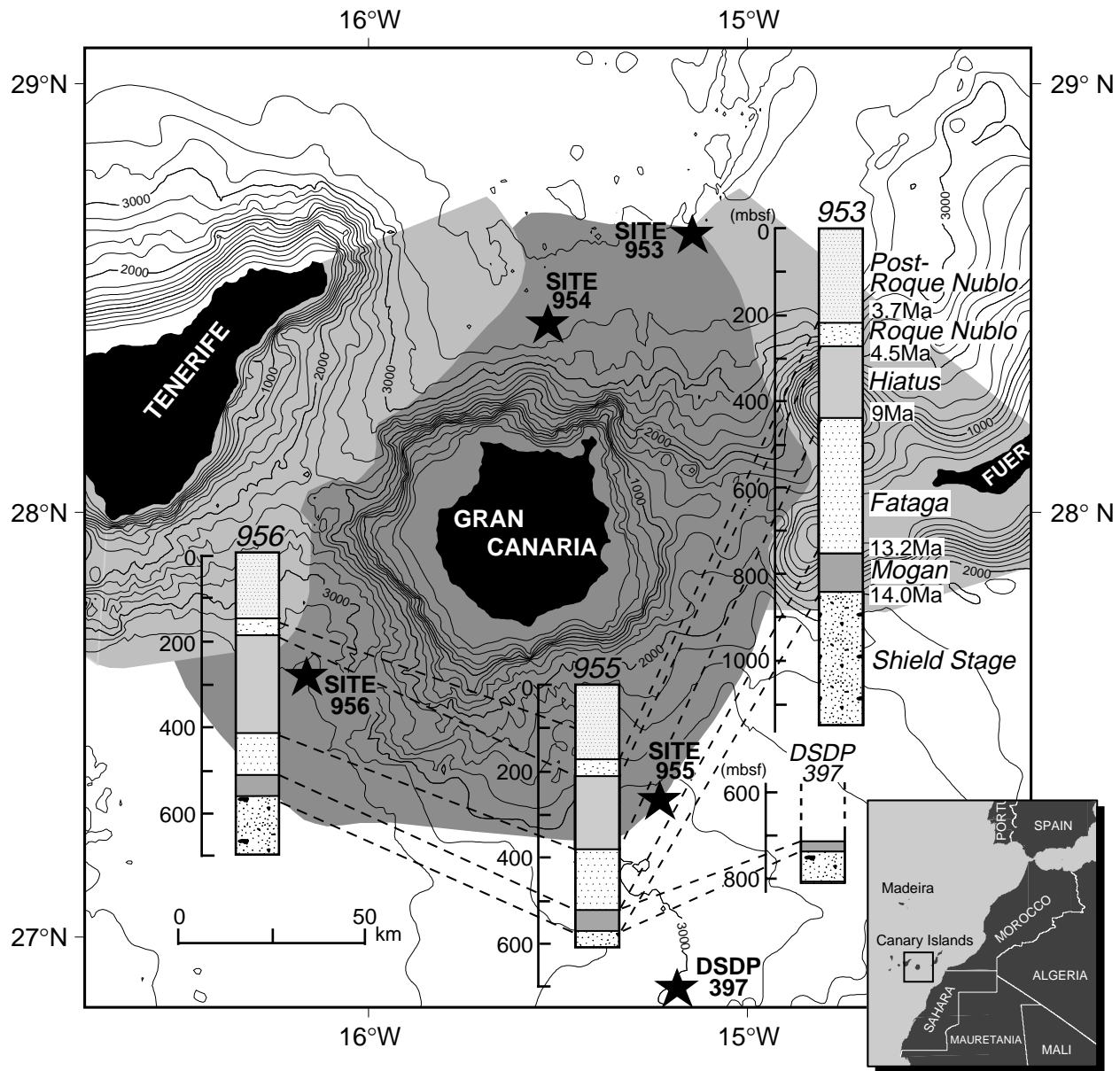


Figure 1. Gran Canaria and the neighboring islands of Fuerteventura and Tenerife, showing the shingled volcanic apron, four Leg 157 sites, DSDP Site 397, and simplified lithostratigraphic columns of Sites 953, 955, and 956.

sion of the emplacement mechanisms of the volcanioclastic layers (Schmincke and Sumita, Chap. 16, this volume) is based fundamentally on establishing a reliable stratigraphic framework. Finally, the stratigraphic, sedimentological, volcanological, and compositional data will ultimately result in a more realistic calculation of sediment budgets for the submarine growth, subaerial evolution, and unroofing of Gran Canaria, Fuerteventura, and Tenerife, and ocean islands in general.

We have been faced with several problems in correlating the volcanioclastic layers to the subaerial record. First, it turned out during this study that our geochemical database of the subaerial pyroclasts was insufficient, so we have spent a major effort in strengthening our geochemical database of subaerial rocks by carrying out chemical analyses of ignimbrites and EMP analysis of fresh glass from vitrophyres and of feldspar phenocrysts in many of the subaerial ignimbrite cooling units. The glass data that we present represent only

~20% of the total number of analyses. We have also made plots of the entire database, including glass analyses with totals <90 wt%, and for some units this has resulted in a higher concentration of points and thus clearer stratigraphic signals.

TERMINOLOGY

Volcanioclastic Unit

We subdivided the stratigraphic intervals corresponding to the Mogán and Fataga Groups in the cores of Holes 953C, 955A and 956B into volcanioclastic units during detailed postcruise examinations at the Ocean Drilling Program (ODP) core repository in Bremen (Table 1; e.g., Unit VU-15, Sample 157-953C-65R-1, 50–52 cm). We define a volcanioclastic unit as a volcanioclastic layer that contains >5 vol% of volcanic particles, generally indicated by a darker color.

Table 1. List of volcaniclastic units at Holes 953C, 955A, and 956B.

VU	Top of unit		Base of unit		Depth interval			Remarks
	Core, section	Interval (cm)	Core, section	Interval (cm)	Top (mbsf)	Bottom (mbsf)	Thickness (cm)	
157-953C-								
VU-1	70R-2	85.00	70R-3	22.50	842.86	843.69	82.5	Ignimbrite P1
VU-2	70R-2	11.00	70R-2	68.00	842.12	842.69	57.0	Reworked P1
VU-3	70R-2	0.00	70R-2	11.00	842.01	842.12	11.0	Reworked P1
VU-4	70R-1	86.50	70R-1	111.50	841.67	841.92	25.0	Reworked P1
VU-5	70R-1	77.50	70R-1	86.50	841.58	841.67	9.0	
VU-6	70R-1	74.50	70R-1	77.50	841.55	841.58	3.0	
VU-7	70R-1	40.50	70R-1	66.00	841.21	841.46	25.5	
VU-8	70R-1	15.00	70R-1	40.50	840.95	841.21	25.5	
VU-9	70R-1	0.00	70R-1	15.00	840.80	840.95	15.0	
VU-10	69R-5	37.00	69R-5	51.00	836.97	837.11	14.0	End reworking P1
VU-11a	69R-4	121.00	69R-5	37.00	836.57	836.97	40.0	
VU-11b	69R-4	28.00	69R-4	97.00	835.64	836.33	69.0	V-type
VU-12	69R-4	0.00	69R-4	28.00	835.36	835.64	28.0	
VU-12a	69R-3	91.00	69R-3	126.00	834.81	835.16	35.0	
VU-12b	69R-2	129.00	69R-3	16.00	833.82	834.06	24.0	
VU-12c	69R-3	37.00	69R-3	91.00	834.27	834.81	54.0	
VU-12d	69R-2	106.00	69R-2	130.00	833.59	833.83	24.0	
VU-12e	69R-2	85.00	69R-2	106.00	833.38	833.59	21.0	
VU-13	69R-2	38.00	69R-2	83.50	832.91	833.37	45.5	Ignimbrite P2?
VU-13a	69R-2	35.00	69R-2	38.00	832.88	832.91	3.0	
VU-13b	69R-1	8.00	69R-2	33.00	831.18	832.86	168.0	
VU-14	68R-5	12.00	69R-1	7.00	826.83	831.17	38.0	
VU-14b	68R-4	111.00	68R-4	120.00	826.62	826.71	9.0	
VU-15	68R-4	39.00	68R-4	61.00	825.90	826.12	22.0	
VU-15b	68R-3	121.00	68R-4	39.00	825.27	825.90	63.0	
VU-15c	68R-3	112.00	68R-3	121.00	825.18	825.27	9.0	
VU-15d	68R-3	98.00	68R-3	112.00	825.04	825.18	14.0	
VU-15e	68R-3	94.00	68R-3	98.00	825.00	825.04	4.0	
VU-16	68R-2	123.00	68R-3	72.00	824.03	824.78	75.0	Reworked P2
VU-16a	68R-2	95.00	68R-2	105.00	823.75	823.85	10.0	
VU-16b	68R-1	87.00	68R-1	130.00	822.27	822.70	43.0	End V-type
VU-16c	68R-2	105.00	68R-2	113.00	823.85	823.93	8.0	
VU-16d	68R-2	91.00	68R-2	93.00	823.71	823.73	2.0	
VU-16e	68R-2	80.00	68R-2	91.00	823.60	823.71	11.0	
VU-16f	68R-2	70.00	68R-2	80.00	823.50	823.60	10.0	
VU-16g	68R-2	59.00	68R-2	61.00	823.39	823.41	2.0	
VU-16h	68R-1	131.00	68R-2	30.00	822.71	823.10	39.0	
VU-17	68R-1	56.00	68R-1	88.00	821.96	822.28	32.0	Ignimbrite TL?
VU-17a	68R-1	42.00	68R-1	48.00	821.82	821.88	6.0	
VU-18	68R-1	7.00	68R-1	20.00	821.47	821.60	13.0	
VU-18a	67R-5	123.00	68R-1	7.00	818.62	821.47	34.0	
VU-18b	67R-5	98.00	67R-5	123.00	818.37	818.62	25.0	
VU-18c	67R-5	83.00	67R-5	98.00	818.22	818.37	15.0	
VU-18d	67R-5	28.00	67R-5	39.00	817.67	817.78	11.0	
VU-19	67R-5	12.00	67R-5	28.00	817.51	817.67	16.0	
VU-19a	67R-4	127.00	67R-5	12.00	817.23	817.51	28.0	
VU-19b	67R-4	97.00	67R-4	125.00	816.93	817.21	28.0	
VU-20	67R-3	6.00	67R-4	58.00	814.65	816.54	189.0	Ignimbrite X
VU-20a	67R-2	104.00	67R-2	112.00	814.25	814.33	8.0	
VU-20b	67R-2	92.00	67R-2	104.00	814.13	814.25	12.0	
VU-21	67R-1	118.00	67R-2	83.00	812.88	814.04	116.0	
(VU-21a)	67R-1	118.00	67R-1	150.00	812.88	813.20	32.0	Ignimbrite O
VU-22	67R-1	16.00	67R-1	148.00	811.86	813.18	132.0	
VU-23	66R-5	36.00	66R-5	39.00	807.59	807.62	3.0	Ignimbrite A
VU-24	66R-5	7.00	66R-5	31.00	807.30	807.54	24.0	Reworked A
VU-25	66R-4	92.00	66R-4	102.00	807.15	807.25	10.0	
VU-25a	66R-4	81.00	66R-4	89.00	807.04	807.12	8.0	
VU-26	66R-4	53.00	66R-4	77.00	806.76	807.00	24.0	
VU-27	66R-3	133.00	66R-3	135.00	806.20	806.22	2.0	
VU-27a	66R-3	102.00	66R-3	133.00	805.89	806.20	31.0	
VU-28	66R-3	38.00	66R-3	102.00	805.25	805.89	64.0	T4?
VU-29	66R-2	93.00	66R-3	34.00	804.34	805.21	87.0	Reworked A
VU-30	66R-2	15.00	66R-2	35.00	803.56	803.76	20.0	Ignimbrite B?
VU-30a	66R-1	103.00	66R-1	114.00	803.13	803.24	11.0	
VU-30b	66R-1	100.00	66R-1	103.00	803.10	803.13	3.0	
VU-30c	66R-1	82.00	66R-1	89.00	802.92	802.99	7.0	
VU-30d	66R-1	69.00	66R-1	79.00	802.79	802.89	10.0	
VU-30e	66R-1	43.00	66R-1	49.00	802.53	802.59	6.0	
VU-30f	66R-1	32.00	66R-1	35.00	802.42	802.45	3.0	
VU-30g	66R-1	20.00	66R-1	32.00	802.30	802.42	12.0	
VU-31	65R-5	116.00	65R-6	106.00	798.79	800.05	126.0	Ignimbrite B?
VU-32	65R-5	85.00	65R-5	103.00	798.48	798.66	18.0	Ignimbrite C?
VU-33	65R-5	60.00	65R-5	70.00	798.23	798.33	10.0	
VU-33a	65R-5	20.00	65R-5	37.00	797.83	798.00	17.0	
VU-33aa	65R-5	0.00	65R-5	8.00	797.63	797.71	8.0	
VU-33b	65R-4	130.00	65R-4	143.00	797.49	797.62	13.0	
VU-33c	65R-4	116.00	65R-4	117.00	797.35	797.36	1.0	
VU-33d	65R-4	90.00	65R-4	96.00	797.09	797.15	6.0	
VU-33e	65R-4	71.00	65R-4	73.00	796.90	796.92	2.0	
VU-33f	65R-4	61.00	65R-4	62.00	796.80	796.81	1.0	
VU-33g	65R-4	41.00	65R-4	43.00	796.60	796.62	2.0	
VU-33h	65R-4	15.00	65R-4	37.00	796.34	796.56	22.0	
VU-34	65R-3	41.00	65R-3	81.00	795.20	795.60	40.0	
VU-35	65R-1	78.00	65R-2	102.00	793.18	794.57	139.0	Ignimbrite D?
VU-35a	65R-1	50.00	65R-1	78.00	792.90	793.18	28.0	
VU-35aa	65R-1	37.00	65R-1	42.00	792.77	792.82	5.0	

Table 1 (continued).

VU	Top of unit		Base of unit		Depth interval			Remarks
	Core, section	Interval (cm)	Core, section	Interval (cm)	Top (mbsf)	Bottom (mbsf)	Thickness (cm)	
VU-35b	64R-4	27.00	64R-4	32.00	786.86	786.91	5.0	
VU-36	64R-3	73.00	64R-4	27.00	786.15	786.86	71.0	
VU-36a	64R-2	50.00	64R-3	73.00	784.76	786.15	139.0	Ignimbrite D?
VU-36b	64R-2	13.00	64R-2	40.00	784.39	784.66	27.0	
VU-36c	64R-2	6.00	64R-2	12.00	784.32	784.38	6.0	
VU-37	64R-1	0.00	64R-1	144.00	782.80	784.24	144.0	Ignimbrite E?
VU-38	63R-1	0.00	63R-1	53.00	773.10	773.63	53.0	
VU-39	62R-3	47.00	62R-4	34.00	767.02	768.39	137.0	
VU-39a	62R-3	30.00	62R-3	37.00	766.85	766.92	7.0	
VU-39b	62R-3	18.00	62R-3	22.00	766.73	766.77	4.0	
VU-39c	62R-3	0.00	62R-3	2.00	766.55	766.57	2.0	
VU-39d	62R-2	133.00	62R-2	139.00	766.38	766.44	6.0	
VU-39e	62R-2	76.00	62R-2	82.00	765.81	765.87	6.0	
VU-39f	62R-2	43.00	62R-2	50.00	765.48	765.55	7.0	
VU-39g	62R-2	30.00	62R-2	37.00	765.35	765.42	7.0	
VU-40	62R-1	0.00	62R-2	4.00	763.60	765.09	149.0	
VU-40a	61R-4	15.00	61R-4	22.00	758.48	758.55	7.0	
VU-40b	61R-3	114.00	61R-3	123.00	758.11	758.20	9.0	
VU-41	61R-3	50.00	61R-3	114.00	757.47	758.11	64.0	
VU-41a	61R-2	124.00	61R-3	50.00	756.75	757.47	72.0	
VU-41b	61R-2	89.00	61R-2	106.00	756.40	756.57	17.0	
VU-42	60R-2	21.00	60R-3	18.00	746.13	747.60	147.0	
VU-43	60R-1	0.00	60R-1	47.00	744.50	744.97	47.0	
VU-44	59R-6	63.00	59R-6	113.00	742.55	743.05	50.0	
VU-45	59R-6	0.00	59R-6	19.00	741.92	742.11	19.0	
VU-46	59R-5	3.00	59R-5	129.00	740.56	741.82	126.0	
VU-47	59R-3	36.00	59R-3	118.00	738.09	738.91	82.0	
VU-48	58R-5	113.00	58R-6	37.00	732.14	732.88	74.0	
VU-49	58R-3	85.00	58R-4	84.00	728.96	730.45	149.0	
VU-50	58R-2	25.00	58R-2	125.00	726.92	727.92	100.0	
VU-51	58R-1	54.00	58R-1	82.00	725.74	726.02	28.0	
VU-52	57R-5	24.00	57R-5	45.00	721.51	721.72	21.0	
VU-53	57R-3	15.00	57R-3	74.00	718.46	719.05	59.0	
VU-54	57R-1	56.00	57R-1	76.00	716.06	716.26	20.0	
VU-55	56R-4	0.00	56R-4	35.00	710.31	710.66	35.0	
VU-56	56R-3	39.00	56R-3	105.00	709.25	709.91	66.0	
VU-57	56R-2	0.00	56R-2	110.00	707.40	708.50	110.0	
VU-58	56R-1	20.00	56R-1	81.00	706.20	706.81	61.0	
VU-59	55R-5	50.00	55R-5	117.00	702.56	703.23	67.0	
VU-60	55R-3	77.00	55R-4	54.00	699.86	701.13	127.0	
VU-61	55R-2	102.00	55R-2	118.00	698.78	698.94	16.0	
VU-62	55R-2	28.00	55R-2	77.00	698.04	698.53	49.0	
VU-63	54R-5	104.00	54R-6	32.00	693.70	694.34	64.0	
VU-64	54R-3	17.00	54R-3	59.00	689.83	690.25	42.0	
VU-65	54R-2	82.00	54R-2	95.00	689.22	689.35	13.0	
VU-66	54R-1	32.00	54R-1	81.00	687.32	687.81	49.0	
VU-67	54R-1	0.00	54R-1	14.00	687.00	687.14	14.0	
VU-68	53R-5	105.00	53R-6	25.00	684.01	684.64	63.0	
VU-69	53R-5	26.00	53R-5	48.00	683.22	683.44	22.0	
VU-70	53R-3	132.00	53R-4	98.00	681.55	682.54	99.0	
VU-71	53R-2	31.00	53R-2	36.00	679.16	679.21	5.0	
VU-72	53R-1	130.00	53R-2	8.00	678.70	678.93	23.0	
VU-73	52R-4	70.00	52R-4	109.00	672.31	672.70	39.0	
VU-74	52R-1	110.00	52R-2	25.00	668.80	669.24	44.0	
VU-75	51R-6	30.00	52R-1	1.00	665.05	667.71	9.0	
VU-76	51R-4	85.00	51R-5	107.00	662.67	664.35	168.0	
VU-77	51R-1	110.00	51R-2	45.00	659.20	659.75	55.0	
VU-78	50R-4	2.00	51R-1	10.00	652.82	658.20	153.0	
VU-79	50R-2	89.00	50R-2	112.00	650.83	651.06	23.0	
VU-80	50R-1	90.00	50R-2	8.00	649.40	650.02	62.0	
VU-81	49R-6	92.00	50R-1	16.00	646.50	648.66	131.0	
VU-82	49R-5	83.00	49R-6	4.00	645.29	645.62	33.0	
VU-83	49R-4	112.00	49R-5	16.00	644.38	644.62	24.0	
VU-84	49R-4	29.00	49R-4	75.50	643.55	644.02	46.5	
VU-85	49R-3	101.00	49R-3	104.00	642.77	642.80	3.0	
VU-86	49R-3	75.00	49R-3	85.00	642.51	642.61	10.0	
VU-87	49R-3	50.00	49R-3	67.00	642.26	642.43	17.0	
VU-88	49R-2	71.00	49R-2	112.00	640.97	641.38	41.0	
VU-89	49R-1	121.00	49R-1	137.00	640.11	640.27	16.0	
VU-90	49R-1	51.00	49R-1	71.00	639.41	639.61	20.0	
VU-91	48R-6	45.00	49R-1	4.00	635.55	638.94	74.0	
VU-92	48R-2	56.00	48R-2	93.00	630.79	631.16	37.0	
VU-93	48R-1	35.00	48R-1	46.00	629.65	629.76	11.0	
VU-94	47R-4	14.00	47R-4	27.00	623.17	623.30	13.0	
VU-95a	47R-3	99.00	47R-3	121.00	622.56	622.78	22.0	
VU-95b	47R-3	55.00	47R-3	99.00	622.12	622.56	44.0	
VU-96	47R-2	112.00	47R-2	147.00	621.22	621.57	35.0	
157-955A-								
VU-1	60X-3	134.00	60X-4	29.00	565.24	565.69	45.0	
VU-2	60X-3	116.00	60X-3	121.00	565.06	565.11	5.0	
VU-3	60X-3	65.00	60X-3	66.00	564.55	564.56	1.0	
VU-4	60X-3	54.00	60X-3	62.00	564.44	564.52	8.0	
VU-5	60X-3	40.00	60X-3	43.00	564.30	564.33	3.0	
VU-6	60X-3	20.00	60X-3	24.00	564.10	564.14	4.0	
VU-7	60X-2	140.00	60X-2	144.00	563.80	563.84	4.0	
VU-8	60X-2	114.00	60X-2	117.00	563.54	563.57	3.0	
VU-8/9a	60X-2	18.00	60X-2	21.00	562.58	562.61	3.0	

Table 1 (continued).

VU	Top of unit		Base of unit		Depth interval			Remarks
	Core, section	Interval (cm)	Core, section	Interval (cm)	Top (mbsf)	Bottom (mbsf)	Thickness (cm)	
VU-8/9b	61X-3	81.00	61X-3	84.00	574.31	574.34	3.0	
VU-9	60X-1	140.00	60X-1	145.00	562.30	562.35	5.0	
VU-10	60X-1	117.00	60X-1	121.00	562.07	562.11	4.0	
VU-11	60X-1	8.00	60X-1	11.00	560.98	561.01	3.0	
VU-12	59X-CC	22.00	59X-CC	25.00	560.33	560.36	3.0	
VU-13	59X-6	128.00	59X-6	140.00	559.98	560.10	12.0	
VU-14	59X-6	75.00	59X-6	78.00	559.45	559.48	3.0	
VU-15	59X-6	60.00	59X-6	67.00	559.30	559.37	7.0	
VU-16	59X-6	23.00	59X-6	34.00	558.93	559.04	11.0	
VU-17	59X-5	126.00	59X-5	130.00	558.46	558.50	4.0	
VU-18	59X-5	76.00	59X-5	83.00	557.96	558.03	7.0	
VU-19	59X-4	95.00	59X-4	115.00	556.65	556.85	20.0	
VU-20	59X-3	113.00	59X-3	150.00	555.33	555.70	37.0	
VU-21	59X-3	32.00	59X-3	43.00	554.52	554.63	11.0	
VU-22	59X-2	123.00	59X-2	127.50	553.93	553.98	4.5	
VU-23	59X-2	100.00	59X-2	105.00	553.70	553.75	5.0	
VU-24	59X-1	144.00	59X-2	50.00	552.64	553.20	56.0	
VU-25	59X-1	40.00	59X-1	57.00	551.60	551.77	17.0	
VU-26	58X-CC	24.00	58X-CC	27.00	549.05	549.08	3.0	
VU-27	58X-5	69.00	58X-5	79.00	548.29	548.39	10.0	
VU-28	58X-4	147.00	58X-4	151.00	547.57	547.61	4.0	
VU-29	58X-4	128.00	58X-4	132.00	547.38	547.42	4.0	
VU-30	58X-4	59.00	58X-4	76.00	546.69	546.86	17.0	
VU-31	58X-4	52.00	58X-4	53.00	546.62	546.63	1.0	
VU-32	58X-3	77.00	58X-3	90.00	545.37	545.50	13.0	
VU-33	58X-2	107.00	58X-2	131.00	544.17	544.41	24.0	
VU-34	58X-1	116.00	58X-1	126.00	542.76	542.86	10.0	
VU-35	58X-1	92.00	58X-1	93.50	542.52	542.54	1.5	
VU-36	58X-1	88.00	58X-1	89.50	542.48	542.50	1.5	
VU-37	58X-1	38.00	58X-1	39.00	541.98	541.99	1.0	
VU-38	58X-1	18.00	58X-1	37.00	541.78	541.97	19.0	
VU-39	58X-1	13.00	58X-1	18.00	541.73	541.78	5.0	
VU-40	57X-CC	38.00	57X-CC	70.00	541.38	541.70	32.0	
VU-41	57X-CC	9.00	57X-CC	13.00	541.09	541.13	4.0	
VU-42	57X-6	14.00	57X-6	16.00	539.64	539.66	2.0	
VU-43	57X-5	120.00	57X-5	127.00	539.20	539.27	7.0	
VU-44	57X-5	65.00	57X-5	70.00	538.65	538.70	5.0	
VU-45	57X-5	37.00	57X-5	39.00	538.37	538.39	2.0	
VU-46	57X-4	43.00	57X-4	45.00	536.93	536.95	2.0	
VU-47	57X-3	80.00	57X-3	94.00	535.80	535.94	14.0	
VU-48	57X-3	70.00	57X-3	72.00	535.70	535.72	2.0	
VU-49	57X-3	56.00	57X-3	61.00	535.56	535.61	5.0	
VU-50	57X-3	35.00	57X-3	36.00	535.35	535.36	1.0	
VU-51	57X-3	24.00	57X-3	32.00	535.24	535.32	8.0	
VU-52	57X-2	103.00	57X-2	108.00	534.53	534.58	5.0	Ignimbrite D?
VU-53	57X-2	33.00	57X-2	49.00	533.83	533.99	16.0	
VU-54	57X-2	0.00	57X-2	9.00	533.50	533.59	9.0	
VU-55	57X-1	145.00	57X-1	150.00	533.45	533.50	5.0	
VU-56	57X-1	131.00	57X-1	135.00	533.31	533.35	4.0	
VU-57	57X-1	106.00	57X-1	109.00	533.06	533.09	3.0	
VU-58	56X-3	133.00	56X-3	145.00	526.73	526.85	12.0	
VU-59	56X-3	54.00	56X-3	57.00	525.94	525.97	3.0	
VU-60	56X-3	15.00	56X-3	25.00	525.55	525.65	10.0	Ignimbrite E?
VU-61	56X-2	75.00	56X-2	78.00	524.65	524.68	3.0	
VU-62	56X-2	16.00	56X-2	19.00	524.06	524.09	3.0	
VU-63	56X-1	123.00	56X-1	131.00	523.63	523.71	8.0	Ignimbrite E or F?
VU-64	56X-1	45.00	56X-1	51.00	522.85	522.91	6.0	
VU-66	56X-1	14.00	56X-1	17.00	522.54	522.57	3.0	
VU-67	55X-4	17.00	55X-4	24.00	517.57	517.64	7.0	
VU-68	55X-3	80.00	55X-3	84.00	516.70	516.74	4.0	
VU-69	55X-2	131.00	55X-3	4.00	515.71	515.94	23.0	
VU-70	55X-2	80.00	55X-2	84.00	515.20	515.24	4.0	
VU-71	55X-2	12.00	55X-2	15.00	514.52	514.55	3.0	
VU-72	55X-1	80.00	55X-1	89.00	513.70	513.79	9.0	
VU-73	55X-1	42.00	55X-1	43.00	513.32	513.33	1.0	
VU-74	54X-CC	0.00	54X-CC	21.00	503.40	503.61	21.0	
VU-75	53X-CC	4.00	53X-CC	30.00	499.04	499.30	26.0	
VU-76	53X-4	55.00	53X-4	65.00	498.85	498.95	10.0	
VU-77	53X-4	45.00	53X-4	50.50	498.75	498.81	5.5	
VU-78	53X-4	27.00	53X-4	31.00	498.57	498.61	4.0	
VU-79	53X-3	116.00	53X-3	121.50	497.96	498.02	5.5	
VU-80	53X-3	32.00	53X-3	36.00	497.12	497.16	4.0	
VU-81	53X-3	0.00	53X-3	30.00	496.80	497.10	30.0	
VU-82	53X-2	118.00	53X-2	124.00	496.48	496.54	6.0	
VU-83	53X-2	107.00	53X-2	113.00	496.37	496.43	6.0	
VU-84	53X-2	91.00	53X-2	93.00	496.21	496.23	2.0	
VU-85	53X-2	8.00	53X-2	11.00	495.38	495.41	3.0	
VU-86	53X-1	123.00	53X-1	124.00	495.03	495.04	1.0	
VU-87	53X-1	94.00	53X-1	96.00	494.74	494.76	2.0	
VU-88	53X-1	72.00	53X-1	73.00	494.52	494.53	1.0	
VU-89	53X-1	58.00	53X-1	62.00	494.38	494.42	4.0	
VU-90	52X-3	33.00	52X-3	34.00	487.43	487.44	1.0	
VU-91	52X-3	27.00	52X-3	28.00	487.37	487.38	1.0	
VU-92	52X-2	149.00	52X-3	9.00	487.09	487.19	10.0	
VU-93	52X-2	96.00	52X-2	143.00	486.56	487.03	47.0	
VU-94	52X-2	26.00	52X-2	28.00	485.86	485.88	2.0	
VU-95	52X-1	117.00	52X-1	119.00	485.27	485.29	2.0	
VU-96	52X-1	90.00	52X-1	108.00	485.00	485.18	18.0	

Table 1 (continued).

VU	Top of unit		Base of unit		Depth interval			Remarks
	Core, section	Interval (cm)	Core, section	Interval (cm)	Top (mbsf)	Bottom (mbsf)	Thickness (cm)	
VU-97	52X-1	77.00	52X-1	79.00	484.87	484.89	2.0	
VU-98	52X-1	53.00	52X-1	62.00	484.63	484.72	9.0	
VU-99	52X-1	33.00	52X-1	41.00	484.43	484.51	8.0	
VU-100	51X-CC	0.00	51X-CC	13.00	483.74	483.87	13.0	
VU-101	51X-7	7.00	51X-7	8.00	483.47	483.48	1.0	
VU-102	51X-6	104.00	51X-6	109.00	482.94	482.99	5.0	
VU-103	51X-6	30.00	51X-6	38.00	482.20	482.28	8.0	
VU-104	51X-5	142.00	51X-5	147.00	481.82	481.87	5.0	
VU-105	51X-5	106.00	51X-5	112.00	481.46	481.52	6.0	
VU-106	51X-5	43.00	51X-5	85.00	480.83	481.25	42.0	
VU-107	51X-4	146.00	51X-4	150.00	480.36	480.40	4.0	
VU-108	51X-4	98.00	51X-4	106.00	479.88	479.96	8.0	
VU-109	51X-3	147.00	51X-3	150.00	478.87	478.90	3.0	
VU-110	51X-3	115.00	51X-3	116.00	478.55	478.56	1.0	
VU-111	51X-3	97.00	51X-3	100.00	478.37	478.40	3.0	
VU-112	51X-3	50.00	51X-3	60.00	477.90	478.00	10.0	
VU-113	51X-3	38.00	51X-3	41.00	477.78	477.81	3.0	
VU-114	51X-2	134.00	51X-2	150.00	477.24	477.40	16.0	
VU-115	51X-2	118.00	51X-2	124.00	477.08	477.14	6.0	
VU-116	51X-2	36.00	51X-2	38.00	476.26	476.28	2.0	
VU-117	51X-1	42.00	51X-1	46.00	474.82	474.86	4.0	
VU-118	51X-1	18.00	51X-1	20.00	474.58	474.60	2.0	
157-956B-								
VU-1	43R-6	37.00	43R-6	57.00	568.97	569.17	20.0	
VU-2	43R-6	16.00	43R-6	25.00	568.76	568.85	9.0	
VU-3	43R-5	101.00	43R-5	109.50	568.11	568.20	8.5	
VU-4	43R-5	57.00	43R-5	77.50	567.67	567.88	20.5	
VU-5	43R-4	122.00	43R-5	21.00	566.82	567.31	49.0	
VU-6	43R-3	88.00	43R-4	71.00	564.98	566.31	133.0	
VU-7	43R-2	113.00	43R-3	8.50	563.73	564.19	45.5	Ignimbrite P1
(VU-7a)	43R-3	4.50	43R-3	8.50	564.15	564.19	4.0	Subunit P1
(VU-7b)	43R-2	125.00	43R-3	4.50	563.85	564.15	29.5	Subunit P1
(VU-7c)	43R-2	121.00	43R-2	125.00	563.81	563.85	4.0	Subunit P1
(VU-7d)	43R-2	113.00	43R-2	121.00	563.73	563.81	8.0	Subunit P1
(VU-7e)	43R-2	89.00	43R-2	98.00	563.49	563.58	9.0	Reworked P1?
(VU-7f)	43R-2	77.00	43R-2	89.00	563.37	563.49	12.0	Reworked P1?
VU-8	43R-2	48.50	43R-2	57.00	563.09	563.17	8.5	
VU-8a	43R-2	52.50	43R-2	57.00	563.13	563.17	4.5	
VU-8b	43R-2	48.50	43R-2	52.00	563.09	563.12	3.5	
VU-9	43R-2	20.00	43R-2	21.00	562.80	562.81	1.0	
VU-10	43R-2	3.00	43R-2	10.00	562.63	562.70	7.0	Reworked P1?
VU-11	43R-1	125.50	43R-1	127.00	562.36	562.37	1.5	
VU-12	43R-1	119.00	43R-1	119.50	562.29	562.30	0.5	
VU-12x	43R-1	61.50	43R-1	62.50	561.72	561.73	1.0	
VU-13	43R-1	26.00	43R-1	35.00	561.36	561.45	9.0	V-type
VU-14	43R-1	24.00	43R-1	26.00	561.34	561.36	2.0	Nonvolcanic
VU-15	42R-3	40.00	43R-1	8.00	554.75	561.18	46.0	
VU-16	42R-3	20.00	42R-3	31.00	554.55	554.66	11.0	
VU-17	42R-3	0.00	42R-3	2.00	554.35	554.37	2.0	
VU-18	42R-2	81.00	42R-2	121.00	553.72	554.12	40.0	
VU-19	42R-2	0.00	42R-2	20.00	552.91	553.11	20.0	V-type
VU-20	42R-1	87.00	42R-1	88.00	552.37	552.38	1.0	V-type
VU-21	42R-1	0.00	42R-1	4.00	551.50	551.54	4.0	
VU-22	41R-3	57.00	41R-3	65.00	545.34	545.42	8.0	
VU-23	41R-3	41.00	41R-3	49.00	545.18	545.26	8.0	
VU-24	41R-3	34.00	41R-3	37.00	545.11	545.14	3.0	
VU-25	41R-2	116.00	41R-2	139.00	544.53	544.76	23.0	Ignimbrite P2?
VU-26	41R-2	92.00	41R-2	95.00	544.29	544.32	3.0	
VU-27	41R-2	26.00	41R-2	37.00	543.63	543.74	11.0	
VU-28	41R-1	125.00	41R-1	136.00	543.15	543.26	11.0	
VU-29	41R-1	82.00	41R-1	91.00	542.72	542.81	9.0	VL, P2, TL? reworked
VU-30	41R-1	24.00	41R-1	36.00	542.14	542.26	12.0	
VU-31	41R-1	0.00	41R-1	9.00	541.90	541.99	9.0	Ignimbrite X
VU-32	40R-2	107.00	40R-2	146.00	534.87	535.26	39.0	Ignimbrite A
VU-33	40R-2	92.00	40R-2	96.00	534.72	534.76	4.0	
VU-34	40R-2	88.00	40R-2	90.00	534.68	534.70	2.0	Ignimbrite A?
VU-35	40R-2	70.00	40R-2	71.00	534.50	534.51	1.0	
VU-36	40R-2	23.00	40R-2	38.00	534.03	534.18	15.0	Ignimbrite B?
VU-37	40R-1	117.00	40R-1	149.00	533.47	533.79	32.0	
VU-38	40R-1	90.00	40R-1	98.00	533.20	533.28	8.0	
VU-39	40R-1	69.00	40R-1	72.00	532.99	533.02	3.0	T4?
VU-40	40R-1	51.00	40R-1	52.00	532.81	532.82	1.0	
VU-41	40R-1	39.00	40R-1	40.00	532.69	532.70	1.0	
VU-42	39R-4	89.00	39R-4	93.00	527.17	527.21	4.0	
VU-43	39R-4	74.00	39R-4	80.00	527.02	527.08	6.0	
VU-44	39R-4	32.00	39R-4	57.00	526.60	526.85	25.0	
VU-45	39R-3	83.00	39R-3	95.00	525.91	526.03	12.0	
VU-46	39R-3	35.00	39R-3	38.00	525.43	525.46	3.0	
VU-47	39R-2	106.00	39R-2	120.00	524.94	525.08	14.0	Ignimbrite D
VU-48	39R-2	77.00	39R-2	85.00	524.65	524.73	8.0	
VU-49	39R-2	65.00	39R-2	71.00	524.53	524.59	6.0	
VU-50	39R-2	25.00	39R-2	36.00	524.13	524.24	11.0	
VU-51	39R-2	10.00	39R-2	17.00	523.98	524.05	7.0	
VU-52	39R-2	6.00	39R-2	10.00	523.94	523.98	4.0	
VU-53	39R-1	123.00	39R-1	129.00	523.83	523.89	6.0	
VU-54	39R-1	79.00	39R-1	99.00	523.39	523.59	20.0	Ignimbrite D?
VU-55	39R-1	47.00	39R-1	79.00	523.07	523.39	32.0	

Table 1 (continued).

VU	Top of unit		Base of unit		Depth interval			Remarks
	Core, section	Interval (cm)	Core, section	Interval (cm)	Top (mbsf)	Bottom (mbsf)	Thickness (cm)	
VU-56	39R-1	41.00	39R-1	47.00	523.01	523.07	6.0	
VU-57	39R-1	7.00	39R-1	12.00	522.67	522.72	5.0	
VU-58	38R-3	94.00	38R-3	101.00	516.72	516.79	7.0	
VU-59	38R-3	47.00	38R-3	57.00	516.25	516.35	10.0	
VU-60	38R-3	8.00	38R-3	18.00	515.86	515.96	10.0	
VU-60x	38R-3	0.00	38R-3	0.10	515.78	515.78	0.1	
VU-61	38R-2	146.00	38R-2	150.00	515.74	515.78	4.0	
VU-62	38R-2	121.00	38R-2	126.00	515.49	515.54	5.0	
VU-63	38R-2	84.00	38R-2	87.00	515.12	515.15	3.0	
VU-64	38R-2	38.00	38R-2	51.00	514.66	514.79	13.0	
VU-65	38R-2	22.00	38R-2	24.00	514.50	514.52	2.0	
VU-66	38R-1	133.00	38R-1	138.00	514.23	514.28	5.0	
VU-67	38R-1	113.00	38R-1	125.00	514.03	514.15	12.0	
VU-68	38R-1	105.00	38R-1	111.00	513.95	514.01	6.0	
VU-69	38R-1	61.00	38R-1	64.00	513.51	513.54	3.0	
VU-70	38R-1	21.00	38R-1	30.00	513.11	513.20	9.0	
VU-71	38R-1	0.00	38R-1	8.00	512.90	512.98	8.0	
VU-72	37R-2	141.00	37R-3	87.00	506.21	507.17	96.0	
VU-73	37R-2	138.00	37R-2	141.00	506.18	506.21	3.0	
VU-74	37R-2	125.00	37R-2	130.00	506.05	506.10	5.0	
VU-75	37R-2	92.00	37R-2	102.00	505.72	505.82	10.0	
VU-76	37R-2	60.00	37R-2	67.00	505.40	505.47	7.0	
VU-77	37R-1	126.00	37R-2	18.00	504.56	504.98	42.0	
VU-78	37R-1	94.00	37R-1	96.00	504.24	504.26	2.0	
VU-79	37R-1	64.00	37R-1	69.00	503.94	503.99	5.0	
VU-80	37R-1	7.50	37R-1	8.00	503.38	503.38	0.5	
VU-81	37R-1	0.00	37R-1	7.50	503.30	503.38	7.5	
VU-82	36R-2	0.00	36R-2	48.00	495.04	495.52	48.0	
VU-83	36R-1	119.00	36R-1	124.00	494.79	494.84	5.0	
VU-84	36R-1	80.00	36R-1	81.00	494.40	494.41	1.0	
VU-85	36R-1	14.50	36R-1	44.00	493.75	494.04	29.5	
VU-86	36R-1	13.00	36R-1	14.00	493.73	493.74	1.0	
VU-87	35R-4	0.00	36R-1	6.00	488.21	493.66	75.0	Black Unit 1
VU-88	35R-3	77.00	35R-3	90.00	487.57	487.70	13.0	
VU-89	35R-3	60.00	35R-3	77.00	487.40	487.57	17.0	Black Unit 2
VU-90	35R-3	51.00	35R-3	58.00	487.31	487.38	7.0	
VU-90-X	35R-3	40.00	35R-3	50.00	487.20	487.30	10.0	
VU-91	35R-3	0.00	35R-3	9.00	486.80	486.89	9.0	Black Unit 3
VU-92	35R-2	130.00	35R-2	146.00	486.63	486.79	16.0	
VU-93	35R-2	129.00	35R-2	130.00	486.62	486.63	1.0	
VU-94	35R-2	56.00	35R-2	110.50	485.89	486.44	54.5	Black Unit 4
VU-94X	35R-2	47.00	35R-2	56.00	485.80	485.89	9.0	
VU-95	35R-2	40.00	35R-2	47.00	485.73	485.80	7.0	Black Unit 5
VU-95-X	35R-2	29.00	35R-2	38.00	485.62	485.71	9.0	
VU-96	35R-2	25.00	35R-2	29.00	485.58	485.62	4.0	
VU-97	35R-1	141.00	35R-2	3.00	485.31	485.36	5.0	
VU-98	35R-1	102.00	35R-1	107.00	484.92	484.97	5.0	
VU-99	35R-1	24.00	35R-1	26.00	484.14	484.16	2.0	
VU-100	34R-2	120.00	35R-1	14.00	476.87	484.04	46.0	Black Unit 5X
VU-101	34R-2	109.00	34R-2	120.00	476.76	476.87	11.0	
VU-102	34R-2	26.00	34R-2	75.00	475.93	476.42	49.0	
VU-103	34R-1	134.00	34R-1	140.00	475.64	475.70	6.0	
VU-104	34R-1	78.00	34R-1	100.00	475.08	475.30	22.0	
VU-105	34R-1	23.00	34R-1	77.00	474.53	475.07	54.0	
VU-106	34R-1	14.00	34R-1	22.00	474.44	474.52	8.0	Black Unit 5A
VU-106-X	33R-4	0.00	33R-4	13.00	468.79	468.92	13.0	
VU-107	33R-3	86.00	33R-3	126.00	468.22	468.62	40.0	Black Unit 6
VU-108	33R-3	38.00	33R-3	55.00	467.74	467.91	17.0	
VU-109	33R-3	0.00	33R-3	10.00	467.36	467.46	10.0	Black Unit 6A
VU-110	33R-2	107.00	33R-2	121.00	466.93	467.07	14.0	
VU-111	33R-2	81.00	33R-2	106.00	466.67	466.92	25.0	
VU-112	33R-2	80.00	33R-2	81.00	466.66	466.67	1.0	
VU-113	33R-2	64.00	33R-2	65.00	466.50	466.51	1.0	
VU-114	33R-2	50.00	33R-2	57.00	466.36	466.43	7.0	
VU-115	33R-2	26.00	33R-2	27.00	466.12	466.13	1.0	
VU-116	33R-2	14.00	33R-2	18.00	466.00	466.04	4.0	
VU-117	33R-2	0.00	33R-2	2.00	465.86	465.88	2.0	
VU-118	33R-1	109.00	33R-1	128.00	465.69	465.88	19.0	
VU-119	33R-1	75.00	33R-1	109.00	465.35	465.69	34.0	
VU-120	33R-1	63.00	33R-1	75.00	465.23	465.35	12.0	
VU-121	33R-1	53.00	33R-1	62.00	465.13	465.22	9.0	Black Unit 7
VU-122	33R-1	0.00	33R-1	5.00	464.60	464.65	5.0	
VU-123	32R-4	20.00	32R-4	34.00	459.63	459.77	14.0	
VU-124	32R-3	138.00	32R-3	150.00	459.31	459.43	12.0	
VU-125	32R-3	83.00	32R-3	115.00	458.76	459.08	32.0	
VU-126	32R-2	140.00	32R-3	83.00	457.83	458.76	93.0	Black Unit 8
VU-127	32R-2	45.00	32R-2	100.00	456.88	457.43	55.0	Black Unit 9
VU-128	32R-1	124.00	32R-2	12.00	456.24	456.55	31.0	Black Unit 10
VU-129	32R-1	8.00	32R-1	124.00	455.08	456.24	116.0	Black Unit 11
VU-130	31R-1	105.00	31R-1	125.00	446.35	446.55	20.0	
VU-131	31R-1	0.00	31R-1	87.00	445.30	446.17	87.0	

Note: VU = volcaniclastic unit.

In naming volcaniclastic units, we do not discriminate with respect to grain size, composition, primary vs. reworked origin, or admixture of nonvolcanic components. The latter criterion would have been the most difficult to apply, because even most nonvolcanic sedimentary layers in the Mogán and Fataga stratigraphic intervals contain trace amounts of volcanic glass or volcanic minerals owing to the widespread explosive volcanism on the island over a 5-m.y. interval. The reason for this subdivision was simply to help organize the hundreds of volcaniclastic layers at each site by employing a nongenetic nomenclature. Our most detailed description of volcaniclastic units is of Hole 956B, whereas we have named only the more prominent layers at Hole 953C. The description of the volcaniclastic units from Hole 955A is least satisfactory because the soft nature of the methane-rich, nonvolcanic, interlayered sediments and sedimentary matrix made it difficult to define exact boundaries of volcanic units.

In this paper we present the chemical and mineralogical data by which we correlate these volcaniclastic units to subaerial volcanic cooling units. The origin and emplacement of the volcanic units are discussed in Schmincke and Sumita (Chap. 16, this volume).

Other Terms

We use the terms volcaniclastic layer, volcaniclastic deposits, volcaniclastic rocks, and volcaniclastic turbidite loosely by simply emphasizing the volcaniclastic nature of a layer, etc. We introduce the new term “syn-ignimbrite” for submarine volcaniclastic layers that appear from several lines of evidence to have been emplaced practically synchronously with the parent ignimbrite on land. The criteria are discussed in more detail in the companion paper (Schmincke and Sumita, Chap. 16, this volume). We use the term lithologic unit following ODP guidelines.

XRF AND EMP ANALYTICAL METHODS

X-Ray Fluorescence

Major and trace element concentrations were determined for 40 bulk rocks by X-ray fluorescence (XRF; Philips X'Unique). Forty powders of bulk rocks done on board were reanalyzed. XRF analyses were carried out on melt (glass) pellets using a Philips PW 1400 and a Philips PW 1480 spectrometer. Standard OXIQUANT software was used, and 230 international reference samples and 41 synthetic standards were employed. The pellets were produced from melting of rock powder at 1000°C for ~10 min with an added flux of lithium metaborate and dilithium tetraborate (Merck A 12) at a mixing ratio of 1:4. The melt was cooled in a mold 34 mm in diameter. H₂O was measured by closed system coulombmetric titration. Water degassing from rock powder heated at 1300°C in a Pt-crucible placed in an induction furnace was carried in a nitrogen gas stream and analyzed in Karl Fischer reagent. Sulfur, carbon, and CO₂ were analyzed by infrared photometry using a Rosemount CWA 5003 for CO₂ and a Rosemount CSA 5003 for carbon and sulfur. For trace element determinations, powder pellets were prepared. Trace elements determined include Cr, Ni, V, Cu, Zr, Nb, Ce, Y, Rb, Zn, Ba, and Sr.

Electron Microprobe Analyses

Major elements and Ba, Sr, S, Cl, and F were analyzed with a Cameca SX-50 electron probe at GEOMAR, Kiel. Analytical conditions were 15 kV of accelerating voltage, 60 nA of beam current for felsic glass, 10 nA for sideromelane, feldspar, amphibole, and mica, 20 nA for pyroxene, and 20 s of peak counting time. Analyses were performed with an electron beam rastered to 5 × 5 μm in the scanning mode for felsic glass, sideromelane, feldspar, and 10 × 10 μm for other minerals. Cameca synthetic oxides, basaltic glasses USNM 111240/52 and USNM 113498/1 (VG-A99), apatite USNM 104021, and microcline USNM 143966 (Jarosewich et al., 1980) were used as standards

for calibration. S, F, and Cl were measured as trace elements. Standards used were chalcopyrite for S, scapolite USNM R6600-1 for Cl, and Durango fluorapatite USNM 104021 for F, respectively (Jarosewich et al., 1980). As a monitor sample for S, we used basaltic ALV981R23 (Metrich and Clocchiatti, 1989), and for F and Cl, comenditic glass KN18 (Mosbah et al., 1991). Four to 10 spots were measured within fresh sideromelane. The detection level was estimated to be 0.01 wt% with relative uncertainties of 5%–15% relative for volatile concentrations >0.05 wt%, and up to 20%–40% for concentrations <0.05 wt%.

SUBAERIAL STRATIGRAPHY

One of the main purposes of the drilling project being to correlate the submarine record with subaerial stratigraphy, we begin with a condensed summary of the lithostratigraphy of the Mogán and Fataga Groups on Gran Canaria (Figs. 2, 3). The stratigraphic subdivisions are based on the formalized lithostratigraphic subdivision (groups, formations, members) of the volcanic series by Schmincke (1969, 1976), with later additions and amendments by Schmincke (1994). Here we summarize the subaerial Miocene felsic activity on Gran Canaria.

Miocene Felsic Rocks

The subaerial Miocene cycle started with the rapid formation of the exposed tholeiitic to mildly alkalic shield basalts between 14 and 15 Ma. A 0.6- to 0.7- m.y.-long period of trachytic to rhyolitic composition followed at 14 Ma, generating the largest known volume of silicic volcanic rocks (>300 km³) on any oceanic intraplate island. A large caldera (~20 km in diameter) collapsed during the beginning of this phase. The caldera basin was filled with more than 1000 m of sedimentary, extrusive, and intrusive felsic rocks. After the rhyolitic stage, more than 500 km³ of silica-undersaturated trachyphonolitic ash flows, lava flows, and fallout tephra was erupted between ~13 and 9 Ma. The outflow or extra-caldera facies has been divided into two groups: the lower trachytic to rhyolitic Mogán Group, up to ~400 m thick, and the trachyphonolitic Fataga Group, locally >1000 m thick.

Mogán Group

The Miocene Mogán Group consists of 15–20 dominantly trachytic to pantelleritic, extra-caldera ignimbritic cooling units treated as stratigraphic members (Fig. 2). K/Ar and ⁴⁰Ar/³⁹Ar ages of feldspar, amphibole, and whole rocks from these cooling units and one interbedded basalt flow range from 14 to 13.35 Ma (McDougall and Schmincke, 1977; Bogaard et al., 1988; Bogaard and Schmincke, Chap. 11, this volume). The Mogán Group (Fig. 2) is subdivided into: (1) Lower Mogán Formation members (LMF; cooling units) PI, R, U, and T3 (basalt), VL, and VI; (2) Middle Mogán Formation members (MMF; cooling units) P2, T6 (basalt), TL (locally 2 cooling units), X, and O (locally two cooling units) with a major compositional break between TL and X; and (3) Upper Mogán Formation members (UMF; cooling units) T4 (basalt), A, B, C, D, E, and F (compositionally transitional to Fataga rocks).

Lower Mogán Formation

The LMF begins with the most widespread ignimbrite cooling unit PI (>400 km², 45 km³) on the island, zoned from rhyolite with admixed trachyte in the lower part to basalt at the top (discussed in detail by Freundt and Schmincke 1992, 1995a, 1995b; and Chap. 14, this volume). A feldspar phenocryst-rich rhyolite-basalt ignimbrite PIX, resembling PI but with lesser amounts of crystals, occurs above PI at Barranco de Balos in the east and Risco Faneque in the west (Fig. 3). Ignimbrite R, mixed aphyric rhyolite and dominantly basalt, contains oligoclase, clinopyroxene, hypersthene, and Fe/Ti oxide.

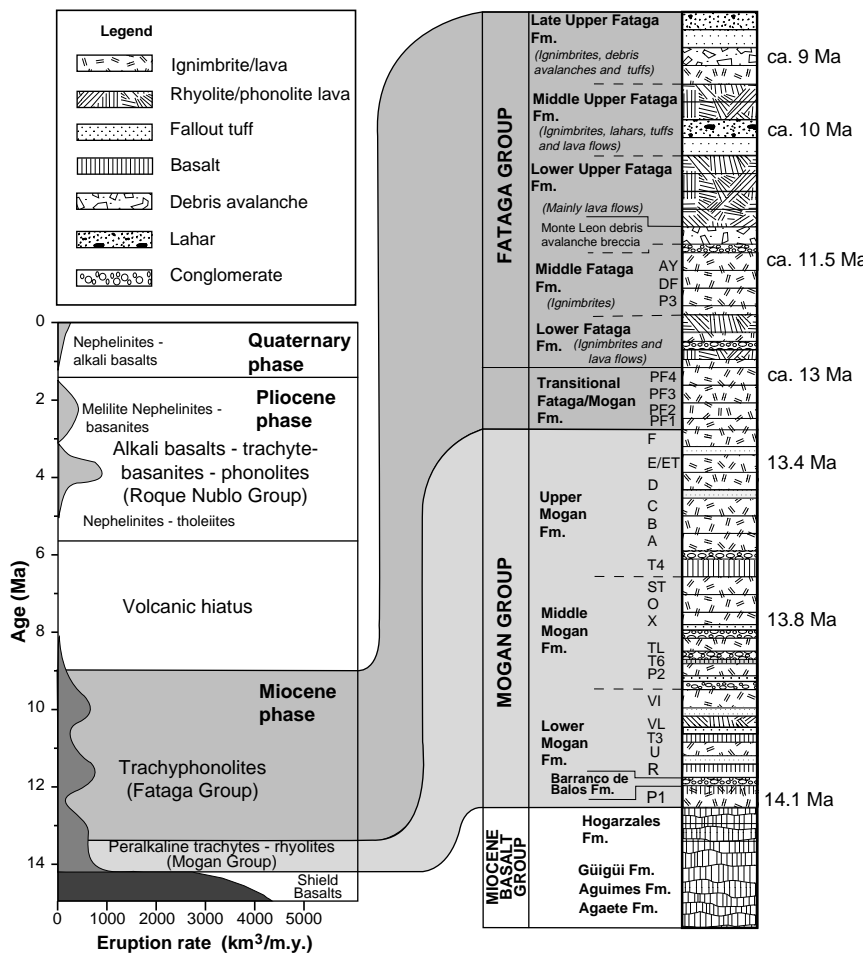


Figure 2. Stratigraphy of volcanic phases on Gran Canaria and detail of Mogán and Fataga stratographies.

The most widespread fallout tuffs in the Mogán group occur below local cooling Unit U and, where U is missing, between Units R and VI. A trachyrhyolitic ignimbrite (U), as yet only positively identified at Anden Verde and in the Horgazales-Cedro area, contains less than 5% oligoclase, clinopyroxene, hypersthene, and Fe/Ti oxide phenocrysts (Fig. 4). Three plagioclase-clinopyroxene-phyric lava flows of intermediate (mugearitic) composition (T3) occur locally between Units U and VI. VL lava flows, underlain in the Mt. Carboneras area by several decimeters of bedded crystal-vitric tuff, locally composed of poorly vesicular shards, suggesting some phreatomagmatic activity, roughly correlate in time with U. These low-silica rhyolite lava flows locally dominate the LMF and largely filled the ancestral Tira-jana canyon in the southeast of the island and canyons between Barranco de Taurito and Barranco de Tasarte in the south (Zr 1300 ppm; Nb 180 ppm) (Fig. 5). The overlying, much more widespread extremely welded high-temperature cooling Unit VI overlies VL, which it resembles in its mineralogy (oligoclase, clinopyroxene, hypersthene, oxides, and zircon) and chemical composition (Zr 1260–1420 ppm; Nb 170 ppm). Thick-bedded fallout tuffs underlying VI form very useful stratigraphic marker horizons from Mt. Cedro in the west to Aguimes in the east.

Middle Mogán Formation

Thin, widespread, highly phryic cooling Unit P2 forms the base of the MMF. Thin conglomerates/fanglomerates and local tuffs underlie, and are mixed with, P2 in the Mt. Carboneras area. In the MMF, P2 is chemically and mineralogically transitional between the LMF and MMF rocks as shown by the presence of >20 vol% oligoclase, sodic as well as calcic amphibole, and large green clinopyroxene phe-

nocrysts, the latter with abundant hypersthene and magnetite inclusions. Locally, the upper part contains only anorthoclase and amphibole. Widespread resorption in the phenocrysts suggests complex disequilibria because of magma mixing. Chemically, P2 is relatively mafic (trachyte) compared to other Mogán Group ignimbrites (Zr 790–1044 ppm; Nb 103–149 ppm). A crystal-poor tuff locally separates P2 and TL. A very plagioclase-phyric mugearite lava flow (T6) containing clinopyroxene and iddingsitized olivine occurs as a small erosional remnant on top of P2 at Mt. Carboneras (Zr 605 ppm; Nb 99 ppm). TL ignimbrite-lava flow cooling unit, locally with a highly irregular, lava-like surface morphology, is exceedingly complex and consists of comendite (anorthoclase and amphibole) and trachyte (oligoclase, clinopyroxene, and rare hypersthene) (Zr 563–1638 ppm; Nb 101–223 ppm). The crystal-rich (20–40 vol%) comenditic cooling Unit X, is relatively thick (>40 m) in the M. Horgazales–Mt. Cedro area. X contains anorthoclase (Or_{32-34}), amphibole (characteristically with chevkinite inclusions), and titanite (Zr 470–2564 ppm; Nb 85–416 ppm). The latter two phases are characteristic of X, except for A, which also contains chevkinite as inclusions in amphibole. The moderately (<15 vol%) crystal-rich comenditic-pantelleritic ignimbrite O exceeds 40 m in the Horgazales–Mt. Vacas area and is chemically zoned from pantelleritic to comenditic rhyolite to comenditic trachyte. Anorthoclase (Or_{27-34}) and richterite amphibole are the phenocrysts (Zr 1721–1911 ppm; Nb 226–272 ppm).

Upper Mogán Formation

Very widespread hawaiite-mugearite lava flows (T4) that contain microphenocrysts of clinopyroxene, plagioclase, and magnetite form the base of the UMF. T4 is thickest in the southwest (up to 20 m),

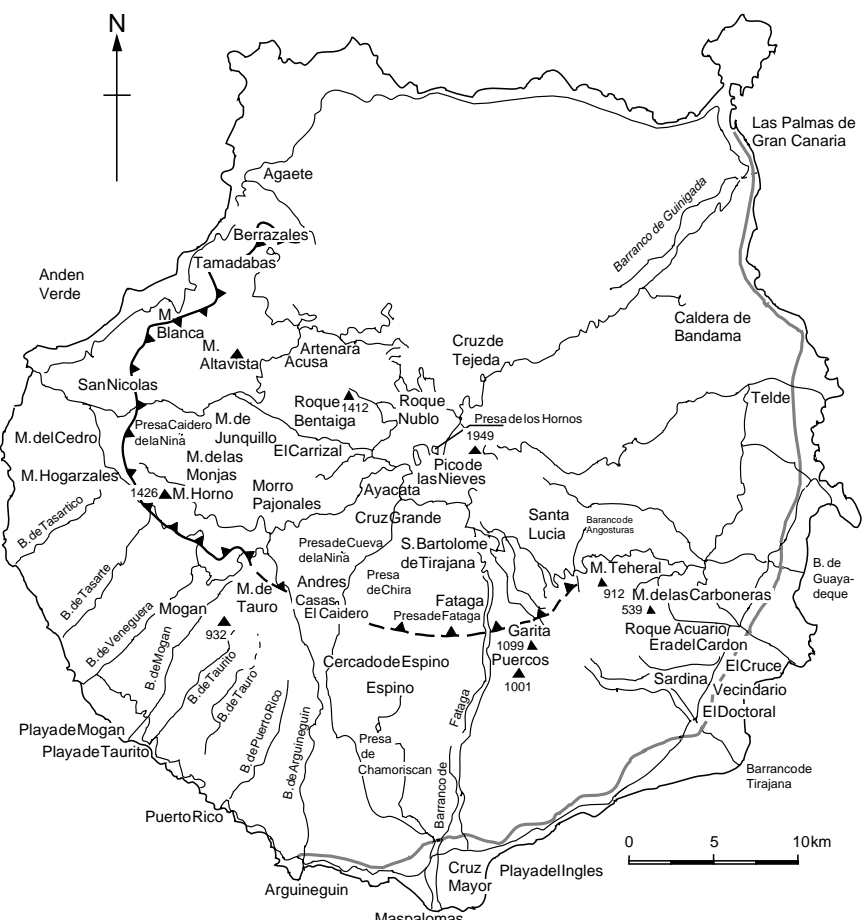


Figure 3. Map showing major Barrancos (canyons) = dashed lines, where not coinciding with roads, towns, and peaks on Gran Canaria. Thick line = freeway, and thin line = roads. Miocene caldera wall = dashed lines where inferred and heavy line with arrows.

connected with two feeder dikes of identical composition which cut through LMF and MMF rocks, and is associated with local scoria cones and lapilli fallout beds (Zr 296–364 ppm; Nb 54–64 ppm).

The lower 4 ignimbrites of the UMF (A through D), all of which are compositionally zoned becoming more mafic and crystal-rich upward in stratigraphy, represent a series of increasing differentiation of the lowermost erupted flow units. Ignimbrite A is the least evolved and D is the most evolved. Ignimbrite A is trachytic, with the highest Ba concentrations in the Mogán Group (Ba 132–2278 ppm), and contains low-K anorthoclase (<10 vol%), amphibole with chevkinite inclusions (<0.2 vol%) and magnetite or ilmenite (Zr 512–1513 ppm; Nb 80–201 ppm). Phlogopite phenocrysts in this ignimbrite are unique in the Mogán Group. Ignimbrite B, the thinnest and least evolved of the three highly evolved pantelleritic ignimbrites, is almost aphyric (generally <1 vol% of rounded, Na-rich anorthoclase [Or_{12-19}]) and contains minor oxides and amphibole (Zr 843–1187 ppm; Nb 115–196 ppm). Ignimbrite C contains mostly anorthoclase and minor richterite and, toward its more mafic top, clinopyroxene (Zr 692–1626 ppm; Nb 105–237 ppm). Ignimbrite D and overlying E are the most widespread ignimbrites of the UMF. Ignimbrite D represents the most evolved magma in the Mogán Group, being extremely enriched in Ti, Fe, Mn, Y, Zr, F, Cl, and Nb (Zr 453–2312 ppm; Nb 81–388 ppm). It is zoned from almost aphyric and xenolith-rich pantellerite in its lower part to phryic trachyte in its upper part. The comenditic to trachytic ignimbrite E contains 5–15 vol% anorthoclase, richterite and Fe/Ti oxides, with clinopyroxene, hypersthene and more sodic feldspar in the trachytic top flow unit of E (Zr 404–2396 ppm; Nb 404–1216 ppm). Trachytic ignimbrite F is compositionally transitional to Fataga compositions (Zr 401–1344; Nb 64–

335 ppm). At its type locality Barranco de Taurito, F is separated from E by up to 30 cm of tuffs and epiclastic sandstone to fanglomerate in local depressions, but regionally overlies E directly.

Ignimbrites Compositionally Transitional Between Mogán and Fataga

In the southeastern sector of the island, as well as in the intra-caldera Montaña Horne Formation, about six oxidized and silicified cooling units transitional in composition between the Mogán and Fataga Groups occur, which are still poorly characterized. These ignimbrites are transitional in the sense that their mineralogy is more Fataga-like (phlogopite instead of amphibole and slightly more potassiac anorthoclase feldspar), whereas their chemistry is Mogán-like, such as Zr/Nb ratios >5 (Zr 678–1161 ppm; Nb 127–195 ppm).

Fataga Group

The Fataga Group, generally ~500 m and locally >1000 m thick, consists of moderately silica-undersaturated trachyphonolitic ignimbrites, lava flows, fallout tephras, debris avalanches, and epiclastic deposits. Fataga cooling units overlie Mogán rocks from Barranco de Veneguera to Barranco de Arguineguín in the south and dominate the area between Barrancos de Arguineguín and Tirajana in the southeast where Mogán rocks occur locally in the canyon bottoms. In the main outcrop area between Tirajana and Arguineguín, six formations are tentatively distinguished. Based on field evidence (Schmincke, 1994) and available ages (Bogaard and Schmincke, Chap. 11, this volume), volcanic activity during Fataga time may have continued as late as 9

Name of cooling units	Single crystal $^{40}\text{Ar}/^{39}\text{Ar}$ ages (Ma)	Phenocrysts (vol.%)	Stratigraphy														
			10	20	30	40	50	Anorthoclase	Oligoclase/Anorthite	Ca-Al amphibole	Richterite-Edenite	Augite	Hypersthene	Phlogopite	Sphene	Fe/Ti-oxides	Chevkinite
F	13.36 ± 0.01	■						●	●	●	●	●					
ET (CT)		■						●	●	●							
E (C)	13.37 ± 0.03	■						●	●	●							
DT (CT)		■						●	●	●							
D (P)	13.44 ± 0.01	■						●									
CT (CT)		■						●	●	●							
C (P)								●									
BT												●					
B (P)		■						●				●					
AT (T)								●				●					
A (C)	13.63 ± 0.04	■						●				●					
OT (CT)								●	●	●		●					
O (C)	13.64 ± 0.01	■						●				●	●				
XT (CT)								●				●					
X (C)	13.71 ± 0.02		■					●				●	●	●			
TL-L (CT)		■						●	●	●		●					
TL-I (C)	13.85 ± 0.01	■						●				●					
P2T (T)								●				●					
P2 (T)	13.89 ± 0.05		■					●	●	●	●	●	●	●			
VIT(SR-T)		□						●	●	●	●	●	●	●			
VI(SR)	13.90 ± 0.03	□						●	●	●	●	●	●	●			
VL (SR-C)	13.97 ± 0.02	□						●	●	●	●	●	●	●			
U (SR)	13.94 ± 0.05	□						●	●	●	●	●	●	●			
R (SR-B)		■						●	●	●	●	●	●	●			
PI (SR-B)	13.95 ± 0.02		■					●	●	●	●	●	●	●			

Figure 4. Summary of type and relative amount of phenocrysts (large symbols = abundant and smaller symbols = minor amount) in major cooling units of Mogán Group. Letters are those of specific ignimbrites: SR = subalkalic rhyolite, T = trachyte, C = comendite, CT = comenditic trachyte, and P = pantellerite.

Ma, but was not continuous. The ignimbrite and lava cooling units typically contain variable amounts of anorthoclase, Fe/Ti oxides, phlogopite (mainly ignimbrites), amphibole, green clinopyroxene (ignimbrites and lava flows), titanite, and nepheline (generally altered to analcime).

LITHOLOGY AND GROSS STRATIGRAPHY OF THE MAIN MIocene VOLCANICLASTIC UNITS

Major Volcaniclastic Lithostratigraphic Intervals

A compositionally distinct volcaniclastic unit correlated to ignimbrite P1 (14 Ma), recognized at 845 mbsf at Hole 953C, at 564 mbsf at Hole 956B, and at 560 mbsf at Hole 955A, forms the base of the Mogán interval (Fig. 2). The transition from the mafic shield volcaniclastics to the felsic volcaniclastic sediments at the logged Holes 953C and 956B is characterized by sharp increases in density, sonic velocity, and resistivity, as well as an abrupt increase in potassium, thorium, and uranium contents. Similarly, an abrupt decrease in potassium, uranium, and thorium contents and, to a lesser degree, resistivity reflects the pronounced decrease in supply of volcaniclastics from lithologic Units IV to III, the late Miocene volcanic hiatus in the evolution of Gran Canaria. In the downhole logs, the Mogán volcanic phase, consisting of highly evolved rhyolitic ash layers, is well characterized by high uranium and thorium values. The density, resistivity, and sonic velocity logs show an increasing lithification trend with depth through the Fataga phase but less indurated lithologies with a higher degree of variance in the Mogán phase. Logging data at Hole 956B also indicate that tuff layers begin to appear in Core 157-956B-

23R at the level where the upper boundary of the Fataga-equivalent sediments (Subunit IVA) was placed. The geochemically similar Mogán and Fataga Formations can be distinguished from each other by the patterns of the natural gamma-ray log. There is generally good agreement between the stratigraphic and lithologic interpretations of the cores and the depositional architecture as derived from the seismic profile (Schmincke, Weaver, Firth, et al., 1995).

The disappearance of volcaniclastic layers marks the less precisely defined top of the main Miocene volcaniclastic interval (398 mbsf at Hole 953C, 374 mbsf at Hole 955A, and 367.5 mbsf at Hole 956B). Unit IV at Hole 953C was subdivided into three subunits, based on the frequency and composition of volcaniclastic mass flow deposits: Subunit IVA (106 m, 398–504 mbsf) and Subunit IVB (250 m, Sections 157-953C-34R-6 through 60R-6, 504–754 mbsf), both correlated to the Fataga stratigraphic interval and Subunit IVC (Sections 157-953C-61R-1 through 70R-6, 754–850 mbsf) corresponding to the Mogán group. At Site 955, Subunit IVA (139 m, Sections 157-955A-40X-5 through 54X-CC, 374–513 mbsf) is correlated to the Fataga interval and Subunit IVB (54 m, Sections 157-955A-55X-1 through 60X-4, 513–567 mbsf) to the Mogán. At Hole 956B, Subunit IVA (Fataga; Sections 157-956B-23R-1 through 38R-4, 367.5–517.5 mbsf) is 150 m thick, and Subunit IVB (Mogán; Sections 157-956B-39R-1 through 43R-2, 522.6–564.1 mbsf) is 41.5 m thick. The volcaniclastic interval corresponding to the Mogán and Fataga Groups therefore is more than twice as thick at Hole 953C (452 m) than at Holes 955A (193 m) and 956B (197 m). This doubled thickness in the northern and more distal site is surprising, because it is the southern half of Gran Canaria that is dominated by great thicknesses of the Mogán and Fataga ignimbrites, lavas, and tuffs (Fig. 1). We suspect this difference results from Hole 953C being drilled on the flat floor of the northern depositional basin, where turbidites probably slowed down and deposited more material, whereas the southern sites are closer to the steeper slopes of the island. A second factor may be that the major northeastern outlet of the caldera basin is thought to have channelized outflow of pyroclastic flows erupted inside the caldera basin.

General Lithology of the Fataga and Mogán Stratigraphic Intervals

Apart from the overall thickness differences and contrasts between particular volcaniclastic units and smaller stratigraphic intervals, the general lithology of the volcaniclastic deposits and their interlayered nonvolcanic sediments is fairly similar between sites and is thus discussed together below. The units have been subdivided primarily based on variations in the type and abundance of major volcaniclastic components as well as mineral and glass compositions.

Fataga Intervals (Subunits IVA and IVB at Hole 953C and Subunit IVA at Holes 955A and 956B)

Volcaniclastic layers correlated to the Fataga phase are green, lithic-crystal-vitrile sandstones and siltstones. Rock fragments are typically clasts of trachyphonolitic lava flows and ignimbrites. The abundance and thickness of volcaniclastic sandstones and pumiceous units increase markedly downcore.

The volcaniclastic sediments alternate with medium-bedded green to dark gray, nannofossil claystone and claystone that grade downward into thin siltstone or sandstone bases. The upper contacts are moderately to extensively bioturbated, whereas lower contacts are almost always sharp. Many of the siltstone and sandstone bases are parallel-laminated, or more rarely, cross-laminated. Such units are interpreted as the deposits of turbidity currents that interrupted the background pelagic sedimentation of nannofossil chalk. The claystone parts of these units consist of ~75 vol% clay minerals, 10 vol% nannofossils, 10 vol% foraminifers, and 5 vol% volcanicogenic crys-

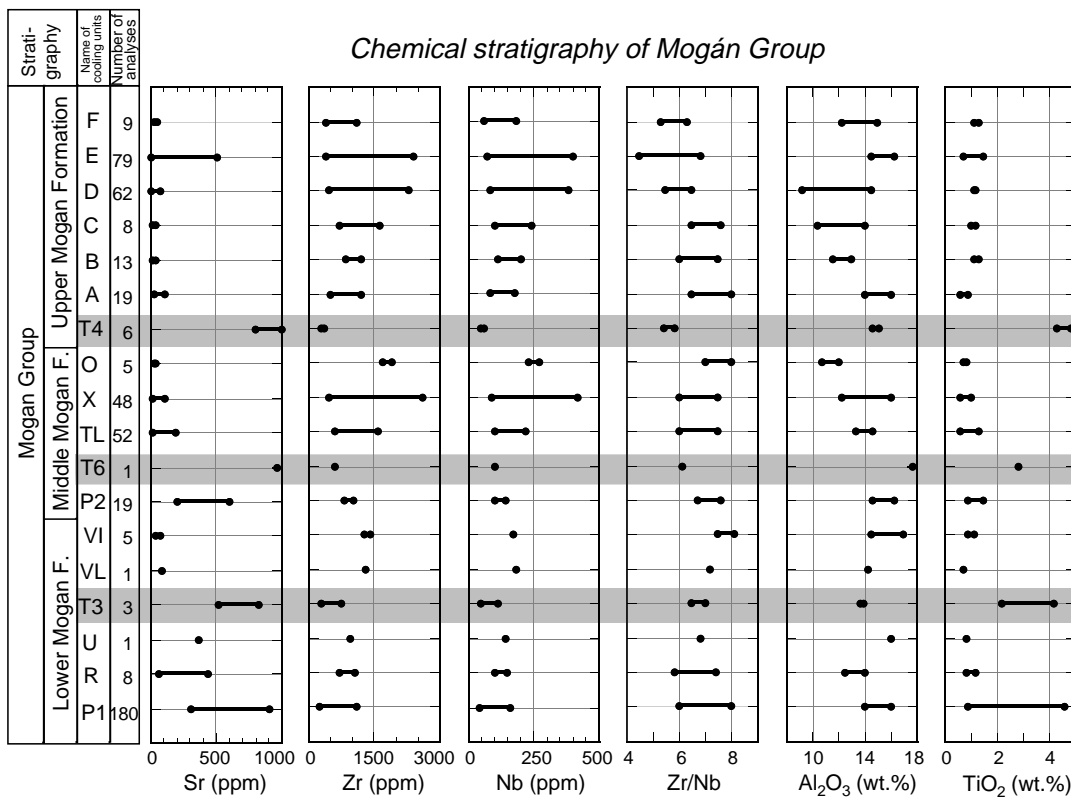


Figure 5. Chemical stratigraphy of Mogán Group.

tals. Nannofossil-bearing sediments may form the top of graded units or occur as interbeds with gradational contacts to the surrounding sediments.

Thickness and grain size of the tuffs and lapillistones increase downward. Thick, bedded tuffs with varying proportions of lithic, crystal, vitric, and biogenic clasts are commonly structureless with sharp basal contacts and bioturbated tops. Normal size grading, reverse in pumice-rich beds, and a transition to parallel-laminated structures in their tops are common. Tuffs contain particles with greatly contrasting density, such as vesicular pumice and dense, mafic rock fragments. Some tuffs are composed almost entirely of vitric components, such as pumice and glass shards, with minor amounts of crystals and lithoclasts. Pumice and scoria fragments range up to 5 mm, vary from white to black, and are highly vesicular. Zeolitized tuffs are common in Subunits IVA and IVB (Hole 953C) and Subunit IVA (Holes 955A and 956B), whereas glass shards are generally less altered in the Lower Mogán subunits at all sites.

Mogán Intervals (Subunit IVC in Holes 953C, 955A, and 956B)

The lower subunits are distinguished from the overlying mixed sediments primarily by a greater abundance of coarse and fine vitric material in the tuffs. Most striking in the lower lithologic units are pumice-rich massive units and thick tuffs consisting entirely of glass shards. Discrete, vitric-rich tuffs and lapillistones commonly occur throughout and are interbedded with subordinate amounts of nannofossil mixed sedimentary rock or nannofossil chalk. Calcareous sands are rare and usually occur as thin beds composed of a mixture of foraminifers, crystals, and lithics. Tuffs commonly grade upward into nannofossil mixed sedimentary rock, nannofossil claystone, or claystone, with abundant fine-grained glass shards and crystals. The deposits typically have sharp bases and bioturbated tops.

Several compositionally distinct ignimbrites studied on land have been recognized in the volcaniclastic units by virtue of their distinctive mineralogical characteristics. For example, a crystal-vitric tuff in Section 157-955A-58X-5 contains trace amounts of titanite, a diagnostic indicator of ignimbrite X from the middle Mogán Group (Schmincke, 1969, 1976). A pumice lapilli tuff in the same section contains phenocrysts of phlogopite, a characteristic feature of ignimbrite A from the Upper Mogán Group on Gran Canaria.

Surprisingly, sideromelane occurs in many volcaniclastic layers chiefly in the Mogán interval at all three sites and even forms a distinct hyaloclastite tuff in Hole 956B. The correlation to two local (T3 and T6) and one widespread (T4) subaerial basalt member is reasonable, but not conclusive. Only the widespread T4 lavas can be considered large enough to be reasonably correlated. The correlation is permissible, although not unique, because sideromelane compositions from other volcaniclastic units that are definitely younger or older could be correlative as well. Instead, we believe the sideromelane shards to have formed during submarine eruptions, roughly synchronously with the silicic/evolved tuffs in which they are contained, as discussed in Schmincke and Sumita (Chap. 16, this volume).

MINERALOGY

Phenocryst Mineralogy of Subaerial Mogán and Fataga Ignimbrites

A summary of the qualitative mineralogy of the ignimbrite cooling units and interbedded fallout tephra layers is presented in Figure 3. The most common phenocryst in the Mogán and Fataga ignimbrites above ignimbrite P1 is anorthoclase. Compositional variations in feldspar phenocrysts through the Mogán and Fataga formations were established by Schmincke (1969), who showed that feldspar,

dominantly anorthoclase, becomes more potassic with decreasing age, most likely reflecting decreasing Na/K ratios of the parental magmas (Fig. 6). This trend is not unidirectional, however, because some units, such as ignimbrite B (UMF), have more sodic feldspar compositions than the underlying ignimbrite. Unfortunately, however, the spectrum of compositions is too large in most units to allow unequivocal discrimination between adjacent cooling units, except in some exceptional cases, such as P1, V, and P2.

Alkalic amphibole (edenite and richterite) is very common in the more evolved, lower parts of most ignimbrites, but more aluminous and calcic amphibole occurs in ignimbrites P1, P2, and A. Clinopyroxene is a minor but common phase in most units and orthopyroxene is present in the Lower Mogán cooling units (U, VI, VL, P2, and TL). Zircon microphenocrysts occur in cooling units P1, U, VI, VL, and P2; titanite has been found only in ignimbrite X, phlogopite only in A and in the transitional ignimbrite F, and chevkinite crystals occur generally as inclusions in amphibole, especially in ignimbrites X, A, and O, and, very rarely, in P1.

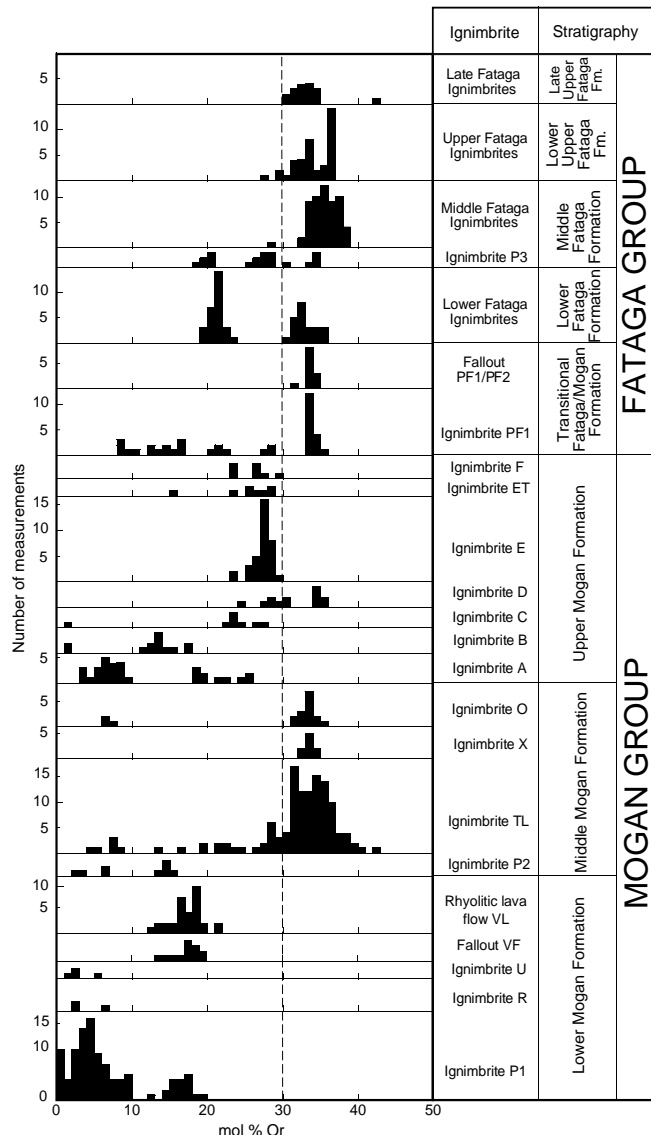


Figure 6. Stratigraphic plot of mol% anorthoclase (Or) in feldspar phenocrysts from the Mogán and Fataga groups.

Clastic Mineral Phases in the Volcaniclastic Units

Feldspars

The most common phenocryst phase in the submarine volcaniclastic layers is anorthoclase approaching sanidine in composition in the Fataga volcaniclastic units. Feldspar crystals were analyzed in 28 polished sections in Hole 953C from VU-7 (836.86 mbsf) to VU-100 (602 mbsf), 20 polished sections in Hole 955A from VU-4 (564.45 mbsf) to VU-85 (495.36 mbsf), and 21 polished sections in Hole 956B from VU-7a (563.45 mbsf) to VU-107 (468.48 mbsf). The data are presented in Table 2 and Figures 6–9. To facilitate stratigraphic correlation of the volcaniclastic units with the land stratigraphy, we have also analyzed feldspar compositions in 20 polished thin sections from both Mogán and Fataga subaerial cooling units (Fig. 6).

Lower Mogán Phase

The chemical feldspar stratigraphy is well developed in all three holes: the bimodal plagioclase/anorthoclase assemblage characteristic for reworked tuff, P1 is found as high as VU-11a at Hole 953C (Sample 157-953C-69R-5, 26–33 cm; 836.86 mbsf), in VU-7 at Hole 955A (Sample 157-955A-60X-2, 140–144 cm; 563.8 mbsf) and in VU-10 at Hole 956B (Sample 157-956B-43R-2, 8–11 cm; 562.68 mbsf). Fairly homogeneous feldspar compositions (anorthoclase Or_{10-15}) at relatively high An_{4-9} correspond to the most homogeneous glass composition intervals of V-type fallout, ignimbrite, and lava intervals on land. At Hole 953C, only one volcaniclastic unit (VU-14) shows this composition corresponding to the relatively thin interval of V-type volcaniclastics. This feldspar composition is found in VU-15 at Hole 955A, whereas at Hole 956B very homogeneous feldspar compositions of V-type extend from VU-15 to VU-25, reflecting the relatively thick succession of this composition in the extra-caldera facies in southwestern Gran Canaria.

Middle Mogán Phase

The compositions of glass shards in tuffs correlated to ignimbrite (see below) V and P2 are similar so we relied on the occurrence of potassic feldspars (Or_{32}) to help identify VU-15 at Hole 953C as P2 comendite fraction rather than V. VU-60 in Hole 953C also appears to represent ignimbrite P2. Feldspars are less potassic and more mixed in VU-24 at Hole 955A, and are more potassic than those in V-type magma, corroborating the stratigraphic correlation made on the basis of glass composition. The absence of volcaniclastic layers correlative to ignimbrite P2 based on glass compositions at Hole 956B is also corroborated by the feldspar data. The submarine equivalent of the compositionally strongly mixed subaerial TL ignimbrite might be correlated to VU-17 at Hole 953C and VU-25 at Hole 955A, but it is not present at Hole 956B. Ignimbrite X is easily distinguished at all three holes by a very heterogeneous feldspar compositional spectrum, with a distinct peak in Or -rich compositions, however. This spectrum may reflect that of the source ignimbrite or may have resulted from erosional mixing by turbidites generated during and after emplacement of ignimbrite X, which incorporated less potassic feldspar from underlying older deposits. VU-21 at Hole 953C and VU-30 at Hole 955A are equivalent to ignimbrite O, but no equivalent was found in Hole 956B, most likely because of the very poor recovery of Cores 157-956B-40R, 41R, and 42R at this hole.

Upper Mogán Phase

Anorthoclase in VU-34 (Hole 955A) is less potassic than in the under- and overlying units as in the more trachytic ignimbrite A. Feldspar compositions are trimodal in VU-32 (Hole 956B), which corresponds to ignimbrite A. Although ignimbrite A is compositionally very heterogeneous, VU-32 is more strongly reworked than some of the other volcaniclastic units, suggesting that the heterogeneity in feldspar compositions has resulted from erosional mixing.

Figure 7. Feldspar compositions at Hole 956B. Samples include: VU-107 (Sample 157-956B-33R-1, 59–63 cm), VU-102 (Sample 157-956B-34R-2, 62–70 cm), VU-94 (Sample 157-956B-35R-2, 101–110 cm), VU-87a (Sample 157-956B-35R-4, 27–35 cm), VU-77b (Sample 157-956B-37R-1, 136–146 cm), VU-47 (Sample 157-956B-39R-2, 114–118 cm), VU-39 (Sample 157-956B-40R-1, 68–71 cm), VU-36 (Sample 157-956B-40R-2, 26–33 cm), VU-32 (Sample 157-956B-40R-2, 129–133 cm), VU-31a and VU-31b (Sample 157-956B-41R-1, 0–9 cm), VU-19 (Sample 157-956B-42R-2, 0–5 cm), VU-15 (Sample 157-956B-43R-1, 0–8 cm), VU-10 (Sample 157-956B-43R-2, 8–11 cm), and VU-7d (Sample 157-956B-43R-2, 85–89 cm).

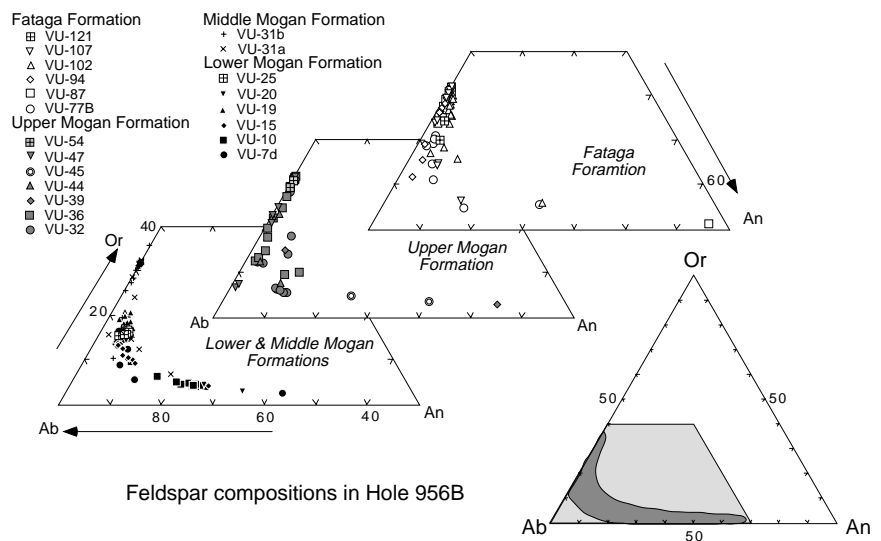
The highly peralkaline compositions of the major ignimbrites of the Upper Mogán (B, C, and D) appear in Hole 953C with VU-32. The feldspars in this unit are heterogeneous, and feldspars with Or-content of 31.2 are present. At Hole 955A, ignimbrite B probably correlates to VU-29 because feldspars in ignimbrite B are relatively sodic. VU-44 in Hole 956B might correlate with ignimbrite B. The correlation of volcaniclastic units to ignimbrite C at all three holes is still uncertain. The highly evolved, pantelleritic ignimbrite D is recognized in all sites by the highly peralkaline composition of glass. At Hole 953C, we correlate VU-36 to ignimbrite D, and the feldspar population contains several very potassic crystals, the most potassic being $\text{Or}_{35.1}$. The feldspar population is quite heterogeneous compositionally, but the nature of the volcaniclastic unit suggests direct derivation from an ignimbrite eruption, so that the more sodic feldspars, which range to albitic plagioclase, may reflect the large compositional spectrum of compositionally zoned ignimbrite D. No feldspar from this unit has been analyzed at Hole 955A.

Transitional Mogán/Fataga and Fataga

Sampling and analysis of volcaniclastic units above ignimbrite D has not been as detailed as that for the Mogán-related volcaniclastic units. At all three holes, feldspars become slightly more potassic with decreasing age. For example, most feldspars in VU-42 to VU-60 at Hole 953C range from Or_{30} to Or_{35} with even more potassic feldspars in younger units. Or contents as high as Or_{39} are found in VU-100 (Sample 157-953C-45R-2, 10–14 cm; 602 mbsf). Or contents as high as 33.5 are reached in VU-67 at Hole 955A, Or = 35.2 is reached in VU-75, and 36.6 is reached in VU-81 at 496.8 mbsf. Feldspars are less potassic in the younger cores at Hole 956B, which is most distant from the presumed Fataga eruptive center. It is not known whether the more potassic ignimbrites erupted during Fataga time reached the coast in southwest Gran Canaria. The compositional heterogeneity is pronounced in most volcaniclastic units of the Fataga interval. This is expected because of the smaller volume of the ignimbrites, their more restricted aerial extent relative to most Mogán ignimbrites, and the terrain in the south, which became more dissected during Fataga volcanism.

Amphibole

Amphibole is the most common mafic phenocryst phase, apart from Fe-Ti-oxides, in the Mogán Formation, but is relatively rare in the Fataga Formation and is generally restricted to ignimbrites. The only stratigraphic intervals where amphibole does not occur in the Mogán are the ignimbrites U, VL, and VI and related fallout tuffs.



The qualitative use of amphibole as a stratigraphically diagnostic phenocryst mineral is compromised by the fact that amphibole also occurs in abundance in an exotic crystal-rich sandstone unit overlying the thick basal debris-flow deposit at Hole 956B and sporadically in other hyaloclastites. We have interpreted this amphibole as “xenocrystic,” probably derived from admixture of Gomera beach sands (Schmincke and Segschneider, Chap. 12, this volume). Qualitatively, this amphibole is commonly slightly darker and more rounded than amphibole derived from Mogán Group ignimbrites. These amphiboles also differ in their composition from those of the Mogán and Fataga Group volcanics.

Amphibole phenocrysts in the Mogán and Fataga volcaniclastic layers occur basically as two end-members with much variation in between (Table 3; Figs. 10–12). One end member is calcic amphibole, mostly kaersutite with relatively low concentrations of Na_2O , F, SiO_2 , MgO , K_2O , FeO^* , MnO , Al_2O_3 , and Cr_2CO_3 . Those in ignimbrite P1, and to a lesser degree in P2, are darker colored and commonly intergrown or associated with Fe/Ti oxide, apatite and, in the case of P1, zircon. The kaersutites mainly occur in volcaniclastic layers derived by erosion of P1, as incorporated crystals in volcaniclastic layers of the V interval, and sporadically in other layers. The other end-member is sodic richterite with relatively high concentrations of Na_2O , F, SiO_2 , MgO , MnO , slightly higher K_2O and FeO^* contents, and lower alumina, calcium and titanium contents. These pale-colored, alkalic amphiboles dominate in nearly all ignimbrites starting with TL up to E. Amphiboles in ignimbrites X and A, and to a lesser extent O, contain deep reddish brown, strongly pleochroic inclusions of chevkinite. The rare amphiboles in the Fataga Group appear to be compositionally similar to those from the Mogán Group.

In Hole 953C and in Core 157-955A-53X, probably the most highly evolved amphibole occurs in volcaniclastic layers correlated to ignimbrites C and D (VU-35 and 36), at Hole 953C in VU-47 and 52 at Hole 955A, and in VU-47 in Hole 956B. In these units, as well as some of those correlated tentatively to ignimbrite B, the elements F, Na, and, in the case of ignimbrite D, Fe reach the highest concentrations. In summary, the amphibole chemical stratigraphy has turned out to be especially diagnostic because of the pronounced differences in chemical composition between the two end-members.

Pyroxenes

Pyroxenes fall into three compositional groups, distinguishable by color: augite and titanaugite, hypersthene, enstatite, and aegirine. Aegirine augites are rare (Figs. 13–15).

Table 2. Representative EMP analyses of feldspars from Holes 953C, 955A, and 956B

Hole, core, section:	953-69R-5C	953C-69R-5	953C-69R-1	953C-68R-4	953C-67R-3	953C-67R1	953C-66R-3	953C-65R-5	953C-64R-3
Interval (cm):	26-33	26-33	0-7	56-60	102-104	148-150	16-22	93-98	72-75
Depth (mbsf):	836.86	836.86	831.1	826.07	815.61	813.18	805.03	798.56	786.14
Volcaniclastic unit:	VU-11a	VU-11a	VU-14	VU-15	VU-20	VU-21	VU-29	VU-32	VU-36
Sample number:	FP-1	FP-3	FP-2	FP-12	FP-1	FP-5	FP-7	FP-2	FP-6
Number of analyses:	2	2	2	2	2	2	1	3	1
(wt%)									
SiO ₂	53.53	65.33	64.92	64.99	66.66	65.53	65.89	64.84	64.46
TiO ₂	0.16	0.03	0.03	0.06	0.07	0.04	0.03	0.05	0.02
Al ₂ O ₃	26.51	19.28	20.52	18.65	18.78	18.01	17.80	19.66	17.26
FeO	0.53	0.45	0.47	0.64	0.97	1.65	1.55	0.45	1.96
MnO	0.01	0.05	0.03	0.02	0.02	0.00	0.04	0.01	0.07
MgO	0.10	0.00	0.00	0.00	0.00	0.00	0.01	0.00	0.00
CaO	10.25	8.80	1.22	0.15	0.09	0.01	0.01	1.22	0.00
Na ₂ O	5.38	9.42	9.53	7.78	8.39	7.96	7.74	9.60	7.44
K ₂ O	0.66	2.71	2.23	5.46	4.58	5.22	5.53	2.20	6.12
BaO	0.143	0.218	0.243	0.090	0.201	0.020	0.074	0.301	0.051
SrO	0.184	0.014	0.027	0.261	0.165	0.229	0.194	0.020	0.187
F	0.026	0.045	0.041	0.050	0.019	0.037	0.000	0.026	0.055
Total:	97.47	98.35	99.25	98.14	99.94	98.70	98.87	98.39	97.63
ab	46.9	80.9	81.7	67.9	73.3	69.8	68.0	81.9	64.9
or	3.8	15.3	12.6	31.4	26.3	30.1	31.9	12.4	35.1
an	49.3	3.8	5.8	0.7	0.4	0.0	0.1	5.8	0.0

Table 2 (continued).

Hole, core, section:	953C-60R-3	953C-59R-6	953C-45R-2	955A-60X-2	955A-59X-6	955A-59X-1	955A-58X-1	955A-55X-4	955A-53X-3
Interval (cm):	0-6	105-112	10-14	140-144	61-67	51-53	119-125	19-25	0-7
Depth (mbsf):	747.42	742.97	602	563.8	559.31	551.71	542.79	517.59	496.8
Volcaniclastic unit:	VU-42	VU-44	VU-100	VU-7	VU-15	VU-25	VU-34	VU-67	VU-81
Sample number:	FP-3	FP-8	FP-5	FP-5	FP-4	FP-5	FP-2	FP-4	FP-7
Number of analyses:	1	2	2	2	2	2	2	2	2
(wt%)									
SiO ₂	65.26	66.26	65.79	60.34	66.70	66.71	66.67	67.06	64.58
TiO ₂	0.08	0.06	0.08	0.08	0.02	0.07	0.09	0.08	0.03
Al ₂ O ₃	18.82	18.49	18.91	23.63	19.55	18.79	19.48	18.54	20.76
FeO	0.72	1.04	0.80	0.42	0.52	0.85	0.48	1.26	0.37
MnO	0.00	0.02	0.01	0.05	0.04	0.01	0.00	0.00	0.00
MgO	0.01	0.00	0.00	0.02	0.00	0.01	0.01	0.01	0.01
CaO	0.10	0.04	0.18	5.37	0.63	0.09	0.36	0.03	1.54
Na ₂ O	8.42	7.81	8.11	8.24	9.61	8.83	8.66	8.30	8.50
K ₂ O	4.80	5.59	5.34	0.77	2.43	4.32	4.07	5.04	3.33
BaO	0.105	0.071	0.056	0.083	0.170	0.034	0.135	0.065	0.703
SrO	0.264	0.145	0.106	0.000	0.018	0.140	0.089	0.156	0.000
F	0.095	0.033	0.042	0.014	0.067	0.032	0.042	0.020	0.000
Total:	98.67	99.56	99.43	99.02	99.76	99.90	100.09	100.55	99.83
ab	72.4	67.9	69.2	70.3	83.1	75.3	75.1	71.3	73.6
or	27.2	32.0	30.0	4.3	13.8	24.3	23.2	28.5	19.0
an	0.5	0.2	0.9	25.3	3.0	0.4	1.7	0.2	7.4

Table 2 (continued).

Hole, core, section:	956B-43R-2	956B-43R-1	956B-41R-2	956B-41R-2	956B-40R-2	956B-40R-2	956B-40R-2	956B-35R-2
Interval (cm):	8-11	0-8	115-132	0-9	129-133	129-133	129-133	27-35
Depth (mbsf):	562.68	561.10	544.52	541.90	535.09	535.09	535.09	488.48
Volcaniclastic unit:	VU10	VU-15	VU-25	VU-31a	VU-32	VU-32	VU-32	VU-87a
Sample number:	FP-2	FP-5	FP-3	FP-11	FP-4	FP-7	FP-14	FP-7
Number of analyses:	2	2	2	2	2	2	1	2
(wt%)								
SiO ₂	61.78	65.75	64.66	66.47	66.15	65.62	63.32	67.20
TiO ₂	0.07	0.01	0.06	0.02	0.04	0.08	0.09	0.05
Al ₂ O ₃	22.72	20.16	19.94	17.90	18.90	19.38	20.66	18.33
FeO	0.47	0.40	0.41	1.53	0.59	0.63	0.48	0.93
MnO	0.03	0.00	0.05	0.01	0.08	0.00	0.00	0.01
MgO	0.02	0.00	0.01	0.00	0.00	0.02	0.02	0.00
CaO	4.79	1.12	1.04	0.02	0.18	0.73	2.16	0.05
Na ₂ O	8.42	9.12	9.17	7.71	8.31	9.90	9.73	7.69
K ₂ O	0.88	2.48	2.99	5.44	5.04	2.22	1.05	5.97
BaO	0.159	0.253	0.277	0.036	0.091	0.291	0.408	0.041
SrO	0.000	0.272	0.006	0.249	0.135	0.124	0.000	0.187
F	0.031	0.049	0.063	0.036	0.027	0.000	0.032	0.022
Total:	99.35	99.60	98.66	99.41	99.55	99.00	97.95	100.48
ab	72.3	80.3	78.3	68.2	70.9	84.2	83.7	66.1
or	5.0	14.3	16.8	31.7	28.3	12.4	6.0	33.7
an	22.7	5.4	4.9	0.1	0.8	3.4	10.3	0.2

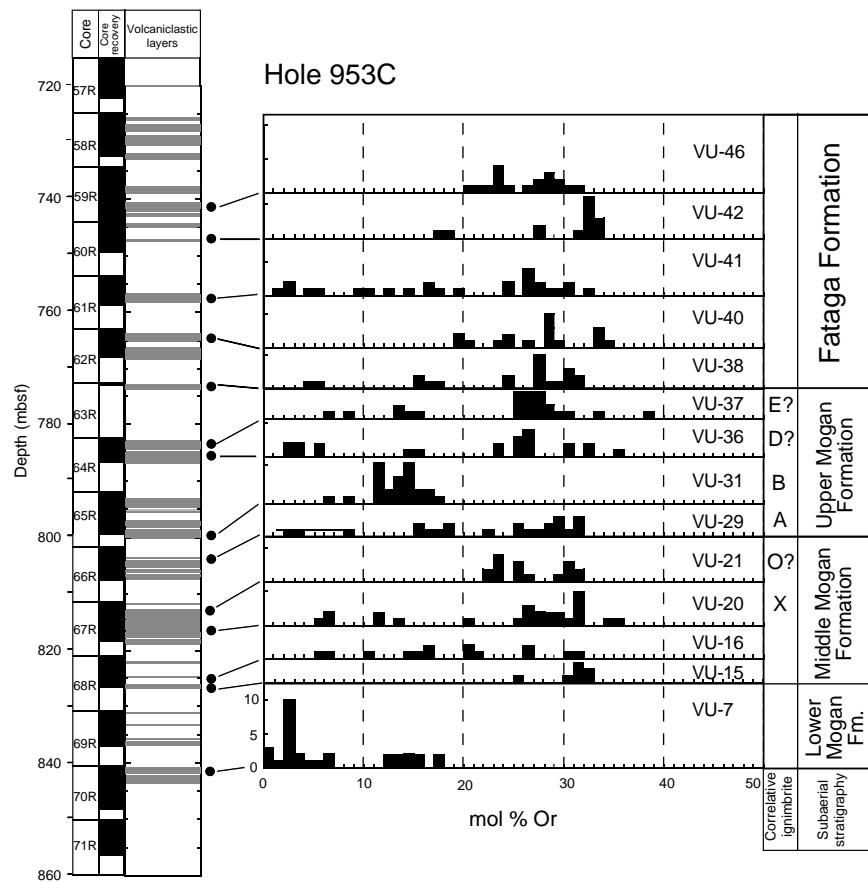


Figure 8. Stratigraphic plot of mol% Or in feldspar for Hole 953C. Samples include VU-60 (Sample 157-953C-55R-3, 74–82 cm), VU-46 (Sample 157-953C-59R-5, 104–107 cm), VU-42 (Sample 157-953C-60R-3, 0–6 cm), VU-41 (Sample 157-953C-61R-3, 109–114 cm), VU-40 (Sample 157-953C-62R-1, 100–118 cm), VU-38 (Sample 157-953C-63R-1, 40–48 cm), VU-37 (Sample 157-953C-64R-1, 62–74 cm), VU-36 (Sample 157-953C-64R-3, 72–75 cm), VU-31 (Sample 157-953C-65R-6, 103–107 cm), VU-29 (Sample 157-953C-66R-3, 16–22 cm), VU-21 (Sample 157-953C-67R-1, 148–150 cm), VU-20 (Sample 157-953C-67R-4, 53–59 cm), VU-16 (Sample 157-953C-68R-3, 60–66 cm), VU-15 (Sample 157-953C-68R-4, 56–60 cm), and VU-7 (Sample 953C-70R-1, 57–65 cm).

Clinopyroxene

Brownish to lilac titanaugite is the most common mafic phenocryst in the submarine and subaerial shield basalts of Gran Canaria, and occurs as a ubiquitous detrital phase derived by erosion of the shield basalts and hyaloclastites wherever a basaltic component is admixed to the felsic volcaniclastic layers. Indeed, “basaltic” clinopyroxene even occurs in those volcaniclastic layers which lack tachylite and crystallized basalt clasts. The basaltic titanaugites are richer in CaO (>20 wt%), TiO₂ (1–5 wt%), Al₂O₃ (up to 8 wt%) and Cr₂O₃ (up to 1 wt%) and poorer in FeO* and SiO₂ than augites from the felsic ignimbrites. Basaltic clinopyroxene is absent only in the purest, ignimbrite-derived, sandy volcaniclastic layers and in the vitric shard tuffs. It also occurs as a phenocryst phase in the submarine hyaloclastites. Extremely mafic (Cr-, Ni- and Mg-rich) clinopyroxene occurs in the black lapillistones in Core 157-956B-32R, which are stratigraphically equivalent to the Middle Fataga Formation (Table 4).

Colorless to light green clinopyroxenes, slightly more Fe-rich and Ca-poor than the basaltic titanaugites, are most common in the upper LMF stratigraphic interval, represented by cooling units U, VL, and VI and associated fallout volcaniclastic layers. They also occur in the uppermost mafic trachyte flow units of most ignimbrites of the MMF and UMF, and in P1, as well as in several Fataga-equivalent volcaniclastic units. Clinopyroxene is more prevalent than orthopyroxene in the subaerial deposits but even more common in the submarine volcanicastics because hypersthene is much more susceptible to alteration than clinopyroxene. The FeO* and MnO concentrations in these augites increase significantly in the Middle and Upper Mogán compared to the V-type tephra layers of the LMF. They remain high in most volcanicastic units of the Fataga interval. Clinopyroxene transitional to aegirine (aegirine-augite) has been analyzed in a few polished thin sections from Upper Mogán and Fataga volcanicastic layers from Hole 955A (Fig. 14).

Orthopyroxene

Orthopyroxene occurs as hypersthene with several compositional subgroups distinguished by their trace-element concentrations (Table 5), especially high Mn concentrations. Mg-rich enstatite with very low Mn concentrations occurs sporadically in some volcanicastic layers and are likely derived from mantle peridotite nodules. Hypersthene occurs chiefly in the subaerial upper LMF pyroclastics corresponding to cooling units U, VL, VI, and associated fallout tuffs. The lowermost MMF (P2) is also contains hypersthene. Smaller amounts of hypersthene occur in the uppermost mafic trachyte flow unit of several ignimbrites of the MMF and UMF, up to ignimbrite E and also in the trachyte component of ignimbrite P1.

Aegirine

Aegirine is by far the most common mafic phase in most subaerial Middle and Upper Mogán ignimbrites as well as Fataga ignimbrites and lava flow cooling units. Aegirine, responsible for the striking green color of these rocks on land, occurs, however, exclusively as a groundmass phase in the generally coarsely crystallized ignimbrites and lava flows. Aegirine is not present in the peraluminous volcanicastic units from the Lower Mogán or in those volcanicastic layers related to fallout ash layers or to ignimbrites that entered the sea, because it formed only during cooling of the hot sheets. In addition, erosion was minor during the Mogán stratigraphic interval in southern Gran Canaria and the ignimbrites were, therefore, generally not dissected into their fully crystallized interior. Aegirine thus appears in minor traces only in volcanicastic layers equivalent to the Upper Mogán but is more common in those equivalent to the Fataga interval as well as in younger ash layers (Pl. 2, Fig. 3). Aegirine occurs in several volcanicastic units starting with D-equivalent tephra (VU-36 in Hole 953C) and many aegirines have been analyzed in volcanicastic units from Hole 955A (Table 6). Aegirine with TiO₂ concentrations

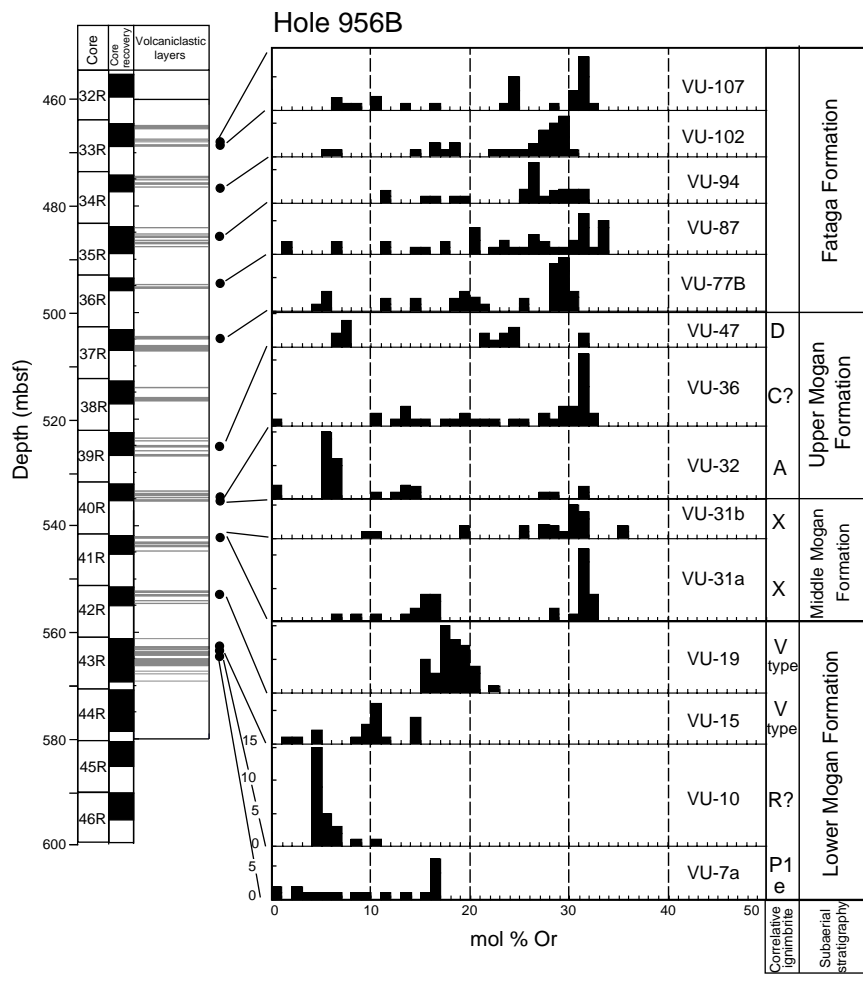


Figure 9. Stratigraphic plot of mol% Or in feldspar for Hole 956B. Samples include VU-121 (Sample 157-956B-33R-1, 59–63 cm), VU-107 (Sample 157-956B-33R-1, 59–63 cm), VU-102 (Sample 157-956B-34R-2, 62–70 cm), VU-94 (Sample 157-956B-35R-2, 101–110 cm), VU-87a (Sample 157-956B-35R-4, 27–35 cm), VU-77B (Sample 157-956B-37R-1, 136–146 cm), VU-47 (Sample 157-956B-39R-2, 114–118 cm), VU-36 (Sample 157-956B-40R-2, 26–33 cm), VU-32 (Sample 157-956B-40R-2, 129–133 cm), VU-31a and VU31b (Sample 157-956B-41R-1, 0–9 cm), VU-19 (Sample 157-956B-42R-2, 0–5 cm), VU-15 (Sample 157-956B-43R-1, 0–8 cm), VU-10 (Sample 157-956B-43R-2, 8–11 cm), and VU-7d (Sample 956B-43R-2, 85–89 cm).

as high as 10 wt% occur in the pantellerites from Gran Canaria (Schmincke, 1969) and TiO_2 concentrations as high as 7.5 wt% were analyzed from Fataga volcaniclastic units at Hole 953C (Fig. 13).

In summary, the pyroxene compositions are more useful for stratigraphic correlation than those of the amphiboles. Moreover, the pyroxenes form magnificent differentiation series similar to the classic evolutionary trend of the amphiboles discussed earlier. The petrologic implications of this broad spectrum of amphibole and clinopyroxene compositions will be discussed elsewhere.

Phlogopite

Phlogopite, like titanite, is unit specific in the Mogán Group where it exclusively occurs as a common but not abundant phenocryst phase in ignimbrite A, and in the topmost Mogán ignimbrite F, which is compositionally transitional to the Fataga Group. Phlogopite also occurs sporadically and in trace amounts in the Lower Mogán (e.g., in ignimbrite P1 and pre-U-ignimbrite-correlated fallout volcaniclastic units). These rare occurrences cannot be used as a stratigraphic tool, however, because phlogopite—commonly but not always partially to completely chloritized—was also supplied to the depositional basins from an external source, most likely erosion of phlogopite-bearing syenites on Gomera and possibly Fuerteventura (Schmincke and Segschneider, Chap. 12, this volume). Because mica settles slowly through the water column, this xenocrystic mica is a mineralogical “vagabond” joining the common xenocrystic alkalic amphibole (see above) but much less common than locally derived

xenocrystic basaltic titanite. Phlogopite is the most common mafic phase in ignimbrites and fallout tephras throughout the ~4.5-m.y.-long Fataga phase. No temporal changes in phlogopite composition have been identified, but the appearance of phlogopite in the volcaniclastic units above the Mogán volcaniclastic units has been an extremely useful criterion to identify the beginning of Fataga-related volcaniclastic units.

The composition of dark mica in Mogán-equivalent volcaniclastic layers (P1, A) and those from Fataga volcaniclastic layers was determined in eight polished sections from Hole 953C and five polished sections from Hole 956B (Plate 2, Fig. 1; Table 7). All micas are phlogopite with very little variation. Fluorine concentrations are lower in phlogopites from volcaniclastic layers equivalent to ignimbrite A, whereas Na_2O and FeO^* contents are slightly higher in this unit compared to those from most volcaniclastic layers of the Fataga stratigraphic interval. In summary, phlogopite, in contrast to all other phenocrysts, shows little variation in chemical composition with stratigraphy; its composition therefore is not useful as a stratigraphic tool.

Titanite

Titanite is practically unique as a phenocryst phase in the Mogán Group where it is the stratigraphically diagnostic phase in ignimbrite X of the MMF. Hand-lens identification of titanite in ignimbrite X has been extremely useful on land, and the recognition of titanite under the microscope aboard ship allowed us to unequivocally identify

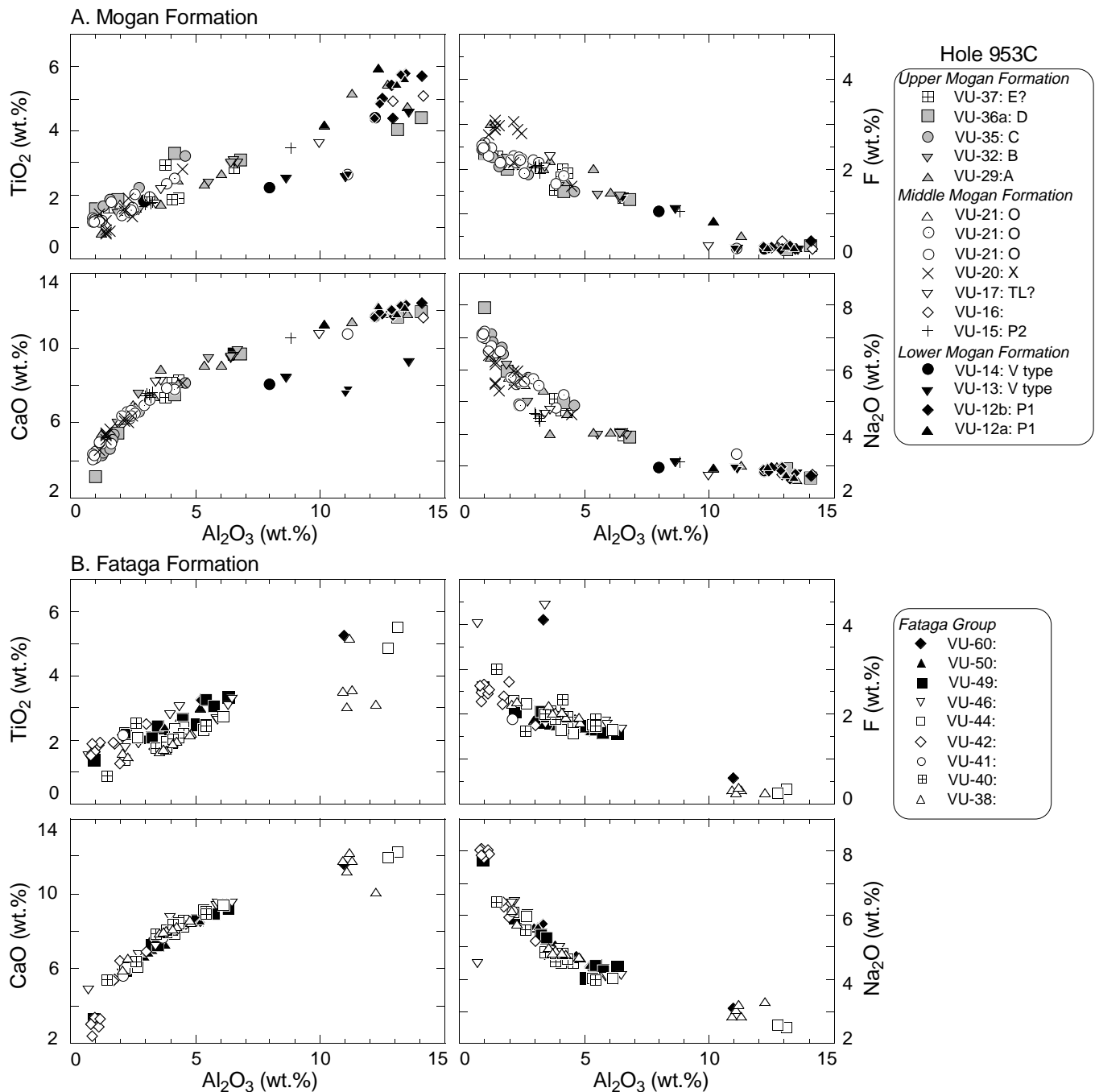


Figure 10. CaO, TiO₂, Na₂O, and F plotted vs. Al₂O₃ in amphibole phenocrysts and xenocrysts from Hole 953C for the (A) Mogán Formation and (B) Fataga Formation. Sample numbers include VU-60 (Sample 157-953C-55R-3, 74–82 cm), VU-50 (Sample 157-953C-58R-2, 76–80 cm), VU-49 (Sample 157-953C-58R-4, 41–45 cm), VU-46 (Sample 157-953C-59R-5, 104–107 cm), VU-44 (Sample 157-953C-59R-6, 105–112 cm), VU-42 (Sample 157-953C-60R-3, 0–6 cm), VU-41 (Sample 157-953C-61R-3, 109–114 cm), VU-36 (Sample 157-953C-64R-3, 72–75 cm), VU-35 (Sample 157-953C-63R-1, 40–48 cm), VU-37 (Sample 157-953C-64R-1, 62–74 cm), VU-32 (Sample 157-953C-65R-3, 93–98 cm), VU-29 (Sample 157-953C-66R-3, 16–22 cm), VU-21-3 (Sample 157-953C-67R-1, 131–138 cm), VU-21-2 (Sample 157-953C-67R-2, 148–150 cm), VU-21-1 (Sample 157-953C-67R-2, 75–84 cm), VU-20 (Sample 157-953C-67R-4, 53–59 cm), VU-17 (Sample 157-953C-68R-1, 80–97 cm), VU-16 (Sample 157-953C-68R-3, 60–66 cm), VU-15 (Sample 157-953C-68R-4, 56–60 cm), VU-14 (Sample 157-953C-69R-1, 0–7 cm), VU-13 (Sample 157-953C-69R-2, 64–69 cm), VU-12b (Sample 157-953C-69R-2, 75–81 cm), and VU-12a (Sample 157-953C-69R-4, 22–29 cm).

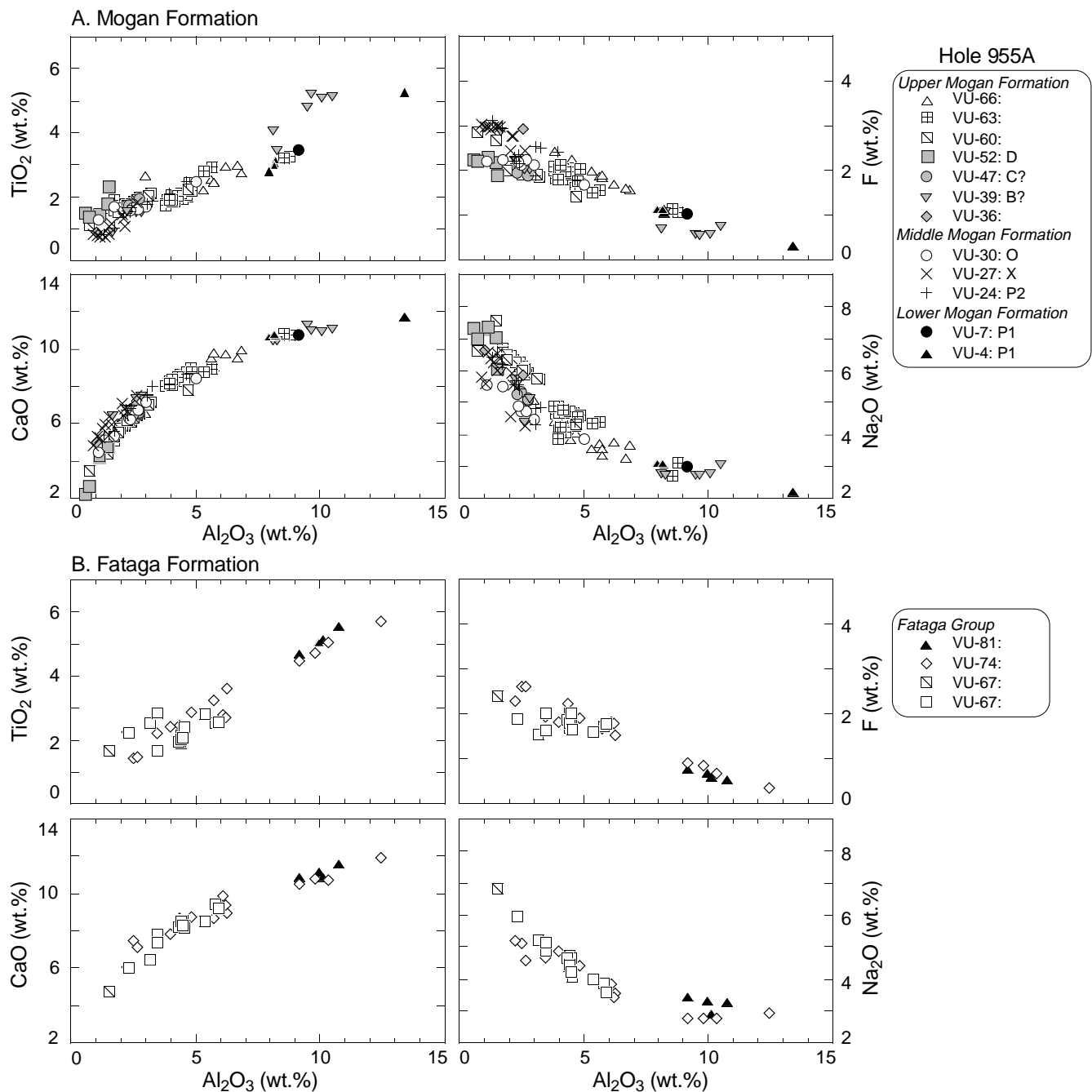


Figure 11. CaO, TiO₂, Na₂O, and F plotted vs. Al₂O₃ in amphibole phenocrysts and xenocrysts from Hole 955A for the (A) Mogán Formation and (B) Fataga Formation. Sample numbers include VU-81 (Sample 157-955A-55X-3, 0–7 cm), VU-74 (Sample 157-955A-54X-CC, 10–14 cm), VU-67-2 (Sample 157-955A-55X-4, 8–13 cm), VU-67-1 (Sample 157-955A-55X-4, 19–25 cm), VU-66 (Sample 157-955A-55X-4, 19–25 cm), VU-63 (Sample 157-955A-56X-1, 126–131 cm), VU-60 (Sample 157-955A-56X-3, 16–25 cm), VU-52 (Sample 157-955A-57X-2, 104–110 cm), VU-47 (Sample 157-955A-57X-3, 90–94 cm), VU-39 (Sample 157-955A-58X-1, 16–17 cm), VU-36 (Sample 157-955A-58X-1, 86–90 cm), VU-30 (Sample 157-955A-58X-4, 71–76 cm), VU-27 (Sample 157-955A-58X-5, 72–78 cm), VU-24 (Sample 157-955A-59X-2, 44–46 cm), VU-7 (Sample 157-955A-60X-2, 140–144 cm), and VU-4 (Sample 157-955A-60X-3, 55–61 cm).

the volcaniclastic layer equivalent to ignimbrite X in all three holes. Titanite also occurs, in lesser amounts, in several ignimbrites and lava flows of the Fataga Group. Similarly, it occurs sporadically in some volcaniclastic layers of the Fataga interval, but we have not yet attempted unit-specific correlations. More detailed analysis of trace-element concentrations, which has proved stratigraphically useful in titanite-bearing ash layers from Tenerife (Rodehorst et al., Chap. 18,

this volume), is being extended to titanite from Gran Canaria (M. Sumita, unpubl. data).

Fe/Ti Oxides

The ubiquitous Fe/Ti oxides have not yet been analyzed in many samples and it is uncertain if their compositions will be of stratigraphic importance.

Table 3. Representative EMP analyses of amphiboles from Holes 953C, 955A, and 956B.

Hole, core, section:	953C-69R-4	953C-69R-2	953C-68R-4	953C-67R-4	953C-67R-4	953C-66R-4	953C-65R-2	953C-64R-3	953C-60R-3	953C-58R-2
Interval (cm):	22-29	75-81	56-60	53-59	53-59	16-22	94-98	72-75	0-6	76-80
Depth (mbsf):	835.58	833.74	826.07	816.49	816.49	805.03	794.49	786.14	747.42	727.43
Tephra unit:	U-12a	U-12b	U-15	U-20	U-20	U-29	U-35	U-36	U-42	U-50
Sample no.:	AMP-1	AMP-1	AMP-1	AMP-2	AMP-6	AMP-5	AMP-4	AMP-6	AMP-8	AMP-5
Number of analyses:	2	2	1	1	2	2	2	1	1	2
(wt%)										
SiO ₂	39.38	38.36	49.64	50.58	47.34	39.02	52.79	52.65	51.40	49.87
TiO ₂	5.60	5.70	1.76	1.21	2.82	5.45	1.65	1.56	1.84	2.40
Al ₂ O ₃	13.42	14.08	3.25	1.43	4.47	12.72	1.27	1.02	1.14	3.80
FeO*	10.84	10.96	13.05	14.15	9.66	12.64	11.20	13.27	14.90	9.91
MnO	0.17	0.09	1.15	1.78	1.03	0.19	0.99	0.95	0.91	0.99
MgO	12.99	12.53	15.50	13.71	16.59	11.90	16.12	15.24	13.57	16.88
CaO	12.20	12.40	7.66	5.43	8.13	11.83	4.25	3.12	2.87	7.32
Na ₂ O	2.60	2.65	4.54	6.18	4.60	2.95	7.11	7.95	8.03	5.02
K ₂ O	0.82	1.05	0.79	1.02	0.76	1.06	0.92	0.98	1.16	1.04
P ₂ O ₅	0.03	0.07	0.10	0.00	0.07	0.14	0.00	0.03	0.04	0.02
BaO	0.173	0.065	0.065	0.078	0.057	0.160	0.000	0.000	0.000	0.100
F	0.246	0.393	2.028	2.899	1.635	0.264	2.256	2.350	2.439	1.762
Cl	0.013	0.021	0.000	0.000	0.021	0.023	0.008	0.003	0.006	0.011
Cr ₂ O ₃	0.01	0.02	0.02	0.05	0.02	0.05	0.00	0.05	0.01	0.04
NiO	0.00	0.03	0.00	0.00	0.03	0.04	0.01	0.00	0.00	0.01
Total:	98.47	98.43	99.56	98.51	97.23	8.44	98.57	99.16	98.30	99.18

Table 3 (continued).

Hole, core, section:	955A-60X-3	955A-60X-3	955A-59X-2	955A-58X-5	955A-58X-1	955A-58X-1	955A-57X-2	955A-56X-1	955A-56X-1	955A-53X-3
Interval (cm):	55-61	55-61	44-46	72-78	16-17	16-17	104-110	126-131	126-131	0-7
Depth (mbsf):	564.45	564.45	553.14	548.32	541.76	541.76	534.54	523.66	523.66	496.80
Tephra unit:	U-4	U-4	U-24	U-27	U-39	U-39	U-52	U-63	U-63	U-81
Sample no.:	AMP-3	AMP-10	AMP-1	AMP-4	AMP-1	AMP-15	AMP-2	AMP-4	AMP-10	AMP-2
Number of analyses:	2	2	2	2	1	2	1	2	2	2
(wt%)										
SiO ₂	45.18	38.69	49.73	49.80	51.47	40.52	50.26	48.46	44.83	42.34
TiO ₂	2.78	5.22	1.85	1.07	1.53	5.07	1.45	2.80	3.27	4.66
Al ₂ O ₃	7.97	13.41	3.27	1.52	2.27	10.09	1.16	5.35	8.74	9.18
FeO*	10.69	10.34	9.18	15.05	10.55	10.20	13.04	9.63	10.47	10.34
MnO	1.01	0.14	1.07	2.05	1.45	0.31	1.25	0.98	0.74	0.62
MgO	15.82	12.77	17.05	12.82	16.04	13.30	14.42	17.13	15.53	14.26
CaO	10.61	11.64	8.03	5.43	6.73	10.87	4.16	8.79	10.77	10.82
Na ₂ O	3.08	2.15	4.84	6.54	5.70	2.73	7.26	4.36	3.12	3.41
K ₂ O	0.60	1.03	0.79	1.06	0.76	0.76	0.87	0.73	0.69	0.96
P ₂ O ₅	0.06	0.05	0.02	0.00	0.01	0.06	0.00	0.07	0.05	0.06
BaO	0.019	0.112	0.032	0.059	0.075	0.107	0.093	0.046	0.070	0.137
F	1.113	0.303	2.515	3.016	2.198	0.553	2.272	1.507	1.054	0.735
Cl	0.022	0.010	0.015	0.017	0.010	0.011	0.020	0.010	0.029	0.031
Cr ₂ O ₃	0.03	0.00	0.00	0.01	0.01	0.03	0.02	0.01	0.00	0.02
NiO	0.02	0.03	0.01	0.03	0.05	0.04	0.07	0.01	0.01	0.00
Total:	99.00	95.90	98.41	98.46	98.85	94.65	96.34	99.88	99.37	97.57

Table 3 (continued).

Hole, core, section:	956B-43R-2	956B-43R-2	956B-41R-1	956B-41R-1	956B-40R-2	956B-39R-2	956B-39R-1	956B-33R-3
Interval(cm):	85-89	8-11	0.9	0.9	26-33	114-118	90-98	112-118
Depth(mbsf):	563.45	562.68	541.90	541.90	534.10	525.00	523.50	468.48
Tephra unit:	U-7a	U-10	U-31a			U-36	U-47	U-54
Sample no.:	AMP-5	AMP-3	AMP-6	AMP-14	AMP-9	AMP-4	AMP-1	AMP-2
Number of analyses:	2	2	2	2	2	2	2	2
(wt%)								
SiO ₂	45.66	44.96	43.37	51.51	52.99	42.32	47.16	48.94
TiO ₂	1.87	2.86	3.41	1.20	1.45	3.79	2.57	2.93
Al ₂ O ₃	8.07	8.01	8.75	2.01	1.06	14.15	6.03	4.16
FeO*	9.68	10.58	10.50	12.10	13.46	13.05	10.10	8.99
MnO	0.20	1.05	0.60	1.66	1.36	0.17	1.02	0.67
MgO	17.71	16.41	15.53	15.36	15.17	6.18	16.36	17.21
CaO	9.98	10.43	10.69	6.24	3.76	12.57	9.51	7.76
Na ₂ O	4.13	3.06	3.00	5.14	7.51	4.42	3.95	4.73
K ₂ O	0.74	0.65	0.76	1.01	1.05	1.28	0.71	0.87
P ₂ O ₅	0.06	0.12	0.12	0.03	0.02	0.97	0.03	0.08
BaO	0.075	0.014	0.049	0.055	0.024	0.066	0.046	0.040
F	0.204	1.160	1.021	2.935	2.222	0.183	1.352	1.656
Cl	0.007	0.057	0.041	0.005	0.014	0.038	0.007	0.014
Cr ₂ O ₃	0.01	0.03	0.01	0.03	0.03	0.05	0.01	0.00
NiO	0.06	0.02	0.02	0.03	0.01	0.05	0.02	0.00
Total	98.44	99.40	97.87	99.29	100.13	99.30	98.88	98.07

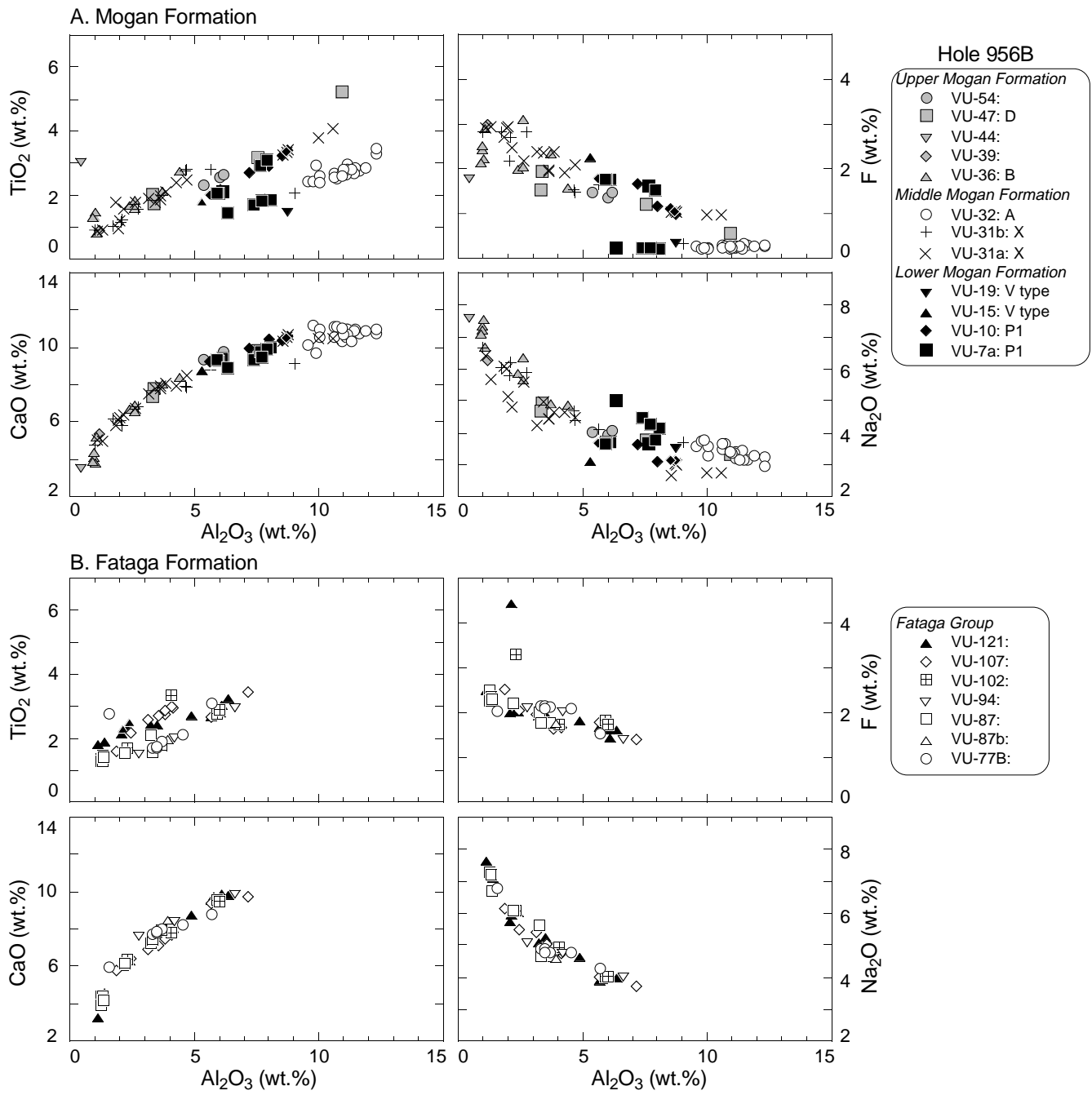


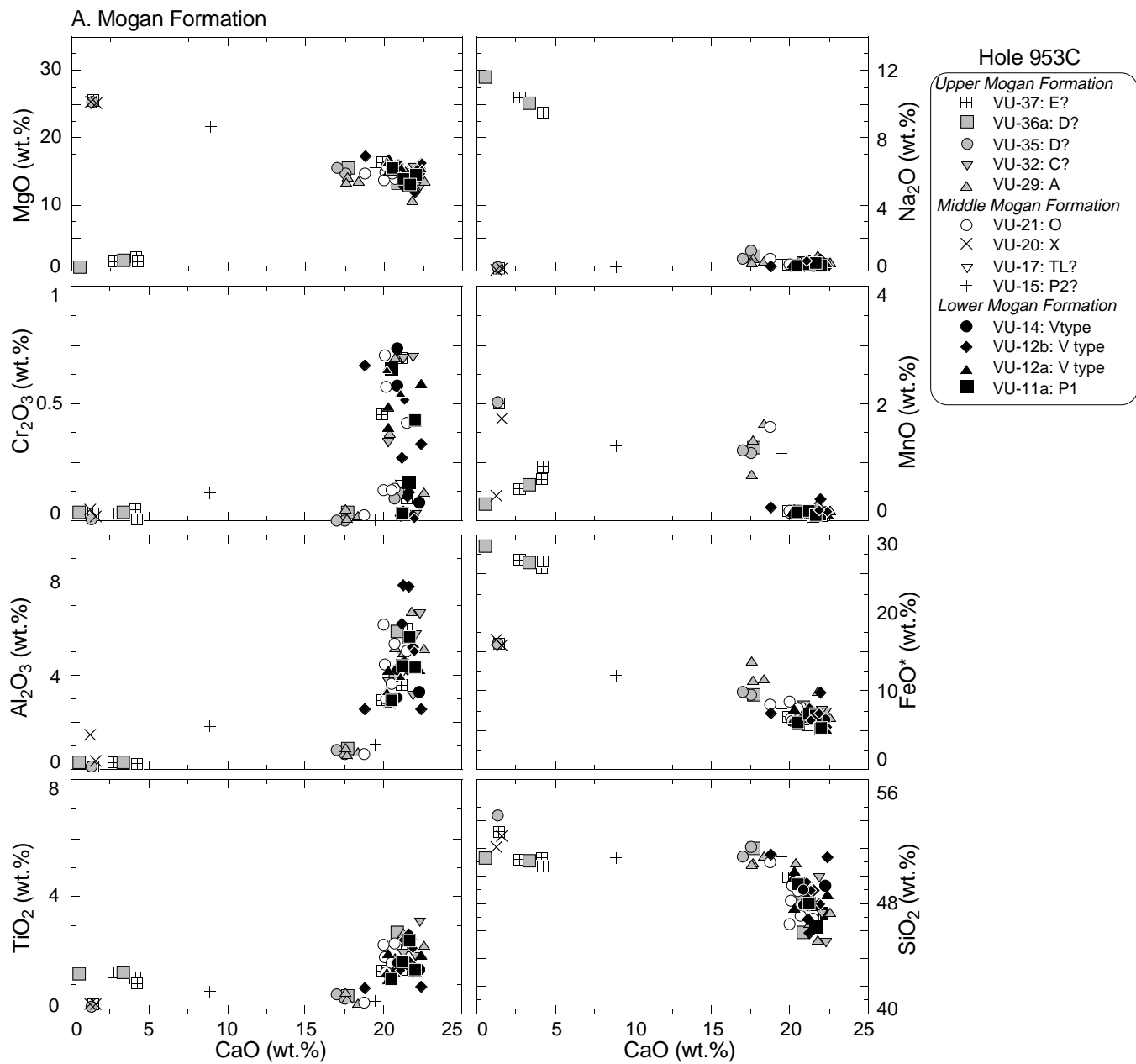
Figure 12. CaO, TiO₂, Na₂O, and F vs. Al₂O₃ in amphibole phenocrysts and xenocrysts from Hole 956B for the (A) Mogán Formation and (B) Fataga Formation. For sample numbers see Figure 9.

Chevkinite

The rare and small accessory phase chevkinite, characterized by very strong pleochroism, occurs as a common accessory phase within amphibole in ignimbrites X and A, less commonly in O, and extremely rarely in P1. In tuffs correlated with ignimbrite X it also occurs in rare large phenocrysts (Pl. 2, Fig. 2). Both chevkinite and zircon have been very useful in correlating specific volcaniclastic layers to their correlative subaerial unit.

Zircon

Zircon is a characteristic accessory phase in all peraluminous ignimbrite units and fallout tuffs of the LMF. It is typically intergrown with amphibole and magnetite in ignimbrite P1 and with magnetite in the other units. Zircon crystals do not occur in the more evolved, peralkaline units most likely because it is more soluble in peralkaline magmas. We have found zircon in most volcaniclastic units corresponding to Lower Mogán ignimbrites.

Figure 13. A. TiO_2 , Al_2O_3 , Cr_2O_3 , MgO , SiO_2 , FeO , MnO , and Na_2O vs. CaO in pyroxenes from Hole 953C for the Mogán Formation.

CHEMICAL COMPOSITION OF FELSIC GLASS SHARDS AND BULK VOLCANICLASTIC ROCKS AND COMPARISON WITH IGNIMBRITES

Ignimbrites

Chemical analyses of the subaerial ignimbrites (Fig. 16) are mainly of whole rocks, although some individual fiamme have been analyzed. These rocks contain variable amounts of phenocrysts, are commonly comprised of two or more magmatic components, and are crystallized (devitrified at high and low temperature), or, in the case of vitrophyres, diagenetically altered. Moreover, nearly all Gran Canaria ignimbrite cooling units are strongly compositionally zoned, with the most evolved compositions occurring generally at the base of a cooling unit.

Bulk Composition of Volcaniclastic Sediments

Forty bulk-rock samples, mainly vitric tuffs with <10 vol% other clasts, chiefly foraminifers and nannofossils, were selected from thicker volcaniclastic units for bulk XRF analysis of major and trace elements. We did not separate xenoclasts (e.g., bioclasts and basaltic lithoclasts) from the vitroclasts, because we have already analyzed volcanic glass and major phenocryst minerals in the same samples. We have also reanalyzed the powders of 40 whole-rock samples prepared and analyzed aboard ship. We note that the agreement is excellent for nearly all major and trace elements. Both coarse (sand) and fine-grained (silty) sediments were analyzed. The samples include relatively pure vitric tuffs as well as sandstones composed of biogenic debris, volcanic rock clasts and single crystals. We subdivided the analyzed rocks into three simple categories: (1) vitric tuffs composed

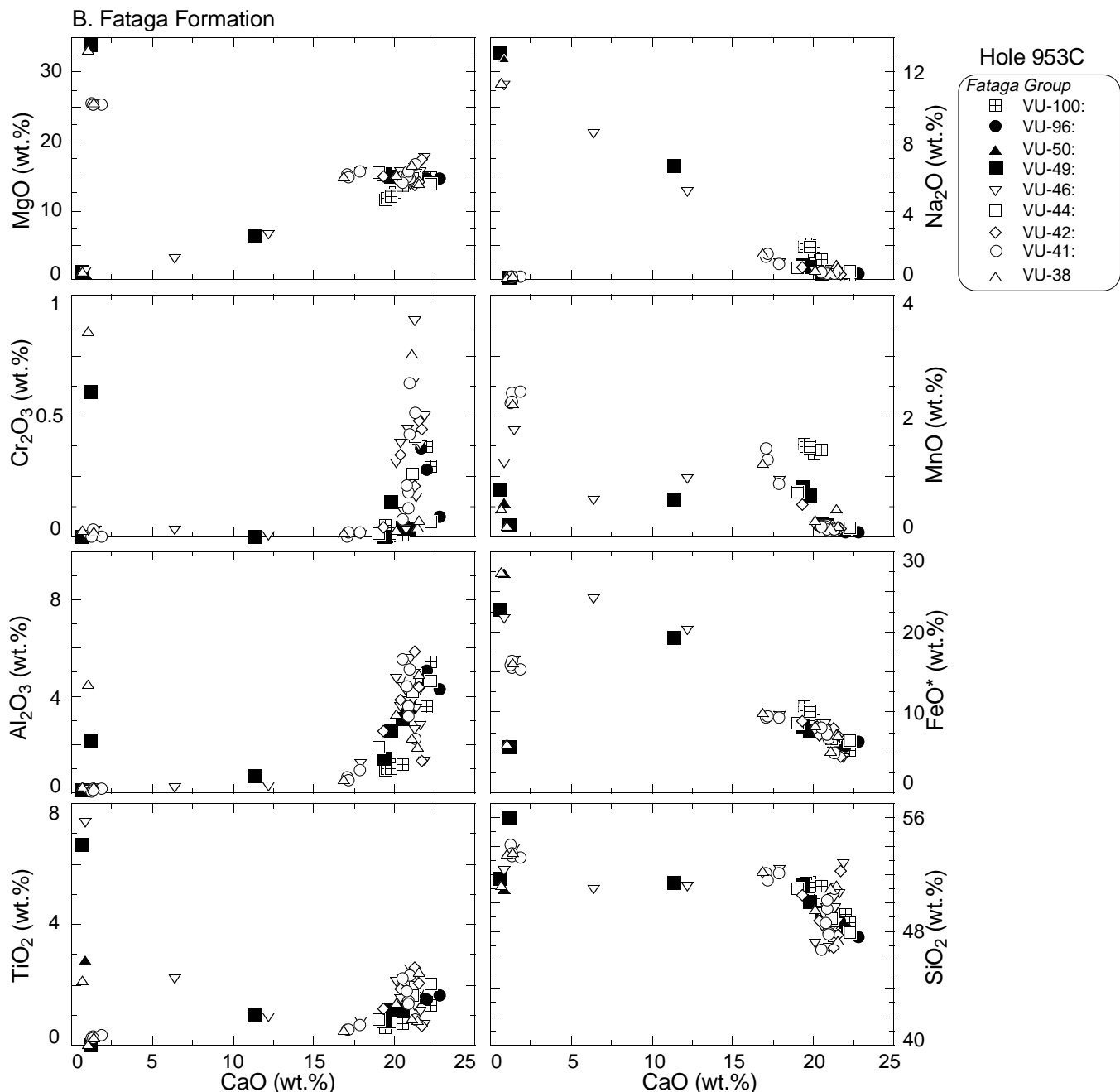


Figure 13 (continued). **B.** TiO_2 , Al_2O_3 , Cr_2O_3 , MgO , SiO_2 , FeO , MnO , and Na_2O vs. CaO in pyroxenes from Hole 953C for the Fataga Formation. Samples include VU-100 (Sample 157-953C-45R-2, 10–14 cm), and those mentioned in Figure 10.

dominantly (generally >90%) of bubble-wall and bubble-junction shards and, less commonly, nonvesicular blocky shards and pumice; (2) mixed rocks consisting of varying proportions of glass and crystals from the felsic volcanics, basaltic accidental clasts, mostly from the shield basalts, and sideromelane shards. These compositions are especially heterogeneous, because they commonly contain a large proportion of a very broad spectrum of skeletal debris, especially foraminifers, echinoderms, coralline algae, and shell fragments; (3) basaltic sandstones that consist dominantly of basaltic lithoclasts and underlie the felsic volcaniclastic sequence or occur in the lower part above tephra equivalent to ignimbrite P1. All analyses were recalculated carbonate-free to account for the abundance of CaCO_3 contrib-

uted from biogenic material. The results are given in Table 8 and shown in Figure 16.

EMP Analyses of Glass Shards and Vitrophyre Glasses

Glass shards were analyzed in 19 polished sections from Hole 953C, 19 from Hole 955A, and 16 from Hole 956B. On average, ~15 shards were analyzed in each section, resulting in more than 3000 analyses of glass shards. In some sections, we analyzed up to 25 shards and each analysis is the average of two to three points on one shard. On some of the large glass shards, we have run traverses with up to 10 analyses (Table 9). The compositions of fresh glass shards

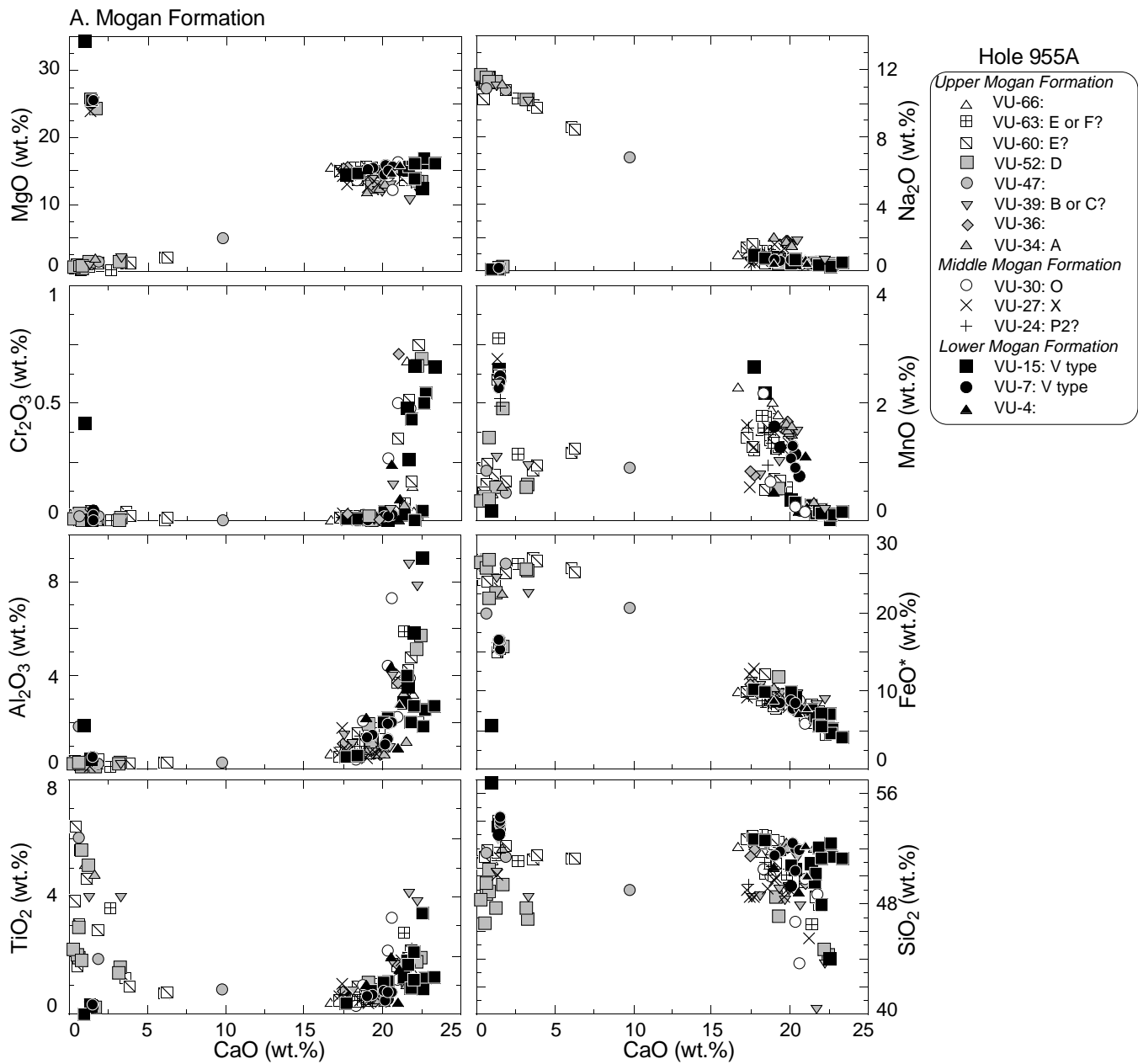


Figure 14. A. TiO_2 , Al_2O_3 , Cr_2O_3 , MgO , SiO_2 , FeO , MnO , and Na_2O vs. CaO in pyroxenes from Hole 955A for the Mogán Formation. For sample numbers see Figure 11.

were compared to those of the vitrophyres of 12 ignimbrites on Gran Canaria. Results of these analyses are shown in Table 10 and in Figures 17–19.

The following types of glass were analyzed: (1) fresh vitrophyric glasses from 12 ignimbrite cooling units; (2) colorless, glassy bubble-wall and bubble-junction shards; (3) brown glass that occurs commonly in compact, blocky, nonvesicular clasts derived from welded ignimbrite; (4) glass rims around feldspar crystals; and (5) glass inclusions in feldspars, amphiboles, and clinopyroxenes. Here, we will concentrate on the bulk of the analyses represented by groups 1, 2, 3, and 4. The difference in chemical composition between glass shards and melt inclusions in phenocrysts will be discussed elsewhere. The quality of the analyses, as expressed by the totals, varies significantly with glass composition, stratigraphy, and between holes.

At Hole 955A, glass shards were analyzed in 21 samples, from interval 157-955A-60R-2 (140–144 cm; 563.8 mbsl) through 53R-2 (0–7 cm; 496.8 mbsl). In this 60-m interval, relatively good glass analyses with totals between 95 and 99 wt% are found in each sample, and are thus regarded as the best data set. Most low totals (98–95 wt%) occur in VU-52 (Sample 157-955A-57X-2, 104–110 cm), which corresponds to the peralkaline glass of ignimbrite D. At both Holes 955A and 956B, many samples contained 10 or more shards with analytical totals exceeding 93 wt%, thus permitting reasonable conclusions to be drawn. In a few cases, totals as low as 90 wt% were included, provided the Na_2O concentrations were significantly higher than those of K_2O . In all samples from Hole 953C, totals >93 wt% are exceptional and indeed totals >91 wt% are rare. In about one-third of the samples, totals as low as 90 wt% and rarely as low as 89.5 wt%

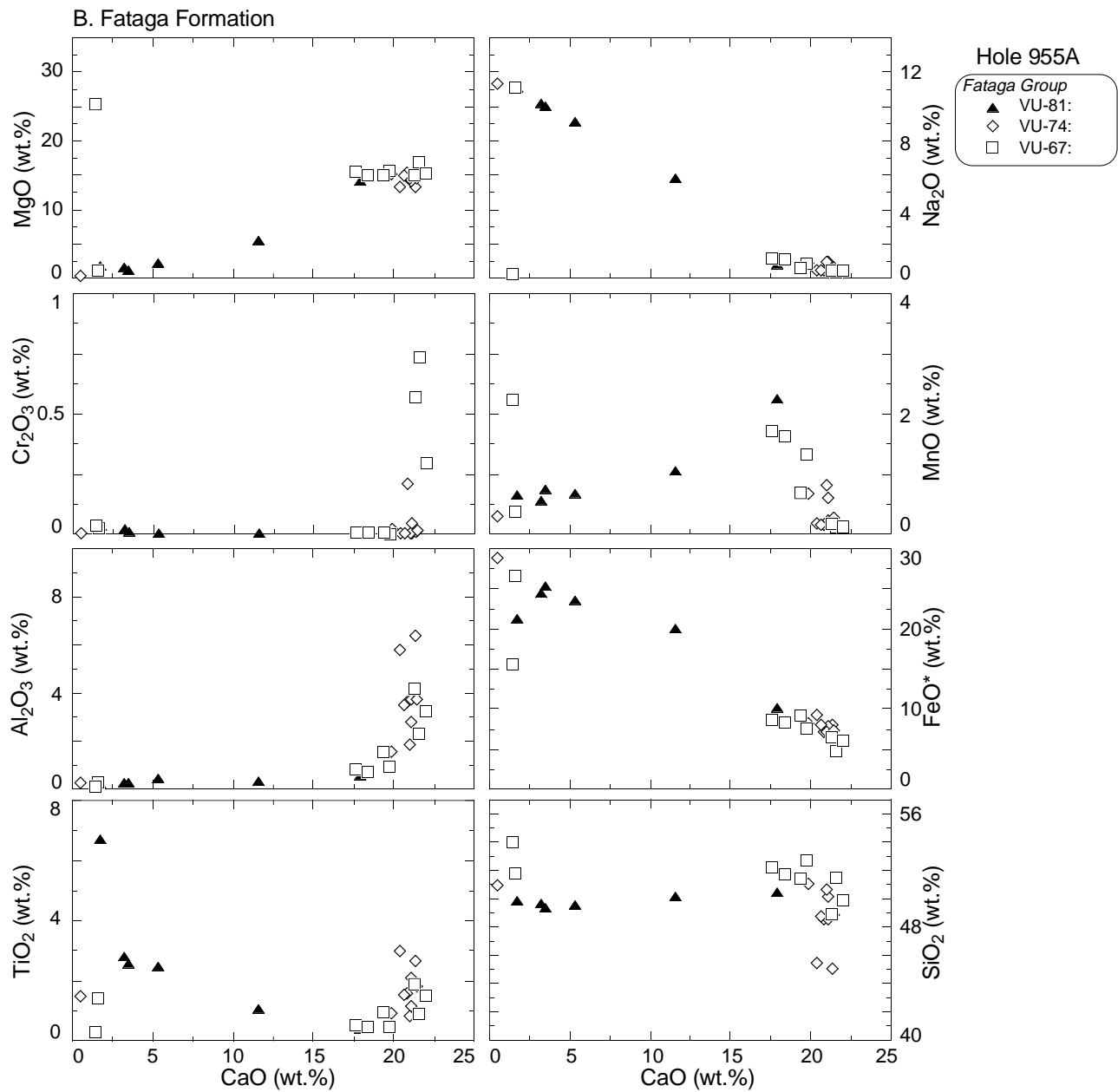


Figure 14 (continued). **B.** TiO_2 , Al_2O_3 , Cr_2O_3 , MgO , SiO_2 , FeO , MnO , and Na_2O vs. CaO in pyroxenes from Hole 955A for the Fataga Formation. For sample numbers see Figure 11.

were included to provide a significant number of glass analyses to identify the chemical stratigraphy of Hole 953C and to aid in determining the stratigraphic correlation of a volcaniclastic unit. In these analyses, the elements alumina, iron, and titanium turned out to be most stable. No analyses were selected with $\text{K}_2\text{O} > \text{Na}_2\text{O}$. Because of the strict criteria for selection, less than five compositions were chosen for half of the samples, and only one sample (VU-41) had >10 glass analyses whose analytical sums fell within the limits.

Glass shards from Hole 953C tend to be more altered, based on the low analytical totals. Glass was analyzed in 40 samples from this hole from VU-12a to VU-49. Throughout the 14 samples representing the Mogán and six samples representing the transitional group, totals are generally less than 92 wt%, except in the more alumina-rich glasses from VU-29 (Sample 157-953C-66R-3, 16–22 cm), which correlates to the trachytic ignimbrite A. Totals between 91 and 97

wt% are slightly more common in stratigraphically higher samples. The closer proximity of Hole 953C to the area of young subaerial and submarine volcanism in northeast Gran Canaria is considered the most important factor in causing more advanced alteration of the felsic glasses; unfortunately, no detailed temperature measurements were taken at Hole 953C.

CHEMICAL STRATIGRAPHY

Subaerial Deposits

The stratigraphic subdivisions of the Mogán Group into the LMF, MMF, and UMF were based on chemical and mineralogical differences and on major lithological changes (Figs. 3, 20). The volcanic rocks of the LMF are characterized by relatively high silica concen-

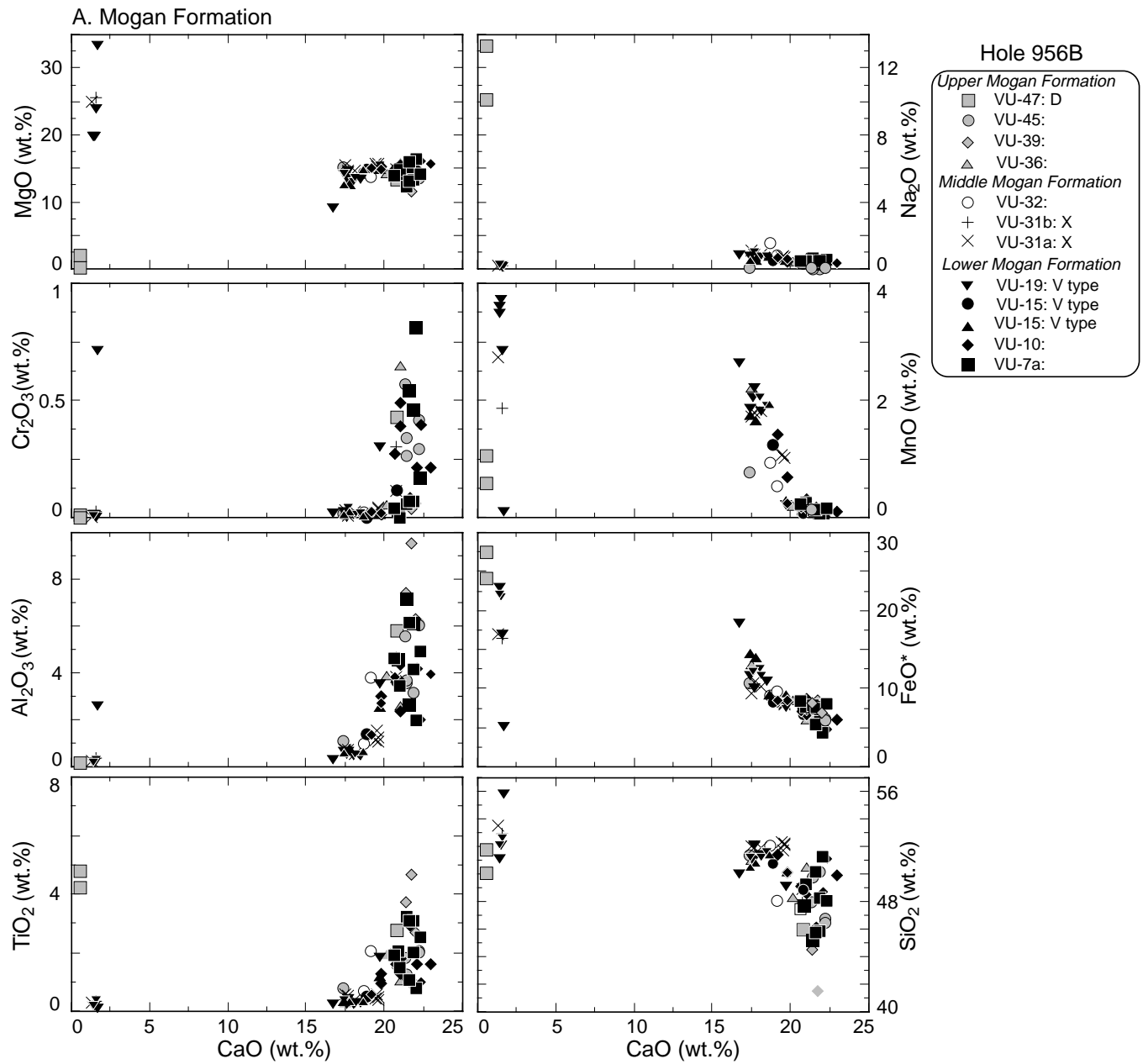


Figure 15. A. TiO_2 , Al_2O_3 , Cr_2O_3 , MgO , SiO_2 , FeO , MnO , and Na_2O vs. CaO in pyroxenes from Hole 956B for the Mogán Formation. For sample numbers see Figure 9.

trations (70–71 wt%) and Na/K ratios and low Fe and Ti concentrations. Incompatible trace element concentrations are relatively low. The LMF can be further subdivided into the basal composite rhyolite/basalt cooling Units P1 and the much smaller subsequent R, and the compositionally much more homogeneous cooling Units U, VL, and VI.

A very voluminous eruption of basalt (T4) covered at least the southern half of the island after the end of the MMF, terminating with the highly evolved ignimbrites X and O. The absence of basaltic activity before this time (~13.7 Ma) suggests that the likely basaltic parental magmas of the 10 cooling units of the LMF and MMF, remained trapped beneath the low-density magma lid, apart from basaltic magmas erupted in ignimbrites P1 and R and the spatially restricted lavas T3 (below VI) and T6 (below TL).

The gradually increasing differentiation of the felsic magmas was abruptly terminated by a major pulse of new more mafic magma that had moderately differentiated from primitive basaltic magma. The system then started a new cycle of increasingly differentiated magmas, beginning with trachytic ignimbrite A and culminating with ignimbrites D and E.

Most cooling units of the Middle and Upper Mogán Group are slightly to strongly peralkaline (comenditic and pantelleritic), trachytic to low-silica rhyolitic ignimbrites, whose chemical composition can largely be explained by crystal fractionation, chiefly by anorthoclase feldspar (Fig. 6), with additional processes having led to extreme trace-element concentrations in the magma reservoir cupolas. Rather constant Zr/Nb ratios of 5–7 suggest differentiation of the Mogán felsic rocks from similar basaltic parents (Fig. 16). Variations

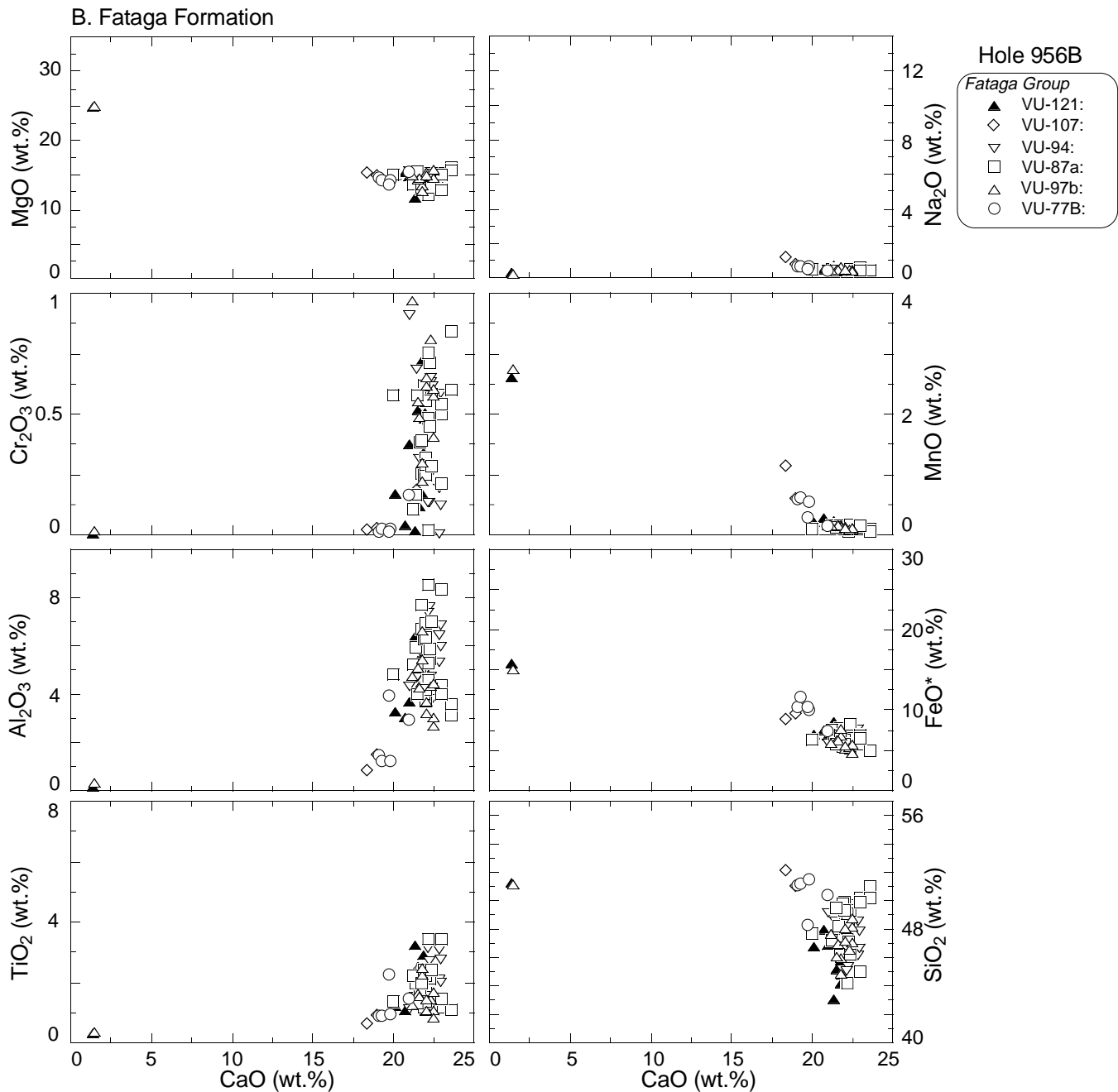


Figure 15 (continued). **B.** TiO_2 , Al_2O_3 , Cr_2O_3 , MgO , SiO_2 , FeO , MnO , and Na_2O vs. CaO in pyroxenes from Hole 956B for the Fataga Formation. For sample numbers see Figure 9.

in the differentiation processes generated a series of evolved magma batches, each with a distinctive composition.

Many of the cooling units show a wide compositional spectrum, resulting from mixing of several magma batches. The lower, compositionally most evolved flow units in a given cooling unit are usually crystal-poor, low-silica rhyolites, whereas the uppermost, more mafic, trachytic flow units may contain up to 15 vol% crystals. Dark, mafic (trachytic) fiamme, commonly with large, partially resorbed, plagioclase phenocrysts are common in ignimbrites P2, TL, X, O, A, B, D, E, and F.

Silica concentrations in the evolved, basal part of ignimbrites of the MMF and UMF are commonly between 69 and 70 wt%. In the Fa-

taga Formation, however, silica concentration generally does not exceed 62 wt% and may be as low as 59 wt%. Alumina concentrations are very diagnostic of the rocks in the Mogán Group. They are highest between 13–16 wt% in the rocks of the LMF, but are as low as 9 wt% in the most peralkaline pantellerite of ignimbrites C and D. The less peralkaline comendites have between 11 and 14 wt% alumina. Alumina is characteristically higher in the trachyphonolitic rocks of the Fataga Group where it always exceeds 15 wt% and can be as high as 19 wt%. Total Fe, as FeO^* , also shows characteristic changes from ~5 wt% in the rocks of the LMF to >7 wt% in the most peralkaline pantellerite such as ignimbrites C and D. In the trachytic rocks of the Fataga Group, however, FeO^* rarely exceeds 5.5 wt%. TiO_2 general-

Table 4. Representative EMP analyses of clinopyroxenes from Holes 953C, 955A, and 956B.

Hole, core, section:	953C-69R-4	953C-69R-2	953C-69R-2	953C-67R-2	953C-67R-1	953C-66R-3	953C-65R-5	953C-65R-5	953C-65R-2	953C-65R-2	953C-64R-3
Interval:	22-29	75-81	75-81	75-84	148-150	16-22	93-98	93-98	94-98	94-98	72-75
Depth (mbsf):	835.58	833.74	833.74	813.96	813.18	805.03	798.56	798.56	794.49	794.49	786.14
Volcaniclastic unit:	VU-12a	VU-12b	VU-12b	VU-21	VU-21	VU-29	VU-32	VU-32	VU-35	VU-35	VU-36
Sample number:	PX-7	PX-2	PX-9	PX-1	PX-4	PX-6	PX-1	PX-2	PX-3	PX-4	PX-3
Number of analyses:	2	2	2	2	2	2	3	3	1	2	2
(wt%)											
SiO ₂	49.77	51.26	48.96	48.20	47.08	51.38	49.80	47.18	52.14	48.62	52.00
TiO ₂	1.36	0.88	1.78	1.93	2.42	0.33	1.33	1.94	0.50	1.75	0.62
Al ₂ O ₃	3.28	2.52	4.24	4.50	5.37	0.74	3.09	5.73	0.68	3.95	0.91
Cr ₂ O ₃	0.64	0.32	0.10	0.71	0.14	0.02	0.69	0.02	0.00	0.09	0.03
FeO*	6.31	5.24	7.32	6.53	8.05	11.43	5.25	7.46	9.62	7.59	9.54
MnO	0.15	0.14	0.12	0.13	0.16	1.66	0.09	0.13	1.15	0.13	1.26
MgO	16.27	16.12	14.52	14.75	13.74	13.39	15.39	13.37	14.66	14.73	15.42
CaO	20.26	22.46	21.57	20.05	20.65	18.37	21.93	22.06	17.55	20.73	17.67
Na ₂ O	0.38	0.29	0.33	0.33	0.50	0.58	0.38	0.34	1.24	0.36	0.90
P ₂ O ₅	0.11	0.12	0.10	0.10	0.23	0.08	0.12	0.13	0.07	0.09	0.13
Total:	98.54	99.35	99.04	97.21	98.34	97.97	98.07	98.35	97.60	98.05	98.47
Si	1.853	1.891	1.828	1.856	1.775	1.967	1.865	1.778	1.977	1.832	1.953
Al ^{IV}	0.144	0.109	0.172	0.144	0.225	0.033	0.135	0.222	0.023	0.168	0.040
Al ^{VI}	0.000	0.000	0.015	0.060	0.014	0.000	0.001	0.033	0.007	0.008	0.000
Ti	0.038	0.024	0.050	0.000	0.069	0.010	0.037	0.055	0.014	0.050	0.018
Cr	0.019	0.009	0.003	0.022	0.004	0.001	0.020	0.001	0.000	0.003	0.001
Fe ³⁺	0.073	0.061	0.068	0.078	0.085	0.048	0.056	0.091	0.072	0.076	0.072
Fe ²⁺	0.124	0.101	0.161	0.132	0.169	0.317	0.109	0.144	0.233	0.163	0.227
Mn	0.005	0.004	0.004	0.004	0.005	0.054	0.003	0.004	0.037	0.004	0.040
Mg	0.903	0.886	0.808	0.846	0.770	0.765	0.859	0.751	0.829	0.827	0.862
Ca	0.808	0.888	0.863	0.827	0.836	0.755	0.880	0.891	0.713	0.837	0.712
Na	0.000	0.000	0.000	0.000	0.000	0.022	0.004	0.000	0.083	0.000	0.051
P	0.003	0.004	0.003	0.003	0.007	0.003	0.004	0.004	0.002	0.003	0.004
Total:	3.97	3.98	3.97	3.97	3.96	3.97	3.97	3.97	3.99	3.97	3.98
Mg#	82.13	84.57	77.95	80.10	75.21	67.69	83.93	76.16	73.09	77.57	74.21
Wo	40.57	43.89	43.23	36.18	42.74	38.76	44.13	42.84	36.05	42.27	36.29
En	50.31	49.43	45.50	54.82	44.65	42.24	47.98	45.87	47.07	46.25	47.88
Fs	9.13	6.69	11.28	9.00	12.60	19.00	7.88	11.29	16.88	11.48	15.83

Table 4 (continued).

Hole, core, section:	953C-64R-1	953C-64R-1	953C-63R-1	953C-63R-1	953C-61R-3	953C-61R-3	953C-61R-3	953C-61R-3	953C-60R-3	953C-60R-3	953C-59R-6
Interval:	62-74	62-74	40-48	40-48	109-114	109-114	109-114	109-114	0-6	0-6	105-112
Depth (mbsf):	783.42	783.42	773.50	773.50	758.06	758.06	758.06	758.06	747.42	747.42	742.97
Volcaniclastic unit:	VU-37	VU-37	VU-38	VU-38	VU-41	VU-41	VU-41	VU-41	VU-42	VU-42	VU-44
Sample number:	PX-2	PX-3	PX-5	PX-7	PX-2	PX-5	PX-7	PX-9	PX-5	PX-9	PX-1
Number of analyses:	2	2	2	2	1	3	2	1	1	1	2
(wt%)											
SiO ₂	47.14	49.50	49.50	51.04	50.21	47.85	46.73	51.04	46.85	50.54	47.76
TiO ₂	2.31	1.52	1.36	0.87	1.35	2.33	2.23	0.87	2.53	1.19	1.92
Al ₂ O ₃	6.02	3.59	3.25	2.26	3.21	5.13	5.52	2.22	5.84	2.53	4.90
Cr ₂ O ₃	0.09	0.70	0.02	0.75	0.12	0.63	0.07	0.51	0.21	0.04	0.41
FeO*	6.92	5.58	8.27	5.20	7.17	6.71	8.09	4.92	7.92	8.89	6.89
MnO	0.08	0.11	0.25	0.14	0.13	0.11	0.16	0.12	0.14	0.53	0.14
MgO	13.93	15.63	15.03	16.59	15.67	14.63	14.00	16.65	13.60	14.84	14.84
Ca	21.52	21.13	20.18	21.14	20.90	20.96	20.49	21.32	21.30	19.37	21.30
Na ₂ O	0.46	0.44	0.54	0.36	0.33	0.44	0.42	0.32	0.47	0.64	0.40
P ₂ O ₅	0.22	0.24	0.25	0.18	0.19	0.25	0.25	0.19	0.19	0.15	0.12
Total:	98.69	98.44	98.65	98.60	99.26	98.97	97.96	98.22	99.03	98.70	98.68
Si	1.764	1.846	1.852	1.893	1.860	1.784	1.766	1.897	1.753	1.893	1.784
Al ^{IV}	0.236	0.154	0.143	0.099	0.140	0.216	0.234	0.097	0.247	0.107	0.216
Al ^{VI}	0.030	0.004	0.000	0.000	0.000	0.009	0.012	0.000	0.011	0.005	0.000
Ti	0.065	0.043	0.038	0.024	0.038	0.065	0.063	0.024	0.071	0.034	0.054
Cr	0.003	0.021	0.001	0.022	0.004	0.019	0.002	0.015	0.006	0.001	0.012
Fe ³⁺	0.086	0.053	0.092	0.047	0.069	0.072	0.100	0.045	0.104	0.066	0.113
Fe ²⁺	0.131	0.121	0.167	0.115	0.153	0.138	0.156	0.108	0.144	0.121	0.102
Mn	0.003	0.003	0.008	0.004	0.004	0.003	0.005	0.004	0.004	0.017	0.004
Mg	0.775	0.867	0.836	0.918	0.867	0.811	0.789	0.925	0.759	0.826	0.826
Ca	0.862	0.843	0.810	0.839	0.829	0.839	0.830	0.848	0.854	0.779	0.853
Na	0.000	0.006	0.000	0.005	0.000	0.007	0.000	0.000	0.000	0.019	0.000
P	0.007	0.008	0.008	0.008	0.006	0.006	0.008	0.008	0.006	0.005	0.004
Total:	3.96	3.97	3.95	3.97	3.97	3.97	3.96	3.97	3.96	3.96	3.97
Mg#	78.17	83.29	76.37	85.05	79.60	79.50	75.52	85.81	75.37	74.79	79.33
Wo	42.77	42.41	41.68	41.87	41.44	42.14	40.82	42.71	42.69	40.22	41.45
En	46.66	49.17	46.85	50.41	48.59	47.15	47.46	50.34	45.53	45.83	49.75
Fs	10.57	8.42	11.47	7.72	9.96	10.71	11.71	6.95	11.79	13.95	8.79

Table 4 (continued).

Hole, core, section:	953C-59R-6	953C-59R-5	953C-59R-5	953C-58R-4	953C-47R-2	953C-45R-2	953C-45R-2	955A-60X-3	955A-60X-3	955A-60X-2	955A-59X-6
Interval:	105-112	104-107	104-107	41-45	141-146	10-14	10-14	55-61	55-61	140-144	61-67
Depth (mbsf):	742.97	741.57	741.57	730.02	621.51	602.00	602.00	564.45	564.45	563.80	559.31
Volcaniclastic unit:	VU-44	VU-46	VU-46	VU-49	VU-96	VU-100	VU-100	VU-4	VU-4	VU-7	VU-15
Sample number:	PX-2	X-11	PX-4	PX-8	PX-3	PX-4	PX-7	PX-1	PX-4	PX-1	PX-3
Number of analyses:	2	1	2	2	2	2	1	2	2	2	2
(wt%)											
SiO ₂	51.04	52.36	50.31	48.67	47.61	49.21	51.19	48.80	52.25	52.02	49.59
TiO ₂	0.87	0.77	1.26	1.73	1.66	1.42	0.58	1.96	0.36	0.53	1.84
Al ₂ O ₃	1.89	1.16	2.58	3.51	4.28	3.61	0.94	4.37	0.90	1.30	4.02
Cr ₂ O ₃	0.01	0.01	0.89	0.03	0.08	0.37	0.05	0.24	0.00	0.02	0.48
FeO*	8.73	9.57	5.13	7.82	6.29	6.56	10.74	7.02	7.65	7.75	7.04
MnO	0.72	0.92	0.11	0.18	0.07	0.14	1.54	0.15	1.08	1.13	0.14
MgO	15.44	15.49	16.13	14.73	14.58	14.85	11.55	14.74	15.76	15.70	14.77
CaO	19.04	17.92	21.35	20.85	22.78	22.03	19.46	20.56	21.04	20.37	21.59
Na ₂ O	0.66	0.91	0.33	0.41	0.30	0.30	1.90	0.40	0.66	0.54	0.46
P ₂ O ₅	0.11	0.15	0.17	0.11	0.10	0.12	0.09	0.11	0.09	0.08	0.07
Total:	98.52	99.25	98.26	98.05	97.75	98.59	98.04	98.34	99.78	99.44	100.00
Si	1.914	1.950	1.878	1.836	1.795	1.841	1.951	1.832	1.929	1.929	1.832
Al ^{IV}	0.084	0.050	0.113	0.156	0.190	0.159	0.042	0.168	0.039	0.057	0.168
Al ^{VI}	0.000	0.001	0.000	0.000	0.000	0.001	0.000	0.026	0.000	0.000	0.007
Ti	0.025	0.022	0.035	0.049	0.047	0.040	0.017	0.055	0.010	0.015	0.051
Cr	0.000	0.000	0.026	0.001	0.002	0.011	0.002	0.007	0.000	0.001	0.014
Fe ³⁺	0.077	0.058	0.042	0.093	0.136	0.078	0.152	0.042	0.123	0.087	0.071
Fe ²⁺	0.197	0.240	0.119	0.154	0.062	0.127	0.190	0.178	0.113	0.153	0.147
Mn	0.023	0.029	0.003	0.006	0.002	0.004	0.050	0.005	0.034	0.035	0.004
Mg	0.863	0.860	0.896	0.828	0.819	0.828	0.656	0.825	0.867	0.868	0.813
Ca	0.765	0.714	0.852	0.843	0.920	0.883	0.795	0.827	0.832	0.809	0.855
Na	0.014	0.052	0.023	0.000	0.000	0.000	0.097	0.029	0.019	0.009	0.012
P	0.003	0.005	0.005	0.004	0.003	0.004	0.003	0.003	0.003	0.003	0.002
Total:	3.96	3.98	3.99	3.97	3.98	3.98	3.95	4.00	3.97	3.97	3.98
Mg#	75.92	74.27	84.83	77.05	80.51	80.14	65.71	78.91	78.59	78.31	78.90
Wo	39.93	36.38	41.32	43.37	44.60	43.37	41.82	41.00	43.03	41.93	43.09
En	47.00	47.81	49.82	45.08	47.88	47.59	39.96	46.41	45.96	46.74	45.84
Fs	13.06	15.81	8.86	11.55	7.52	9.04	18.22	12.59	11.00	11.33	11.07

Table 4 (continued).

Hole, core, section:	955A-59X-6	955A-59X-2	955A-58X-5	955A-58X-4	955A-58X-4	955A-58X-1	955A-58X-1	955A-58X-1	955A-58X-1	955A-58X-1	955A-57X-2
Interval:	61-67	44-46	72-78	71-76	71-76	119-125	86-90	86-90	16-17	86-90	104-110
Depth (mbsf):	559.31	553.14	548.32	546.81	546.81	542.79	542.46	542.46	541.76	542.46	534.54
Volcaniclastic unit:	VU-15	VU-24	VU-27	VU-30	VU-30	VU-34	VU-36	VU-36	VU-39	VU-39	VU-52
Sample number:	PX-9	PX-5	PX-17	PX-3	PX-4	PX-1	PX-1	PX-3	PX-20	PX-22	PX-6
Number of analyses:	2	2	2	2	2	2	2	2	2	2	2
(wt%)											
SiO ₂	52.70	51.29	48.49	50.05	48.69	52.02	51.91	49.45	47.80	43.61	48.50
TiO ₂	0.38	0.58	1.02	0.99	1.64	1.01	0.71	1.65	1.76	3.82	1.09
Al ₂ O ₃	0.54	1.00	1.75	2.09	3.89	1.16	0.96	3.65	3.98	7.80	1.96
Cr ₂ O ₃	0.01	0.02	0.03	0.03	0.48	0.06	0.02	0.71	0.15	0.00	0.02
FeO*	10.33	8.31	12.19	8.60	5.98	6.86	10.72	6.03	7.69	8.76	8.78
MnO	2.61	1.22	0.58	0.66	0.11	0.30	0.75	0.16	0.17	0.16	0.55
MgO	14.40	15.45	14.17	14.91	15.02	15.42	15.37	15.60	14.23	11.69	14.72
CaO	17.72	18.86	17.45	18.72	21.72	21.57	17.74	21.02	20.71	22.27	19.14
Na ₂ O	0.88	0.82	0.52	0.76	0.40	0.58	0.58	0.42	0.44	0.61	0.74
P ₂ O ₅	0.07	0.12	0.06	0.13	0.16	0.12	0.10	0.13	0.09	0.12	0.08
Total:	99.63	97.66	96.26	96.94	98.08	99.10	98.86	98.82	97.02	98.82	95.58
Si	1.975	1.937	1.884	1.908	1.826	1.935	1.953	1.840	1.822	1.650	1.876
Al ^{IV}	0.024	0.045	0.080	0.092	0.172	0.051	0.043	0.160	0.178	0.348	0.089
Al ^{VI}	0.000	0.000	0.000	0.002	0.000	0.000	0.000	0.001	0.000	0.000	0.000
Ti	0.011	0.016	0.030	0.028	0.046	0.028	0.020	0.046	0.050	0.109	0.032
Cr	0.000	0.001	0.001	0.001	0.014	0.002	0.001	0.021	0.005	0.000	0.001
Fe ³⁺	0.063	0.096	0.124	0.075	0.082	0.053	0.044	0.064	0.097	0.169	0.143
Fe ²⁺	0.261	0.167	0.272	0.199	0.106	0.161	0.294	0.124	0.148	0.108	0.141
Mn	0.083	0.039	0.019	0.021	0.003	0.009	0.024	0.005	0.005	0.005	0.018
Mg	0.804	0.870	0.821	0.847	0.840	0.855	0.862	0.865	0.808	0.659	0.849
Ca	0.711	0.763	0.727	0.765	0.873	0.859	0.715	0.838	0.846	0.903	0.793
Na	0.047	0.040	0.026	0.025	0.000	0.042	0.040	0.005	0.000	0.000	0.033
P	0.002	0.004	0.002	0.004	0.005	0.004	0.003	0.004	0.003	0.004	0.003
Total:	3.98	3.98	3.99	3.97	3.97	4.00	4.00	3.97	3.96	3.95	3.98
Mg#	71.30	76.82	67.45	75.55	81.74	80.03	71.87	82.18	76.73	70.40	74.93
Wo	36.38	39.14	36.92	39.76	43.64	42.88	35.85	42.12	42.78	45.96	40.77
En	46.03	47.60	43.00	46.82	48.13	45.19	46.20	48.72	46.10	41.26	45.29
Fs	17.59	13.26	20.08	13.42	8.23	11.92	17.95	9.16	11.12	12.78	13.94

Table 4 (continued).

Hole, core, section:	955A-56X-3	955A-56X-3	955A-56X-3	955A-56X-1	955A-56X-1	955A-56X-1	955A-55X-4	955A-55X-4	955A-54X-CC	956B-43R-2	956B-43R-2
Interval:	16-25	16-25	16-25	126-131	14-17	14-17	19-25	19-25	10-14	85-89	85-89
Depth (mbsf):	525.59	525.59	525.59	523.66	522.54	522.54	517.59	517.59	503.50	563.45	563.45
Volcaniclastic unit:	VU-60	VU-60	VU-60	VU-63	VU-66	VU-66	VU-67	VU-67	VU-74	VU-7a	VU-67
Sample number:	PX-14	PX-17	PX-24	PX-1	PX-14	PX-15	PX-2	PX-5	PX-13	PX-1	PX-7
Number of analyses:	2	2	2	2	2	2	2	2	2	2	1
(wt%)											
SiO ₂	52.33	51.92	48.50	52.46	47.74	51.83	52.67	51.52	48.80	51.27	47.68
TiO ₂	0.74	0.81	1.95	0.50	2.25	0.38	0.47	0.89	1.79	0.83	2.06
Al ₂ O ₃	1.29	1.31	4.25	0.87	4.71	0.59	0.93	2.32	3.73	2.03	4.60
Cr ₂ O ₃	0.00	0.01	0.51	0.02	0.14	0.00	0.00	0.74	0.01	0.81	0.03
FeO*	8.79	9.26	6.58	8.78	6.96	9.91	7.56	4.85	7.27	4.51	8.08
MnO	0.70	0.69	0.14	1.58	0.11	1.78	1.31	0.13	0.25	0.10	0.23
MgO	15.54	14.82	14.82	15.38	14.20	14.43	15.62	16.81	14.41	16.48	14.30
CaO	19.04	19.34	21.69	18.33	21.93	19.26	19.69	21.61	21.51	22.04	20.86
Na ₂ O	0.85	0.76	0.42	1.07	0.44	0.94	0.84	0.36	0.59	0.34	0.45
P ₂ O ₅	0.12	0.14	0.09	0.10	0.19	0.11	0.08	0.12	0.20	0.14	0.19
Total:	99.42	99.05	98.95	99.10	98.66	99.23	99.18	99.35	98.55	98.52	98.48
Si	1.944	1.944	1.808	1.954	1.789	1.943	1.957	1.894	1.829	1.903	1.793
Al ^{IV}	0.056	0.056	0.187	0.038	0.208	0.026	0.041	0.101	0.165	0.089	0.204
Al ^{VI}	0.000	0.001	0.000	0.000	0.000	0.000	0.000	0.000	0.000	0.000	0.000
Ti	0.021	0.023	0.055	0.014	0.063	0.011	0.013	0.025	0.050	0.023	0.058
Cr	0.000	0.000	0.015	0.001	0.004	0.000	0.000	0.022	0.000	0.024	0.001
Fe ³⁺	0.064	0.051	0.096	0.092	0.098	0.124	0.072	0.055	0.099	0.047	0.107
Fe ²⁺	0.209	0.238	0.110	0.181	0.120	0.187	0.163	0.094	0.129	0.093	0.148
Mn	0.022	0.022	0.004	0.050	0.003	0.057	0.041	0.004	0.008	0.003	0.007
Mg	0.860	0.827	0.823	0.854	0.793	0.806	0.865	0.921	0.805	0.912	0.802
Ca	0.758	0.776	0.866	0.732	0.880	0.774	0.784	0.851	0.864	0.876	0.841
Na	0.040	0.043	0.000	0.051	0.000	0.048	0.035	0.004	0.000	0.013	0.000
P	0.004	0.004	0.003	0.003	0.006	0.003	0.004	0.004	0.006	0.004	0.006
Total:	3.98	3.99	3.97	3.97	3.98	3.97	3.97	3.96	3.99	3.97	3.97
Mg#	75.91	74.04	80.06	75.74	78.43	72.19	78.64	86.07	77.94	86.69	75.93
Wo	38.95	39.39	43.79	37.86	44.72	39.70	40.49	42.60	45.26	43.21	42.34
En	47.23	45.38	46.64	48.18	45.41	44.34	47.93	50.45	44.57	49.78	46.35
Fs	13.82	15.23	9.57	13.96	9.87	15.97	11.58	6.96	10.17	7.01	11.31

Table 4 (continued).

Hole, core, section:	956B-43R-2	956B-43R-2	956B-43R-1	956B-43R-1	956B-42R-3	956B-42R-2	956B-42R-2	956B-41R-1	956B-39R-3	956B-39R-3	956B-37R-1
Interval:	8-11	8-11	0-8	0-8	53-57	0-5	0-5	0-9	88-92	88-92	136-146
Depth (mbsf):	562.68	562.68	561.10	561.10	554.88	552.91	552.91	541.90	525.96	525.96	504.66
Volcaniclastic unit:	VU-10	VU-10	VU-15	VU-15	VU-15	VU-19	VU-19	VU-31a	VU-45	VU-45	VU-77B
Sample number:	PX-4	PX-6	PX-2	PX-4	PX-1	PX-4	PX-7	PX-14	PX-6	PX-7	PX-3
Number of analyses:	2	2	3	2	1	1	2	2	2	2	2
(wt%)											
SiO ₂	51.10	46.18	50.78	51.36	48.93	52.13	49.11	52.35	51.39	48.05	50.38
TiO ₂	0.97	2.94	0.35	0.35	1.59	0.41	1.85	0.45	0.83	1.82	1.47
Al ₂ O ₃	2.02	6.17	0.75	0.66	3.67	0.66	3.55	1.13	1.14	5.57	2.96
Cr ₂ O ₃	0.40	0.08	0.03	0.01	0.12	0.04	0.30	0.02	0.02	0.57	0.17
FeO*	4.78	7.52	14.03	9.28	6.67	10.01	7.43	8.25	10.87	6.41	7.49
MnO	0.12	0.16	1.65	1.93	0.08	2.21	0.22	1.07	0.77	0.15	0.15
MgO	16.08	12.95	12.60	14.80	15.11	14.69	15.47	15.74	15.15	14.17	15.47
CaO	22.39	21.66	17.80	18.69	20.77	17.66	19.74	19.49	17.33	21.33	20.99
Na ₂ O	0.37	0.51	0.49	0.74	0.32	0.97	0.43	0.65	0.08	0.09	0.40
P ₂ O ₅	0.12	0.12	0.11	0.12	0.14	0.10	0.18	0.17	0.11	0.14	0.14
Total:	98.32	98.28	98.58	97.92	97.39	98.88	98.27	99.30	97.69	98.29	99.59
Si	1.902	1.746	1.951	1.946	1.851	1.961	1.843	1.944	1.965	1.809	1.865
Al ^{IV}	0.089	0.254	0.034	0.029	0.149	0.029	0.157	0.049	0.035	0.191	0.129
Al ^{VI}	0.000	0.020	0.000	0.015	0.000	0.000	0.000	0.017	0.056	0.000	0.000
Ti	0.027	0.084	0.010	0.010	0.045	0.012	0.052	0.013	0.024	0.052	0.041
Cr	0.012	0.002	0.001	0.000	0.004	0.001	0.009	0.001	0.001	0.017	0.005
Fe ³⁺	0.057	0.091	0.070	0.103	0.051	0.087	0.058	0.069	0.000	0.008	0.070
Fe ²⁺	0.091	0.147	0.380	0.191	0.160	0.228	0.175	0.187	0.348	0.194	0.162
Mn	0.004	0.005	0.054	0.062	0.003	0.070	0.007	0.034	0.025	0.005	0.005
Mg	0.892	0.730	0.721	0.836	0.852	0.824	0.865	0.871	0.864	0.795	0.854
Ca	0.893	0.877	0.733	0.759	0.842	0.712	0.794	0.775	0.710	0.860	0.833
Na	0.013	0.016	0.018	0.033	0.005	0.050	0.012	0.016	0.006	0.007	0.004
P	0.004	0.004	0.004	0.004	0.004	0.003	0.006	0.005	0.004	0.004	0.004
Total:	3.98	3.98	3.98	3.97	3.98	3.98	3.98	3.96	4.00	4.00	3.97
Mg#	85.71	75.43	61.55	73.97	80.15	72.34	78.77	77.27	71.30	79.76	78.64
Wo	44.73	44.59	37.51	38.97	42.36	36.58	40.20	40.29	34.93	39.69	42.64
En	47.99	42.74	39.08	46.01	47.01	46.74	47.94	47.45	44.76	47.27	46.17
Fs	17.28	12.67	23.41	15.03	10.63	16.68	11.85	12.26	20.31	13.04	11.19

Table 4 (continued).

Hole, core, section:	956B-37R-1	956B-36R-1	956B-35R-4	956B-35R-4	956B-35R-2	956B-35R-2	956B-33R-3	956B-33R-3	956B-33R-1	956B-33R-1
Interval:	136-146	0-6	27-35	27-35	101-110	101-110	112-118	112-118	59-63	59-63
Depth (mbsf):	504.66	493.60	488.48	488.48	486.34	486.34	468.48	468.48	465.19	465.19
Volcaniclastic unit:	VU-77B	VU-87b	VU-87a	VU-87a	VU-94	VU-94	VU-107	VU-107	VU-121	VU-121
Sample number:	PX-4	PX-13	PX-7	PX-19	PX-1	PX-6	PX-1	PX-2	PX-6	PX-7
Number of analyses:	2	2	1	2	2	2	2	2	2	2
(wt%)										
SiO ₂	51.51	47.58	49.07	48.33	48.65	49.20	52.11	50.53	46.71	48.05
TiO ₂	0.94	1.25	1.27	1.52	1.54	1.37	0.60	0.82	2.02	1.45
Al ₂ O ₃	1.22	4.72	4.60	5.49	4.71	4.06	0.84	0.95	5.43	4.19
Cr ₂ O ₃	0.03	0.97	0.76	0.71	0.63	0.65	0.02	0.02	0.27	0.50
FeO*	10.13	5.84	5.44	5.52	5.74	5.53	8.92	18.28	6.78	6.06
MnO	0.54	0.14	0.13	0.06	0.08	0.09	1.13	0.42	0.16	0.13
MgO	14.28	14.90	14.99	14.39	14.69	15.04	15.34	14.74	13.91	14.74
CaO	19.80	21.18	22.20	22.30	22.35	22.33	18.38	13.00	21.79	21.99
Na ₂ O	0.63	0.44	0.37	0.43	0.40	0.40	1.16	0.28	0.45	0.44
P ₂ O ₅	0.12	0.06	0.12	0.13	0.09	0.11	0.17	0.13	0.07	0.07
Total:	99.18	97.06	98.93	98.88	98.85	98.77	98.64	99.15	97.57	97.59
Si	1.935	1.800	1.822	1.799	1.811	1.831	1.948	1.934	1.767	1.810
Al ^{IV}	0.054	0.200	0.178	0.201	0.189	0.169	0.037	0.043	0.233	0.186
Al ^{VI}	0.000	0.011	0.024	0.040	0.017	0.009	0.000	0.000	0.009	0.000
Ti	0.027	0.036	0.035	0.043	0.043	0.038	0.017	0.024	0.057	0.041
Cr	0.001	0.029	0.022	0.021	0.019	0.019	0.001	0.001	0.008	0.015
Fe ³⁺	0.056	0.116	0.077	0.074	0.088	0.083	0.100	0.050	0.127	0.123
Fe ²⁺	0.262	0.069	0.092	0.098	0.090	0.089	0.179	0.535	0.087	0.068
Mn	0.017	0.004	0.004	0.002	0.003	0.003	0.036	0.014	0.005	0.004
Mg	0.800	0.840	0.830	0.798	0.815	0.834	0.855	0.841	0.784	0.828
Ca	0.797	0.859	0.883	0.889	0.891	0.890	0.736	0.533	0.883	0.888
Na	0.046	0.000	0.000	0.000	0.000	0.000	0.064	0.021	0.000	0.000
P	0.004	0.002	0.004	0.004	0.003	0.003	0.005	0.004	0.002	0.002
Total:	4.00	3.97	3.97	3.97	3.97	3.97	3.98	4.00	3.96	3.96
Mg#	71.53	81.97	83.08	82.29	82.02	82.90	75.40	58.97	78.53	81.26
Wo	39.81	40.36	42.22	42.67	43.23	43.56	37.77	26.62	42.93	43.22
En	42.97	52.82	50.35	49.08	48.95	49.17	47.75	42.86	48.35	49.67
Fs	17.22	6.82	7.44	8.26	7.82	7.27	14.48	30.52	8.71	7.11

Table 5. Representative EMP analyses of orthopyroxene from Holes 953C, 955A, and 956B.

Hole, core, section:	953C-68R-4	953C-67R-4	953C-65R-2	953C-64R-1	953C-63R-1	953C-63R-1	953C-61R-3	953C-59R-5	953C-58R-4	955A-59X-6
Interval:	56-60	53-59	94-98	62-74	40-48	40-48	109-114	104-107	41-45	61-67
Depth (mbsf):	826.07	816.49	794.49	783.42	773.50	773.50	758.06	741.57	730.02	559.31
Volcaniclastic unit:	VU-15	VU-20	VU-35	VU-37	VU-38	VU-38	VU-41	VU-46	VU-49	VU-15
Sample number:	PX-1	PX-6	PX-1	PX-5	PX-4	PX-6	PX-1	PX-18	PX-6	PX-5
Number of analyses:	5	2	2	1	2	2	2	1	2	1
(wt%)										
SiO ₂	51.33	52.16	54.36	53.23	53.42	53.55	53.51	53.83	56.00	53.72
TiO ₂	0.78	0.33	0.25	0.33	0.00	0.26	0.24	0.31	0.01	0.28
Al ₂ O ₃	1.82	1.48	0.13	0.12	4.48	0.22	0.12	0.18	2.13	0.42
Cr ₂ O ₃	0.12	0.05	0.01	0.03	0.85	0.02	0.03	0.03	0.60	0.00
FeO*	12.05	16.68	16.16	16.07	5.98	16.06	16.42	16.39	5.60	16.01
MnO	1.28	0.42	2.03	2.00	0.16	2.19	2.25	1.74	0.18	2.57
MgO	21.57	25.27	25.39	25.58	33.20	25.64	25.38	25.24	34.08	25.54
CaO	8.89	1.26	1.31	1.44	1.09	1.43	1.30	1.46	1.14	1.42
Na ₂ O	0.28	0.11	0.25	0.21	0.11	0.18	0.20	0.20	0.07	0.13
P ₂ O ₅	0.09	0.04	0.00	0.02	0.03	0.01	0.00	0.00	0.00	0.00
Total:	98.21	97.78	99.89	99.02	99.32	99.56	99.45	99.38	99.81	100.08
Si	1.905	1.932	1.982	1.952	1.848	1.956	1.959	1.973	1.930	1.956
Al ^{IV}	0.080	0.055	0.000	0.000	0.152	0.002	0.000	0.000	0.070	0.010
Al ^{VI}	0.000	0.000	0.000	0.000	0.031	0.000	0.000	0.000	0.017	0.000
Ti	0.022	0.000	0.001	0.004	0.000	0.000	0.001	0.001	0.000	0.000
Cr	0.004	0.001	0.000	0.001	0.023	0.001	0.001	0.001	0.016	0.000
Fe ³⁺	0.075	0.056	0.035	0.086	0.102	0.075	0.077	0.044	0.042	0.063
Fe ²⁺	0.297	0.461	0.458	0.408	0.071	0.417	0.425	0.458	0.119	0.425
Mn	0.040	0.013	0.063	0.062	0.005	0.068	0.070	0.054	0.005	0.079
Mg	1.195	1.397	1.380	1.399	1.712	1.394	1.386	1.376	1.751	1.386
Ca	0.353	0.050	0.051	0.057	0.040	0.056	0.051	0.057	0.042	0.055
Na	0.000	0.000	0.024	0.029	0.000	0.018	0.022	0.024	0.000	0.009
P	0.003	0.001	0.000	0.001	0.001	0.000	0.000	0.000	0.000	0.000
Total:	3.97	3.97	3.99	4.00	3.99	3.99	3.99	3.99	3.99	3.98
Mg#	76.24	72.97	73.69	73.92	90.82	73.92	73.41	73.25	91.56	73.98
W o	18.27	2.17	2.18	2.38	1.33	2.36	2.17	2.45	1.32	2.35
En	63.32	72.97	71.81	71.60	94.62	71.95	71.50	71.05	92.19	72.27
Fs	18.42	24.86	26.01	26.02	4.05	25.69	26.34	26.50	6.49	25.38

Table 5 (continued).

Hole, core, section:	955A-59X-2	955A-58X-1	955A-56X-3	955A-56X-1	955A-55X-4	955A-60X-2	955A-60X-2	956B-42R-2	956B-42R-2	956B-41R-1
Interval:	44-46	16-17	16-25	126-131	19-25	140-144	140-144	0-5	0-5	0-9
Depth (mbsf):	553.14	541.76	525.59	523.66	517.59	563.80	563.80	552.91	552.91	541.90
Volcaniclastic unit:	VU-24	VU-39	VU-60	VU-63	VU-67	VU-7	VU-7	VU-19	VU-19	VU-31a
Sample number:	PX-1	PX-21	PX-8	PX-9	PX-12	PX-2	PX-12	PX-11	PX-1	PX-6
Number of analyses:	2	1	2	2	2	2	2	2	2	2
(wt%)										
SiO ₂	52.16	52.61	53.57	54.01	54.05	53.72	53.13	52.11	52.61	53.55
TiO ₂	0.30	0.25	0.33	0.30	0.26	0.29	0.32	0.21	0.39	0.29
Al ₂ O ₃	0.36	0.17	0.33	0.19	0.10	0.48	0.53	0.17	0.32	0.24
Cr ₂ O ₃	0.01	0.04	0.00	0.00	0.04	0.04	0.00	0.01	0.00	0.00
FeO*	14.97	16.33	15.09	15.32	15.49	15.36	16.56	22.08	16.92	16.95
MnO	2.07	2.33	2.41	3.12	2.25	2.42	2.36	3.61	2.85	2.74
MgO	25.36	23.97	25.86	25.55	25.35	25.54	25.59	19.81	23.94	24.97
CaO	1.46	1.42	1.34	1.40	1.41	1.49	1.53	1.44	1.62	1.32
Na ₂ O	0.16	0.25	0.17	0.19	0.23	0.15	0.20	0.22	0.20	0.18
P ₂ O ₅	0.00	0.00	0.00	0.00	0.00	0.00	0.00	0.00	0.00	0.00
Total:	96.85	97.37	99.09	100.08	99.18	99.48	100.22	99.65	98.82	100.23
Si	1.953	1.977	1.962	1.966	1.983	1.964	1.931	1.975	1.954	1.953
Al ^{IV}	0.007	0.000	0.005	0.000	0.000	0.012	0.014	0.002	0.003	0.002
Al ^{VI}	0.000	0.000	0.000	0.000	0.000	0.000	0.000	0.000	0.000	0.000
Ti	0.000	0.000	0.000	0.000	0.003	0.000	0.000	0.000	0.000	0.000
Cr	0.000	0.001	0.000	0.000	0.001	0.001	0.000	0.000	0.000	0.000
Fe ³⁺	0.072	0.042	0.055	0.058	0.030	0.045	0.113	0.048	0.071	0.080
Fe ²⁺	0.397	0.471	0.407	0.408	0.445	0.425	0.390	0.652	0.454	0.437
Mn	0.066	0.074	0.075	0.096	0.070	0.075	0.073	0.116	0.090	0.085
Mg	1.416	1.342	1.412	1.386	1.386	1.392	1.386	1.119	1.325	1.358
Ca	0.059	0.057	0.053	0.055	0.055	0.058	0.060	0.058	0.064	0.052
Na	0.014	0.023	0.018	0.023	0.026	0.008	0.010	0.019	0.024	0.019
P	0.000	0.000	0.000	0.000	0.000	0.000	0.000	0.000	0.000	0.000
Total:	3.98	3.99	3.99	3.99	4.00	3.98	3.98	3.99	3.99	3.99
Mg#	75.12	72.35	75.34	74.83	74.47	74.77	73.36	61.52	71.61	72.42
Wo	2.42	2.50	2.19	2.31	2.35	2.46	2.52	2.96	2.85	2.24
En	73.18	70.29	73.45	72.74	72.31	73.00	71.68	59.61	69.19	70.55
Fs	24.40	27.20	24.36	24.95	25.34	24.54	25.80	37.43	27.96	27.21

Table 6. Representative EMP analyses of aegirine from Holes 953C, 955A, and 956B.

Hole, core, section:	953C-64R-3	953C-64R-1	953C-59R-5	953A-58X-1	953A-56X-3	953A-56X-1
Interval:	72-75	62-74	104-107	119-125	16-25	126-131
Depth (mbsf):	786.14	783.42	741.57	542.79	525.59	523.66
Volcaniclastic unit:	VU-36	VU-37	VU-46	VU-34	VU-60	VU-63
Sample number:	PX-4	PX-8	PX-15	PX-7	PX-13	PX-2
Number of analyses:	1	2	1	2	2	2
(wt%)						
SiO ₂	51.34	51.32	52.24	52.00	51.26	51.08
TiO ₂	1.35	1.22	7.34	4.77	0.69	3.62
Al ₂ O ₃	0.28	0.27	0.10	0.17	0.28	0.15
Cr ₂ O ₃	0.04	0.05	0.01	0.00	0.00	0.00
FeO*	28.65	25.79	21.62	22.48	25.73	26.26
MnO	0.29	0.71	1.21	0.57	1.16	1.13
MgO	0.63	1.98	1.14	1.79	2.03	0.31
CaO	0.54	4.16	0.89	1.66	6.08	2.67
Na ₂ O	11.63	9.51	11.18	11.09	8.59	10.31
P ₂ O ₅	0.01	0.05	0.03	0.00	0.00	0.00
Total:	94.75	95.06	95.75	94.53	95.83	95.52
Si	2.032	2.036	2.058	2.058	2.033	2.038
Al ^{IV}	0.000	0.000	0.000	0.000	0.000	0.000
Al ^{VI}	0.013	0.013	0.005	0.008	0.013	0.007
Ti	0.040	0.036	0.217	0.142	0.021	0.109
Cr	0.001	0.002	0.000	0.000	0.000	0.000
Fe ³⁺	0.731	0.568	0.299	0.444	0.540	0.498
Fe ²⁺	0.219	0.288	0.413	0.300	0.313	0.378
Mn	0.010	0.024	0.040	0.019	0.039	0.038
Mg	0.037	0.117	0.067	0.106	0.120	0.018
Ca	0.188	0.160	0.048	0.048	0.258	0.075
Na	0.715	0.599	0.855	0.851	0.508	0.797
P	0.000	0.002	0.001	0.000	0.000	0.000
Total:	3.99	3.84	4.00	3.98	3.85	3.96
Mg#	3.77	12.03	8.60	12.43	12.33	2.06
Wo	40.92	42.75	51.76	48.73	13.68	46.04
En	1.30	4.28	2.89	4.12	6.96	0.70
Fs	7.99	11.43	19.57	12.48	20.40	15.68
Ac	49.79	41.54	25.78	34.66	58.96	37.58

Table 7. Representative EMP analyses of phlogopites from Holes 953C, 955A, and 956B.

Hole, core, section:	953C-69R-5	953C-66R-3	953C-62R-1	953C-59R-6	953C-58R-4	953C-47R-2	953C-45R-2	955A-58X-1
Interval:	26-33	16-22	100-118	105-112	41-45	141-146	10-14	119-125
Depth (mbsf):	836.86	805.03	764.60	742.97	730.02	621.51	602.00	542.79
Volcaniclastic unit:	VU-11a	VU-29	VU-40	VU-44	VU-49	VU-96	VU-100	VU-34
Sample number:	MC-1	MC-4	MC-2	MC-4	MC-2	MC-1	MC-1	MC-20
Number of analyses:	2	1	2	2	2	2	2	2
(wt%)								
SiO ₂	36.86	38.36	38.83	38.55	39.97	38.49	36.75	38.20
TiO ₂	8.24	5.07	4.86	5.58	5.64	4.12	7.36	5.09
Al ₂ O ₃	13.38	12.26	11.77	12.11	11.63	11.26	13.03	12.09
FeO*	9.43	12.31	11.37	11.48	10.08	14.04	13.48	11.78
MnO	0.10	0.49	0.58	0.57	0.36	1.07	0.72	0.60
MgO	16.22	17.30	18.35	17.24	18.61	16.15	14.40	17.08
Na ₂ O	0.42	1.25	1.27	0.96	1.03	0.73	0.85	1.04
K ₂ O	9.13	8.27	8.28	8.44	8.59	8.90	8.44	8.61
SrO	0.030	0.145	0.112	0.118	0.087	0.113	0.104	0.066
BaO	0.668	0.113	0.347	0.522	0.065	0.067	0.989	0.234
S	0.025	0.018	0.021	0.009	0.023	0.020	0.019	0.022
F	1.389	1.692	2.456	2.190	2.284	2.138	1.393	1.582
Cl	0.051	0.013	0.013	0.015	0.020	0.020	0.014	0.028
Total:	95.97	97.30	98.27	97.79	98.41	97.14	97.58	96.44

Table 7 (continued).

Hole, core, section:	955A-58X-1	955A-58X-1	955A-54X-CC	955A-54X-CC	956B-40R-2	956B-40R-2	956B-35R-4	956B-34R-2
Interval:	119-125	86-90	10-14	10-14	129-133	129-133	27-35	62-70
Depth (mbsf):	542.79	542.46	503.50	503.50	535.09	535.09	488.48	476.29
Volcaniclastic unit:	VU-34	VU-36	VU-74	VU-74	VU-32	VU-32	VU87a	VU-102
Sample number:	MC-21	MC-6	MC-1	MC-3	MC-1	MC-8	MC-1	MC-5
Number of analyses:	2	1	2	2	1	2	2	2
(wt%)								
SiO ₂	38.36	38.13	39.41	36.96	36.60	37.13	39.55	37.53
TiO ₂	4.88	4.47	5.12	5.32	5.59	4.34	4.88	5.73
Al ₂ O ₃	11.73	11.54	11.70	13.12	16.45	15.69	11.77	12.35
FeO*	11.78	12.20	9.60	14.14	10.90	10.32	10.40	11.62
MnO	0.62	0.72	0.37	0.50	0.00	0.14	0.41	0.38
MgO	17.53	17.26	18.85	15.33	16.87	17.88	19.01	18.02
Na ₂ O	1.17	0.98	1.06	1.04	0.94	1.15	1.33	1.23
K ₂ O	8.16	8.59	7.87	8.64	9.18	8.68	7.97	8.39
SrO	0.111	0.056	0.000	0.002	0.000	0.000	0.103	0.000
BaO	0.082	0.090	0.205	0.283	0.277	0.294	0.448	0.306
S	0.049	0.027	0.030	0.017	0.024	0.039	0.046	0.009
F	1.681	1.974	2.787	1.187	0.449	0.406	2.046	2.432
Cl	0.029	0.005	0.042	0.022	0.025	0.042	0.020	0.020
Total:	96.22	96.07	97.07	96.57	97.32	96.13	98.01	98.01

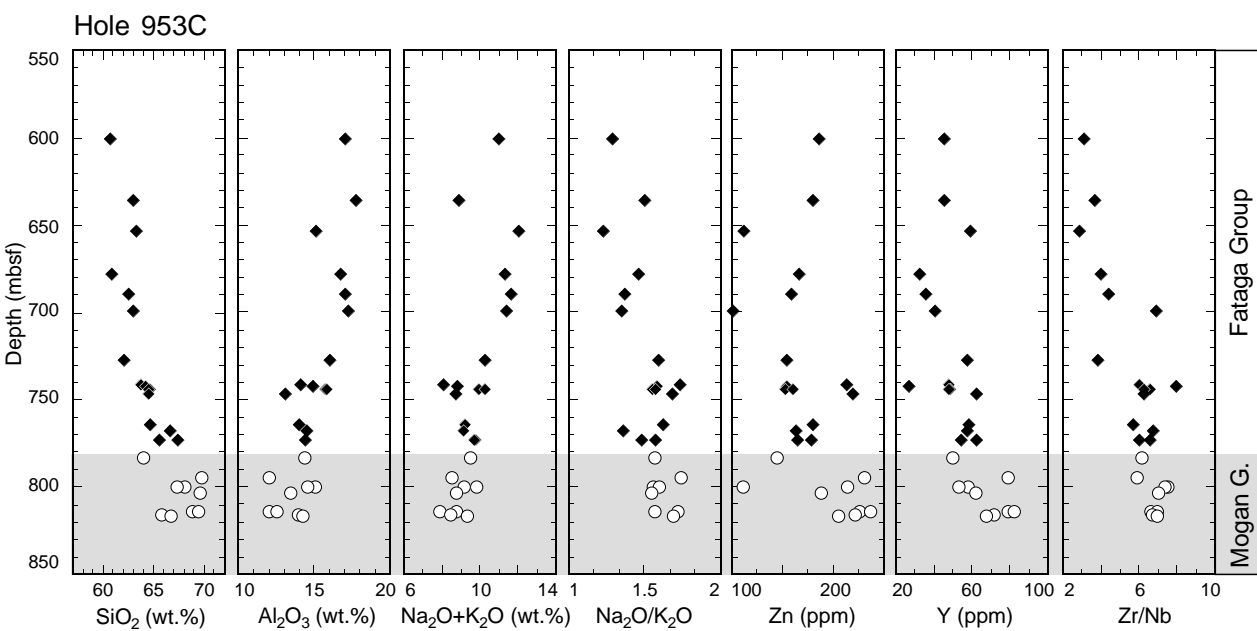


Figure 16. Stratigraphic plot of selected bulk-rock chemical analyses from Hole 953C.

Table 8. Major and trace element analyses of volcanioclastic sediments from Hole 953C.

Hole, core, section:	953C-45R-1	953C-48R-6	953C-50R-4	953C-53R-2	953C-54R-3	953C-55R-3	953C-58R-2	953C-59R-5	953C-59R-6	953C-60R-1	953C-60R-1	953C-60R-2
Interval (cm):	55-58	108-111	81-83	0-8	51-57	74-82	105-113	113-118	105-112	32-34	35-42	145-150
Depth (mbsf):	600.95	636.18	653.61	678.85	690.17	699.83	727.72	741.66	742.97	744.82	744.85	747.37
Volcanioclastic unit:	VU-91	VU-79	VU-72	VU-64	VU-60	VU-50	VU-46	VU-44	VU-43	VU-43	VU-43	VU-42
Major elements (wt%):												
SiO ₂	51.13	49.60	60.85	52.34	54.48	55.06	57.92	56.39	54.41	55.43	56.66	57.99
TiO ₂	1.09	0.78	1.07	1.25	0.79	0.93	1.67	1.21	0.84	0.91	1.19	
Al ₂ O ₃	14.38	14.02	14.56	14.37	14.84	15.09	15.00	12.47	12.71	13.48	13.90	11.81
FeO *	4.83	3.36	6.77	4.90	3.66	3.23	4.92	6.25	5.16	3.93	3.95	6.43
MnO	0.21	0.13	0.10	0.08	0.05	0.03	0.12	0.12	0.04	0.10	0.11	0.14
MgO	2.03	1.67	0.82	1.38	1.71	1.69	1.88	2.66	2.03	1.33	1.41	2.61
CaO	4.94	8.38	0.32	3.76	2.94	3.03	2.19	2.90	4.57	3.45	3.53	2.77
Na ₂ O	5.50	4.61	6.41	5.77	5.86	5.74	5.92	4.61	4.58	5.32	5.53	4.96
K ₂ O	4.28	3.05	5.20	3.93	4.27	4.26	3.71	2.65	2.88	3.41	3.50	2.93
P ₂ O ₅	0.13	0.07	0.05	0.12	0.08	0.10	0.22	0.12	0.07	0.14	0.16	0.14
SO ₃	0.060	0.057	>0.05	0.121	0.09	0.09	0.14	0.10	0.30	0.13	0.08	0.14
LOI	10.28	12.27	1.55	12.42	10.04	9.75	4.71	8.21	10.82	9.81	9.04	7.05
Total:	98.87	98.01	97.71	100.45	98.82	99.01	98.41	97.70	98.42	97.39	98.79	98.18
Trace elements (ppm):												
V	38	19	55	40	51	33	37	38	27	<12	15	35
Cr	30	<18	<18	<18	<18	<18	<18	70	55	20	<18	<18
Co	25	<4	12	<4	<4	5	<4	10	<4	15	<4	<4
Ni	27	16	14	12	<2	<2	<2	37	14	14	<2	4
Cu	32	20	9	14	14	12	18	26	16	17	9	14
Zn	187	180	112	167	159	101	154	214	154	153	161	220
Ga	31	32	44	34	33	32	30	35	19	32	32	37
Rb	75	57	116	79	82	81	51	56	64	77	70	58
Sr	345	316	68	282	243	265	565	292	360	308	329	285
Y	46	46	60	33	36	41	58	48	27	49	48	63
Nb	195	196	197	241	188	152	145	175	181	148	139	176
Ba	326	156	<8	331	269	342	808	283	160	372	516	384
La	175	176	294	223	168	204	162	195	110	179	153	190
Ce	210	234	265	324	248	329	260	266	194	234	221	279
Zr	611	732	574	965	832	1058	558	1056	1450	980	873	1106
Pr	29	31	52	35	29	34	29	32	19	31	26	29
Nd	77	81	157	117	89	122	111	101	70	85	91	113
Sm	11	12	18	11	12	12	15	19	12	17	14	19
Pb	12	18	9	8	14	<4	<4	12	6	9	<4	7
Th	7	8	30	20	10	17	<4	12	16	10	<4	13
Zr/Nb	3.13	3.73	2.91	4.00	4.43	6.96	3.85	6.03	8.01	6.62	6.28	6.28
Zr/Y	13.28	15.91	9.57	29.24	23.11	25.80	9.62	22.00	53.70	20.00	18.19	17.56
Nb/Y	4.24	4.26	3.28	7.30	5.22	3.71	2.50	3.65	6.70	3.02	2.90	2.79

Table 8 (continued)

Hole, core, section:	953C-62R-1	953C-62R-4	953C-63R-1	953C-63R-1	953C-64R-1	953C-65R-2	953C-65R-6	953C-65R-6	953C-66R-2	953C-67R-2	953C-67R-2	953C-67R-3	953C-67R-4
Interval (cm):	134-139	0-7	10-20	49-53	62-74	94-98	59-62	98-100	28-35	61-63	75-84	104-110	47-52
Depth (mbsf):	764.94	768.05	773.2	773.59	783.42	794.49	799.58	799.97	803.69	813.82	813.96	815.63	816.43
Volcaniclastic unit:	VU-40	VU-39	VU-38	VU-38	VU-37	VU-35	VU-31	VU-31	VU-30	VU-21	VU-21	VU-20	VU-20
Major elements (wt%):													
SiO ₂	59.40	57.01	56.17	59.23	57.34	62.82	58.77	55.96	61.26	56.79	60.12	56.10	58.17
TiO ₂	1.34	0.78	0.98	0.79	1.21	1.04	0.58	0.65	0.74	0.86	0.83	0.75	0.86
Al ₂ O ₃	12.85	12.41	12.39	12.64	12.87	10.87	13.00	12.08	11.85	9.96	10.83	11.86	12.39
FeO*	5.15	3.50	3.68	3.59	4.62	5.43	2.85	3.01	4.28	4.37	4.13	4.31	3.72
MnO	0.20	0.13	0.21	0.19	0.16	0.22	0.14	0.14	0.19	0.22	0.19	0.15	0.16
MgO	1.79	1.54	1.20	1.03	1.87	0.73	0.71	0.65	0.92	0.78	0.74	1.46	1.03
CaO	3.75	4.82	5.89	2.87	5.85	1.74	4.11	5.74	2.49	6.26	4.83	6.76	5.71
Na ₂ O	5.26	4.52	5.13	5.17	5.20	4.86	5.16	4.90	4.67	4.14	4.78	4.82	5.11
K ₂ O	3.22	3.32	3.25	3.48	3.32	2.79	3.30	3.07	3.01	2.64	2.78	2.38	3.02
P ₂ O ₅	0.18	0.14	0.13	0.11	0.17	0.13	0.09	0.11	0.09	0.11	0.10	0.24	0.11
SO ₃	0.175	0.231	0.134	0.179	0.097	0.251	0.123	0.356	0.136	0.253	0.115	0.196	0.234
LOI	5.24	9.71	8.43	8.27	5.90	7.07	8.46	10.51	8.06	11.10	8.55	7.83	7.82
Total:	98.56	98.12	97.61	97.55	98.61	97.96	97.30	97.19	97.70	97.50	98.01	96.86	98.34
Trace elements (ppm):													
V	37	20	26	15	50	39	14	24	35	35	34	26	23
Cr	47	<18	<18	<18	63	<18	<18	<18	<18	26	<18	<18	<18
Co	<4	<4	<4	25	<4	<4	<4	9	31	<4	<4	<4	<4
Ni	17	4	<2	21	19	<2	<2	17	<2	24	<2	5	<2
Cu	13	16	8	18	16	8	5	5	13	24	7	12	18
Zn	180	163	165	179	144	231	213	111	188	226	236	221	205
Ga	35	34	34	37	37	39	32	29	37	35	33	34	31
Rb	57	85	67	87	54	60	85	78	75	70	70	56	62
Sr	204	275	181	148	235	1720	205	280	161	621	264	487	245
Y	59	58	55	63	50	79	58	53	62	79	82	72	68
Nb	138	148	137	160	111	161	137	127	127	178	179	183	172
Ba	532	278	534	313	627	856	408	460	583	482	275	622	383
La	158	140	144	182	129	166	162	178	157	221	192	158	180
Ce	188	223	211	240	177	274	214	189	228	262	296	244	279
Zr	794	1008	830	1063	682	943	1022	929	889	1181	1238	1224	1198
Pr	21	23	25	28	20	30	21	26	25	37	32	30	32
Nd	82	98	98	95	86	120	79	87	100	128	128	109	116
Sm	12	10	10	16	11	16	15	12	11	19	19	19	16
Pb	<4	5	<4	14	<4	12	4	12	<4	10	4	15	5
Th	<4	<4	7	11	<4	<4	8	<4	<4	14	<4	13	
Zr/Nb	5.75	6.81	6.06	6.64	6.14	5.86	7.46	7.31	7.00	6.63	6.92	6.69	6.97
Zr/Y	13.46	17.38	15.09	16.87	13.64	11.94	17.62	17.53	14.34	14.95	15.10	17.00	17.62
Nb/Y	2.34	2.55	2.49	2.54	2.22	2.04	2.36	2.40	2.05	2.25	2.18	2.54	2.53

Table 9. EMP analyses of vitrophyre glasses from subaerial ignimbrite on Gran Canaria.

Formation:	Lower Mogán				Middle Mogán				Upper Mogan				Fataga			
	Below VI 17-11-91-3	Ignimbrite TL 105-TL	Ignimbrite O? 95-11-12-10	Ignimbrite A 12-11-95-14	Ignimbrite A 95-11-12-13	Ignimbrite B 12-11-95-18	Ignimbrite C 12-11-95-19	Ignimbrite D 13-12-90-2	Ignimbrite I 12049310a	Ignimbrite P3 12-4-93-9	Ignimbrite Mo 30-4-95-24	Ayagaures 30-4-95-22				
Name of ignimbrite:									Ignimbrite I 12049310a	Ignimbrite P3 12-4-93-9	Ignimbrite Mo 30-4-95-24	Ayagaures 30-4-95-22				
Sample:	3	2	6	3	10	11	16	21	11	9	5	9				
Number of analyses:																
(wt%)																
SiO ₂	69.74	69.56	69.19	68.80	68.47	69.06	68.47	69.05	59.83	60.89	59.55	60.39	60.33			
TiO ₂	0.61	0.50	0.79	0.66	0.67	1.14	0.95	1.14	1.17	1.42	0.82	1.15	1.20			
Al ₂ O ₃	13.47	12.42	9.83	11.81	11.73	10.70	9.09	9.08	15.03	14.95	17.39	15.70	15.78			
FeO	2.25	3.50	4.98	3.67	3.65	5.90	6.53	6.38	5.72	5.79	3.73	4.95	4.90			
MnO	0.18	0.23	0.35	0.24	0.28	0.34	0.44	0.43	0.42	0.43	0.40	0.46	0.50			
MgO	0.29	0.27	0.24	0.28	0.28	0.50	0.26	0.26	0.69	0.72	0.37	0.58	0.57			
CaO	0.36	0.26	0.13	0.14	0.17	0.17	0.10	0.11	0.48	0.49	0.53	0.55	0.57			
Na ₂ O	5.20	5.21	5.55	6.17	6.02	7.52	7.50	7.68	10.24	10.34	8.87	10.08	9.68			
K ₂ O	4.95	5.10	4.69	4.70	4.70	4.53	4.74	5.02	4.97	5.12	5.23	5.14	5.13			
P ₂ O ₅	0.01	0.00	0.01	0.00	0.01	0.09	0.07	0.05	0.11	0.11	0.00	0.05	0.05			
BaO	0.05	0.03	0.04	0.08	0.03	0.09	0.03	0.06	0.05	0.03	0.02	0.04	0.04			
SrO	0.01	0.00	0.01	0.00	0.00	0.01	0.01	0.01	0.00	0.00	0.01	0.01	0.00			
S	0.012	0.033	0.072	0.088	0.067	0.100	0.074	0.083	0.101	0.102	0.041	0.115	0.098			
F	0.16	0.13	0.18	0.15	0.15	0.21	0.41	0.38	0.36	0.35	0.34	0.38	0.36			
Cl	0.11	0.13	0.12	0.15	0.16	0.12	0.19	0.20	0.18	0.19	0.19	0.20	0.22			
Total:	97.39	97.38	96.19	96.93	96.37	100.49	98.87	99.96	99.34	100.94	97.52	99.81	99.42			

Table 10. Representative EMP data of glass shards from Holes 953C, 955A, and 956B

Hole, core, section:	953C-69R-4	953C-68R-4	953C-67R-4	953C-67R-1	953C-66R-3	953C-65R-6	953C-64R-3	953C-64R-1	953C-63R-1	953C-62R-1
Interval (cm):	22-29	56-60	53-59	148-150	16-22	103-107	72-75	62-74	40-48	100-118
Depth (mbsf):	835.58	826.07	816.49	813.18	805.03	800.02	786.14	783.42	773.5	764.6
Volcaniclastic unit:	U-12a	U15	U-20	U-21	U-29	U-31	U-36	U-37	U-38	U-40
Sample number:	CGL-4	PGL-1	CGL-3	CGL-5	CGL-3	CGL-8	GL-r(FP-11)	CGL-5	GL-r(FP-5)	CGL-8
Number of analyses:	3	9	2	2	2	1	2	3	1	2
(wt%)										
SiO ₂	66.05	65.06	67.94	66.11	66.57	66.53	67.40	67.65	65.59	63.39
TiO ₂	0.67	0.59	0.50	0.72	0.51	0.62	0.38	1.07	0.45	0.98
Al ₂ O ₃	13.19	13.46	8.95	11.64	12.33	14.81	14.69	8.85	13.52	10.45
FeO	2.76	2.94	3.88	3.37	2.55	2.49	3.00	6.17	2.19	5.42
MnO	0.18	0.14	0.29	0.22	0.21	0.19	0.13	0.42	0.22	0.31
MgO	0.37	0.36	0.13	0.39	0.25	0.31	0.12	0.35	0.27	0.49
CaO	0.38	0.62	0.16	0.31	0.19	0.41	0.05	0.16	0.30	0.19
Na ₂ O	4.14	5.67	3.95	5.23	5.81	4.00	6.87	6.78	5.75	7.34
K ₂ O	3.71	4.22	2.79	3.71	4.01	4.19	4.35	4.35	4.35	4.78
P ₂ O ₅	0.03	0.08	0.03	0.06	0.07	0.03	0.05	0.12	0.08	0.16
BaO	0.06	0.11	0.10	0.00	0.07	0.01	0.00	0.00	0.00	0.00
SrO	0.084	0.232	0.239	0.230	0.214	0.006	0.247	0.264	0.258	0.243
S	0.034	0.011	0.021	0.020	0.053	0.062	0.020	0.071	0.057	0.076
F	0.200	0.228	0.380	0.248	0.206	0.184	0.086	0.270	0.221	0.249
Cl	0.142	0.080	0.351	0.214	0.158	0.172	0.077	0.168	0.181	0.121
Total:	92.00	93.79	89.73	92.46	93.19	94.00	97.46	96.69	93.43	94.18

Table 10 (continued).

Hole, core, section:	953C-61R-3	955A-60X-2	955A-59X-6	955A-59X-6	955A-59X-2	955A-59X-1	955A-58X-5	955A-58X-4	955A-58X-1	955A-58X-1
Interval (cm):	109-114	140-144	128-140	61-67	44-46	51-53	72-78	71-76	119-125	16-17
Depth (mbsf):	758.06	563.80	559.98	559.31	553.14	551.71	548.32	546.81	542.79	541.76
Volcaniclastic unit:	U-41	U-7	U-13	U-15	U-24	U-25	U-27	U-30	U-34	U-39
Sample number:	CGL-4	GL-r(FP-3)	BGL-1	BGL-3	CGL-9	CGL-10	BGL-12	BGL-2	CGL-5	CGL-1
Number of analyses:	2	2	2	2	2	2	2	2	2	2
(wt%)										
SiO ₂	65.88	67.42	68.49	69.78	64.37	66.82	68.57	63.17	63.22	66.90
TiO ₂	1.09	0.81	0.66	0.61	0.84	0.94	0.53	1.08	0.71	0.59
Al ₂ O ₃	10.88	15.12	13.65	13.39	14.68	11.90	12.38	15.56	15.50	12.71
FeO	5.21	2.44	2.32	2.57	3.03	4.14	2.41	3.61	2.76	3.05
MnO	0.37	0.25	0.14	0.24	0.21	0.23	0.24	0.23	0.21	0.22
MgO	0.50	0.61	0.33	0.30	0.62	0.51	0.27	0.89	0.43	0.28
CaO	0.19	1.22	0.48	0.39	0.69	0.30	0.37	1.15	0.46	0.24
Na ₂ O	7.43	6.17	5.26	5.51	5.67	5.37	5.38	6.92	6.15	5.01
K ₂ O	4.45	3.73	4.14	4.49	3.54	4.31	4.66	4.33	5.14	4.33
P ₂ O ₅	0.19	0.04	0.01	0.00	0.08	0.03	0.03	0.28	0.02	0.00
BaO	0.000	0.130	0.064	0.034	0.201	0.066	0.002	0.184	0.084	0.078
SrO	0.229	0.000	0.100	0.141	0.007	0.108	0.143	0.000	0.036	0.102
S	0.069	0.049	0.023	0.028	0.050	0.027	0.011	0.083	0.084	0.031
F	0.242	0.200	0.133	0.191	0.202	0.205	0.313	0.581	0.257	0.284
Cl	0.153	0.122	0.125	0.106	0.099	0.156	0.089	0.042	0.142	0.194
Total:	96.89	98.32	95.93	97.77	94.29	95.10	95.37	98.10	95.21	94.03

Table 10 (continued).

Hole, core, section:	955A-57X-2	955A-56X-3	955A-56X-1	955A-55X-4	955A-54X-CC	955A-53X-3	956B-43R-1	956B-41R-1	956B-40R-2	956B-39R-4	956B-39R-2
Interval (cm):	104-110	16-25	14-17	19-25	10-14	0-7	0-8	0-9	26-33	43-50	114-118
Depth (mbsf):	534.54	525.56	522.54	517.59	503.50	496.80	561.10	541.9	534.1	526.71	525
Volcaniclastic unit:	U-52	U-60	U-66	U-67	U-74	U-81	U-15	U-31b	U36	U-44	U47
Sample number:	BGL-2	BGL-3	BGL-14	CGL-2	CGL-14	BGL-6	BGL-12	BGL-1	CGL-6	BGL-4	CGL-10
Number of analyses:	2	2	2	2	2	2	2	2	3	2	2
(wt%)											
SiO ₂	62.89	66.39	65.21	66.57	67.63	59.23	66.24	66.76	68.37	64.61	63.60
TiO ₂	1.32	1.29	0.81	1.06	1.10	0.97	0.57	0.95	0.76	0.92	1.24
Al ₂ O ₃	15.19	11.66	14.26	11.32	11.37	16.81	13.34	11.66	9.52	15.23	11.42
FeO	4.30	5.15	2.99	5.61	5.61	2.98	2.17	4.19	4.51	3.27	5.05
MnO	0.26	0.35	0.27	0.30	0.30	0.21	0.10	0.28	0.33	0.16	0.29
MgO	1.19	0.73	0.60	0.50	0.49	0.84	0.30	0.56	0.21	0.73	0.75
CaO	1.45	0.60	0.55	0.20	0.15	1.33	0.52	0.35	0.14	0.96	0.71
Na ₂ O	7.52	7.67	5.88	6.73	6.57	6.90	5.49	5.17	5.10	6.49	6.40
K ₂ O	1.91	3.30	4.98	4.84	4.98	4.43	4.18	5.25	4.36	4.17	3.33
P ₂ O ₅	0.26	0.19	0.08	0.13	0.07	0.14	0.08	0.04	0.00	0.16	0.23
BaO	0.231	0.274	0.080	0.049	0.115	0.299	0.155	0.066	0.078	0.269	0.148
SrO	0.000	0.075	0.000	0.119	0.013	0.037	0.254	0.097	0.122	0.000	0.014
S	0.106	0.060	0.020	0.066	0.095	0.056	0.015	0.029	0.064	0.054	0.130
F	0.381	0.163	0.423	0.215	0.304	0.165	0.157	0.370	0.291	0.188	0.136
Cl	0.029	0.122	0.050	0.130	0.128	0.115	0.104	0.172	0.147	0.077	0.094
Total:	97.04	98.03	96.19	97.84	98.92	94.51	93.67	95.95	94.00	97.30	93.53

Note: CGL = clear glass, PGL = pumice glass, GL-r = glass rim around minerals, and BGL = brown glass.

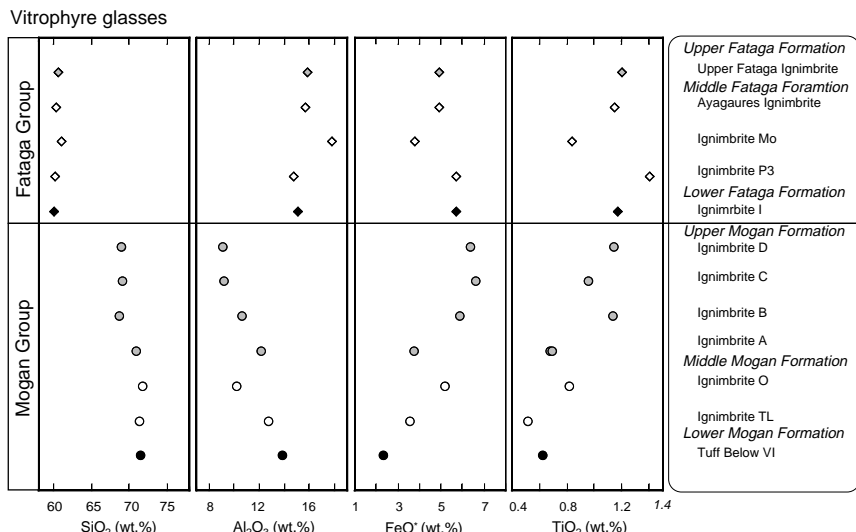


Figure 17. Stratigraphic plot of EMP analyses of fresh vitrophyres of selected subaerial ignimbrites from the Mogán and Fataga Formations

ly increases with iron in the rocks of the Mogán Formation, where it reaches 1.2 wt% in the pantellerite. Interestingly, titania may also exceed 1 wt% in many trachyphonolitic rocks of the Fataga Formation, such that Fe/Ti ratios are much higher in all Mogán rocks relative to those in the Fataga.

Bulk Volcaniclastic Sediments

We analyzed bulk tuffs for two main reasons. First, we wanted to find out whether the bulk composition is useful in verifying and/or defining the chemical stratigraphy established on land and that provided by the microprobe analyses of glass shards. Second, we wanted to contribute to the interpretation of the bulk composition of mixed volcaniclastic rocks that contain varying proportions of accidental lithics and biogenic debris. Such rocks are common in the geologic record, but they are rarely analyzed because of the obvious problems in assessing the magnitude of the effect of multi-component mixing and alteration on the overall chemical composition. We restrict our discussion here to the first goal.

We realize that the interpretation of the composition of bulk rocks is beset with many problems. One has to take into account several factors that modify the chemical composition of the original primary glass. First, glasses have been hydrated and chemically altered to varying degree, as shown also by the low microprobe totals of individual glass shards (see above). This leads to a loss in alkalis, especially Na, and, in the case of alteration of pumice and glass shards to layer silicates, in an uptake of Mg. Second, the admixture of nannofossil matrix and larger bioclasts tends to greatly modify the bulk composition, depending on the type and amount of skeletal debris. Most notably, this leads to significant increases in calcium and, in the case of dolomite cement, magnesium, both elements having concentrations generally <0.5 wt% in the felsic glasses. Taking out an equivalent amount of CaO to the amount of CO_2 measured decreases the calcium excess. Nevertheless, nearly all analyses show a significant excess of magnesium and calcium after carbonate correction, which probably results from the presence of calcium-bearing zeolites in the matrix, basaltic rock fragments, and basaltic clinopyroxene. The ubiquitous admixture of lithic fragments from the shield basalts and mafic crystals tends to increase Ca, Fe, and Mg concentrations and reduce alkalis and silica. The compatible trace element concentrations of Cr, Ni, and, to a lesser degree, V and Cu are also significantly increased. A final, more subtle factor in the interpretation of the composition of the bulk rocks is the fact that—even if the rocks were free of biogenic debris, accidental lithics, and alteration—the ratio of

crystals to glass, representative for the particular level in the magma reservoir, is likely to have changed greatly during transit of the pyroclastic flows.

Despite these complicating factors, however, the main chemical differences in the Mogán and Fataga lithostratigraphic groups are mirrored in remarkable detail in the volcaniclastic units, even by highly alteration-susceptible elements like alkalis (Fig. 16). We now discuss the chemical stratigraphy together with the electron microprobe analyses of the glasses.

Major Elements

The silica concentrations are low in the basaltic sandstones underlying and directly overlying P1, approach 70 wt% in the main Mogán interval, decrease to 64–65 wt% in the transitional interval and decrease further to 59–62 wt% in the Fataga interval, disregarding intermediate concentrations of the mixed rocks. Volcaniclastic sediments in Unit IV of Hole 953C have SiO_2 contents from 49 to 68 wt% (all values on CaCO_3 -free basis), with most values exceeding 55 wt% (Fig. 16). Concentrations of MgO , FeO^* , and TiO_2 are relatively low, whereas alkalis and Al_2O_3 are relatively high. Volcaniclastic sediments with evolved compositions in Subunits IVA and IVB have lower SiO_2 and MgO and generally higher Al_2O_3 , K_2O , and Na_2O than do those in Subunit IVC. These systematic differences in major element compositions clearly reflect the chemical differences between volcanic rocks from the Mogán and Fataga Groups.

It has been known for some time that the Na/K ratios decrease with time from Mogán to Fataga, while total alkalis increase (Schmincke, 1969, 1973). The alkali concentrations of the volcaniclastic sediments preserve these variations, despite the susceptibility of alkalis to alteration. Soda generally shows concentrations of 6–7.5 wt% in the Mogán ignimbrites, but may exceed 10 wt% in fresh glasses of the Fataga Formation (Fig. 20). Interestingly, Na_2O concentrations are, in general, significantly lower in the Fataga ignimbrites relative to those of the fresh vitrophyre glasses, whereas this contrast is less pronounced in Mogán ignimbrites. This most likely results from the less complete and coarse-grained crystallization of the lower temperature Fataga ignimbrites, which results in a diagenetic loss of soda. Potassium, being less mobile than Na_2O , characteristically increases from rocks of the Mogán Group, in which it rarely exceeds 5 wt% to >5 wt% in the Fataga ignimbrites and lava flows. The Na/K ratio decreases throughout the Mogán Formation and is distinctly lower in the Fataga Formation where it is reflected in the more potassic alkali-feldspar phenocrysts. Calcium concentra-

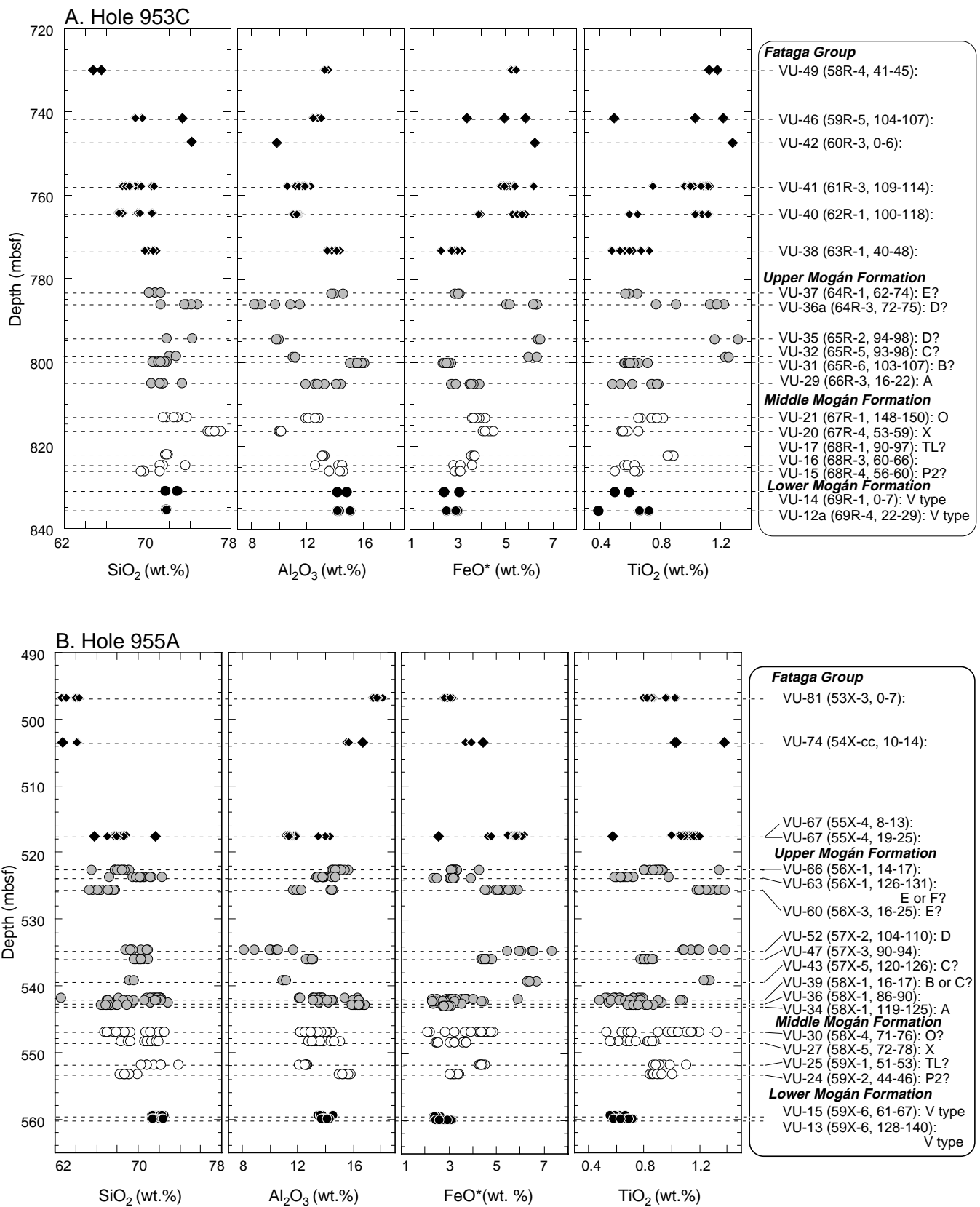
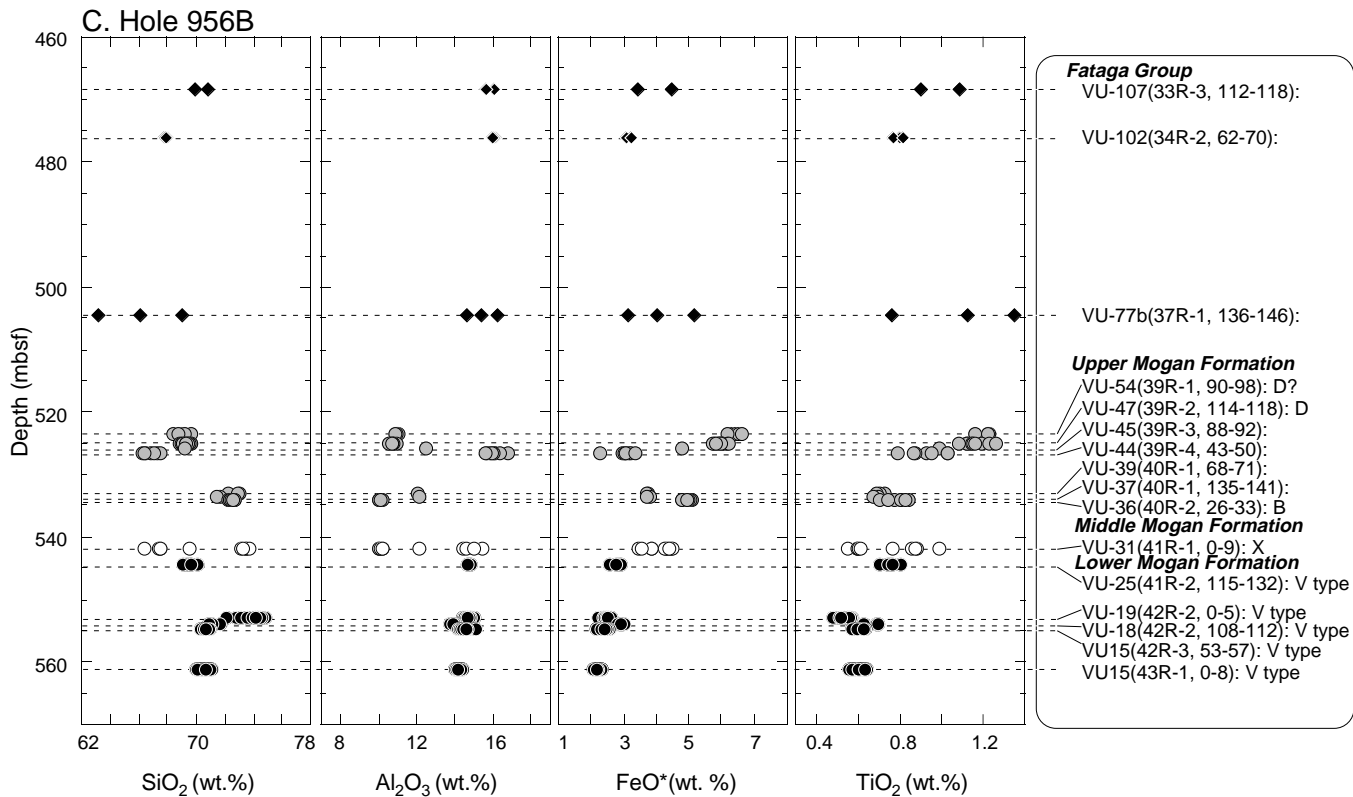


Figure 18. Stratigraphic plot of EMP analyses of glass shards from Holes (A) 953C, (B) 955A, and (C) 956B.



Figures 18 (continued).

tions are generally <0.5 wt% in most Mogán rocks, but are between 0.7 and 0.9 wt% in most Fataga rocks. MgO concentrations are generally less than 0.2 wt% in Mogán rocks, but are as high as 0.5 wt% in many rocks of the Fataga Group.

Trace Elements

High concentrations of many incompatible elements (Zr, Nb, Y, La, and Ce) are characteristic of evolved magmas from the Mogán and Fataga Groups. Rocks from both groups can be distinguished from each other by their Zr/Nb ratios, which mainly result from higher Nb concentration in the Fataga rocks (Schmincke, 1976). Zr/Nb ratios decrease from values >6 in the Mogán and intermediate intervals and are <4 in the vitric sediments of the Fataga interval. Ignimbrites compositionally transitional between Mogán and Fataga are mineralogically more Fataga-like, but their chemical composition is Mogán-like, such as Zr/Nb ratios >5. Volcaniclastic unit with these “transitional” characteristics are abundant in Hole 953C.

Trace element data for sediments in Lithologic Unit IV (Hole 953C) show relatively high concentrations of Nb (40–250 ppm), Zr (330–1310 ppm), Ce (100–430 ppm), and Rb (30–110 ppm), and moderate concentrations of Ba (25–760 ppm) and Sr (70–1090 ppm). Sediments in the lower part of Subunit IVB and in IVC have much higher Zr/Nb ratios (5.9–7.3) than those in the middle and upper parts of Subunit IVB and in IVA (Zr/Nb largely 3.0–4.3), corresponding to the peralkaline rhyolites of the Mogán Group.

In summary, the bulk, major, and trace element compositions of the volcaniclastic layers, which range from nearly pure vitric tuffs through mixed rocks to basaltic lithic sandstones, reflect the major chemical changes between the basaltic shield and the rhyolite, rhyolite to trachyte and trachyte to trachyphonolite of the pre-Mogán, Mogán and Fataga subaerial stratigraphic intervals. Without knowl-

edge of characteristic fingerprint mineralogy or microprobe analysis of individual glass shards, bulk-rock compositions would be sufficient in correlating specific volcaniclastic intervals (except for rare individual ignimbrites and their related volcaniclastic layers) with the known chemostratigraphic subaerial record.

Composition of Glass Shards

Several factors have to be considered when comparing compositions of glass shards with the presumed source ash-flow deposit. The main problem with the glass analyses lies in the variable effects of alteration on their composition (Pls. 1, 2). To minimize this effect we have only used those with analytical totals exceeding 94 wt%. The problem of mixing of glasses of different composition from several ash-flow or fallout deposits is considered negligible in those volcaniclastic layers where significant fractions of the clasts are represented by single glass shards or pumice shards.

Lower Mogán Phase

Compositions corresponding to lava flow VL and overlying high-temperature ignimbrite VI and their associated fallout tephras occur between 835.58 and 822.2 mbsf (13 m in thickness) at Hole 953C, between 563.8 and 553.14 mbsf (10 m in thickness) at Hole 955A, and between 562.68 and 541.9 mbsf (20 m in thickness) at Hole 956B. The enormous thickness of the V-type volcaniclastic layer at Hole 956B, coupled with the more pronounced chemical homogeneity of glass shards in VU-15, probably results from higher ash supply to this area as evidenced by the regionally largest, thickest fallout tephra layers immediately underlying the subaerial ignimbrite VI in the Montaña Horgazales area in southwestern Gran Canaria.

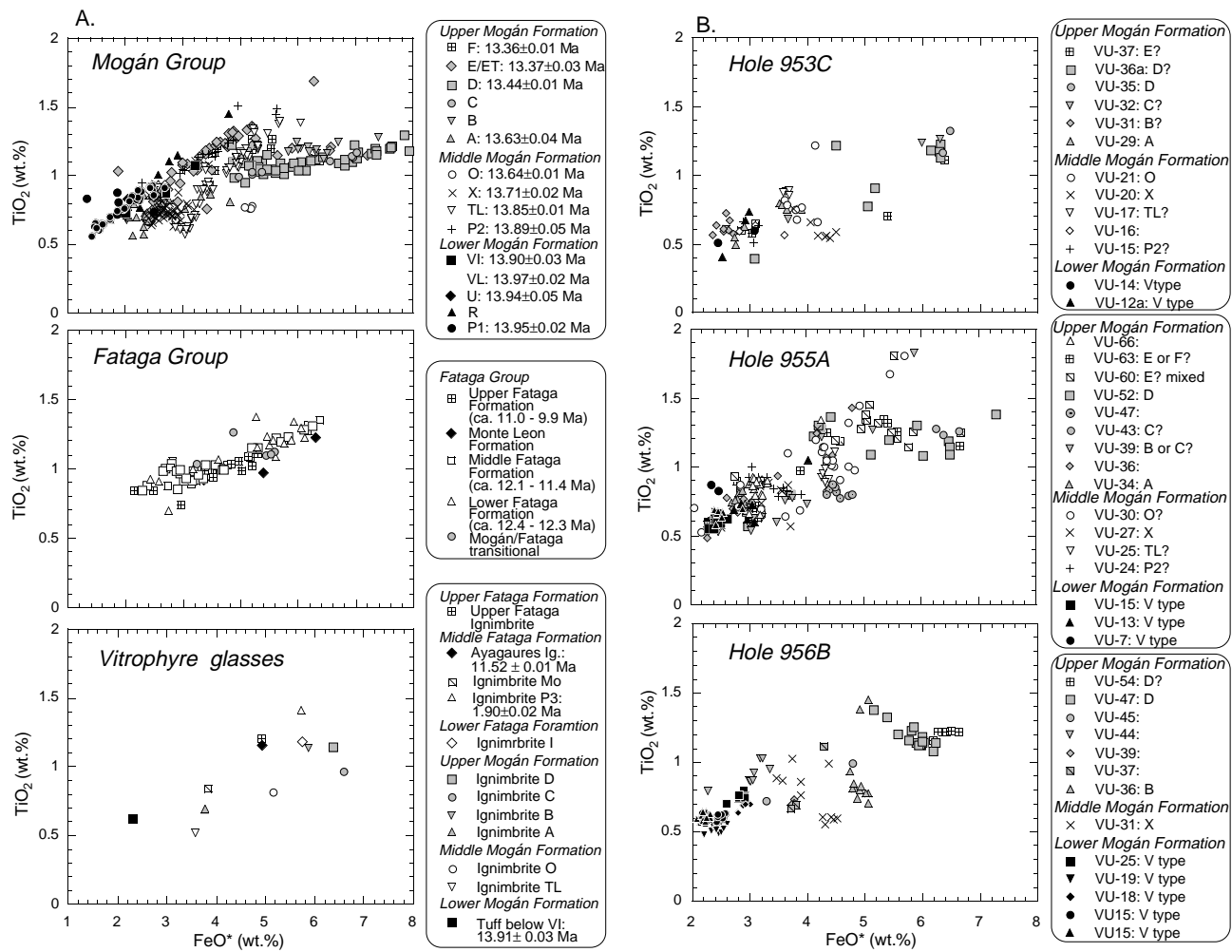


Figure 19 A. TiO_2 vs. FeO^* for major subaerial ignimbrite cooling units of the Mogán and Fataga Groups, and vitrophyre glasses from the Mogán and Fataga Formations. B. EMP analyses of glass shards from volcaniclastic units corresponding to the Mogán Group. (Continued next page.)

Middle Mogán Phase

The interval between the lowermost V-type volcaniclastic layers and volcaniclastic layers derived from ignimbrite X is ~ 2.5 m at Hole 956B. At Hole 955A, this interval is 10 m thick, with X beginning at 548.32 mbsf, and at Hole 953C, the thickness is 8 m, with X beginning at 816.49 mbsf. The two volcaniclastic layers analyzed between V- and X-type volcaniclastic layers (VU-24 and 25) at Hole 955A might correspond to ignimbrite P2 and TL. No volcaniclastic layer has been identified yet at this hole which may correspond to ignimbrites P2 or TL. At Hole 953C, VU-17 might correspond to VL. Interestingly, volcaniclastic units identified positively as being related to ignimbrite X, based on stratigraphic position and the abundance of titanite (see above), are represented by almost entirely pantelleritic composition at Hole 953C, comenditic composition at Hole 955A, and mixed pantellerite-comendite composition at Hole 956B. This difference probably results from regional differences in relative eruption volumes of pantellerite and comendite from cooling Unit X around the eruptive vents, probably being fed from a caldera ring fissure. Most likely, pantelleritic magma erupted dominantly in the north, comenditic magma in the southeast, and both magmas erupted in the southwest.

Upper Mogán Phase

The thickness of the stratigraphic interval between ignimbrites X and A, which is identified by its comenditic and trachytic composition and abundance of phlogopite, is 10 m at Hole 953C, 6 m at Hole 955A, and 14 m at Hole 956B. The volcaniclastic sediments analyzed in the stratigraphic interval between those correlated to ignimbrites X and A are compositionally more heterogeneous and range from pantellerite to comendite. They correspond to pantelleritic-comenditic ignimbrite O. Glass shard compositions in the volcaniclastic unit that correlates to ignimbrite A are very homogeneous at all three holes and differ significantly from those of over- and underlying units. This homogeneity is thought to partially result from the covering of the preceding ignimbrites by widespread basaltic lava flows (T4) which prevented or reduced the incorporation of glass shards from older units. Erosion of this basalt supplied more basaltic lithoclasts to the A-volcaniclastic interval, especially in the two southern holes, compared to most other volcanicastic units related to ignimbrites in the Mogán stratigraphic interval.

The stratigraphic interval between volcanicastic units correlated to A and D is ~ 14 m at Hole 953C, ~ 7 m at Hole 955A, and 1 m at Hole 956B. At Hole 955A, VU-36 and 39 most likely represent re-

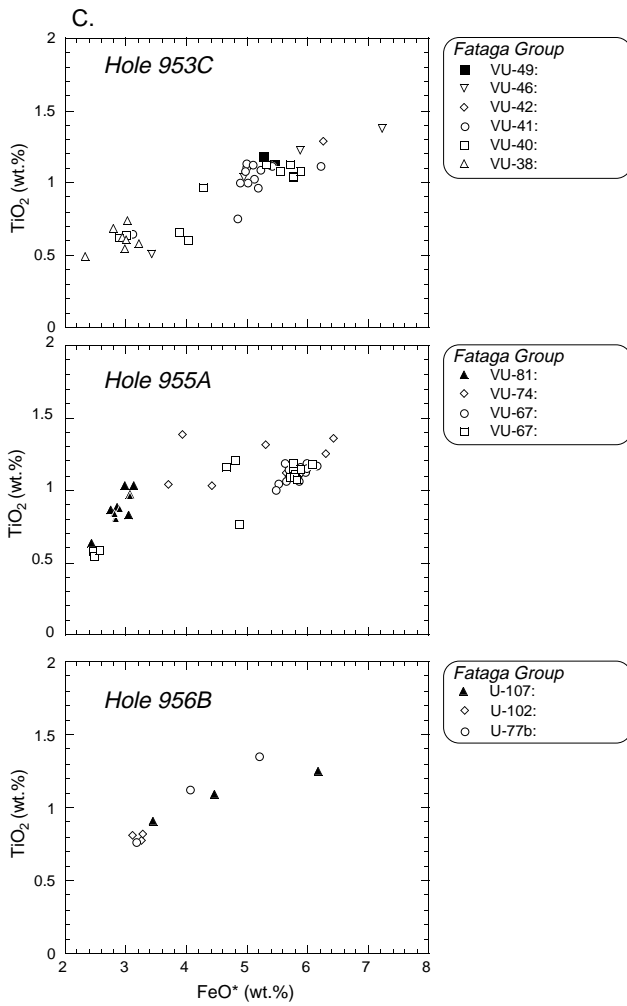


Figure 19 (continued). C. EMP analyses of glass shards from volcaniclastic units corresponding to the Fataga Group.

working of ignimbrite A, the evidence for correlation being based on the compositional similarity of many shards to subaerial ignimbrite A and the extreme heterogeneity in these units. At all three holes, one or two pantelleritic volcaniclastic units occur between syn-ignimbrite A and syn-ignimbrite D (Fig. 18).

We have tentatively identified ignimbrite D of the uppermost UMF at all three holes by its extreme pantelleritic composition. In Hole 953C, we have correlated VU-36 with ignimbrite D. The glass compositions in the five cores from VU-40 through 46 are all pantelleritic trachytic to rhyolitic compositions. Because the petrography of these volcaniclastic layers suggests that they are directly related to ignimbrite emplacement, the question arises as to why these ignimbrites do not occur in the south. We suggest that they correspond to the thick lower part of the intra-caldera Montaña Horno Formation, most of which is pantelleritic in composition. Field evidence suggests that many ignimbrites erupted during this interval ponded inside the caldera basin to the south. We have previously discussed the stronger erosional dissection of the Miocene shield basalts in northeastern Gran Canaria. Our evidence from dips of epiclastic rocks inside the caldera also suggests that drainage of the caldera basin was dominantly to the northeast. We thus view the stratigraphic section in Hole 953C between Cores 157-953C-63R and 58R as largely representing ignimbrites that ponded inside the caldera in the south, possibly be-

cause of a phase of major caldera downsag, following the eruption of widespread basalt unit T4. Ash flows erupted during this time interval were able to leave the basin through the outlet in the northeast and are thus documented at Hole 953C but not the southern holes.

In Hole 956B, the boundary between Mogán type and Fataga type volcaniclastic units is more clearcut. VU-47 up to VU-54 correspond chemically to ignimbrite D. All volcaniclastic units younger than VU-77B show Fataga-type compositions.

Sideromelane

The occurrence of sideromelane and hyaloclastites within felsic ash layers was unexpected. Sideromelane shards occur almost exclusively in submarine volcaniclastic layers corresponding to the Mogán stratigraphic interval in all holes, but most commonly in Hole 955A. Very few were found in Fataga phase volcaniclastic layers. Perhaps the greater magnitude of ash flow eruptions during the Mogán phase triggered the submarine basaltic eruptions.

We suggest that most sideromelane ash particles found within felsic volcaniclastic layers at all three sites were formed by submarine eruptions, because there is an almost complete absence of basalt flows on land, except for the widespread rhyolite-basalt composite ignimbrites, P1 and R, and spatially restricted T3 and T6 basalts. We know of only one widespread basaltic event (T4) that occurred between the eruptions of ignimbrites O and A at the base of the UMF.

We cannot deny that basaltic hyaloclastite cones formed at the shore and were subsequently eroded. We consider this hypothesis unlikely, however, because the only basaltic dikes known to have traversed part of the cooling units of the Mogán Group are those associated with the widespread basaltic eruptive event of T4. We therefore conclude that the sideromelane shards in the felsic volcanicastic layers of Holes 953C, 955A, and 956B are the result of submarine eruptions. Sideromelane, however, is difficult to use as a stratigraphic tool. A more detailed discussion of the origin of these sideromelanes is given in a companion paper (Schmincke and Sumita, Chap. 16, this volume).

CONCLUSIONS AND OPEN QUESTIONS

Major stratigraphic intervals in three holes drilled into the volcanicastic apron of Gran Canaria contain several hundred volcanicastic layers in the age interval between 9 and 14 Ma. This interval is ~450 m thick at Hole 953C, 60 km northeast of Gran Canaria, and slightly <200 m thick in Holes 955A and 956B, southeast and southwest of the island. Most of the major volcanicastic layers are more than 10 cm thick and occur in the stratigraphically lower part of these sections to ~11.5 Ma. The volcanicastic layers have been catalogued and described petrographically based on reexamination in the core repository and ~200 polished sections. Glass shards and major phenocrystic minerals (feldspar, amphibole, pyroxene, phlogopite) have been analyzed by EMP, aided by bulk chemical (XRF) analyses of some 30 tuff samples. In addition more than 30 bulk-rock (XRF) analyses, EMP analyses of fresh vitrophyre and feldspar phenocrysts were also carried out on the subaerial ignimbrites on land that correspond stratigraphically to the volcanicastic units.

The felsic volcanicastic layers, which consist of pumice, blocky vitric shards of welded tuff, bubble-wall and bubble-junction shards, crystals from the ignimbrites and lava flows as well as xenocrysts chiefly of the shield basalts, rock fragments, and nonvolcanic sediments, mainly foraminifers and nannofossil ooze as well as clay, can be correlated to the two main felsic volcanicastic formations on land, the Mogán Group (14–13.35 Ma) and the Fataga Group (13.35 to ~9 Ma). The correlation achieved both between the holes and with the subaerial record is mainly based on the chemical composition of glass shards and minerals, and XRF analyses of bulk rocks. The glass and

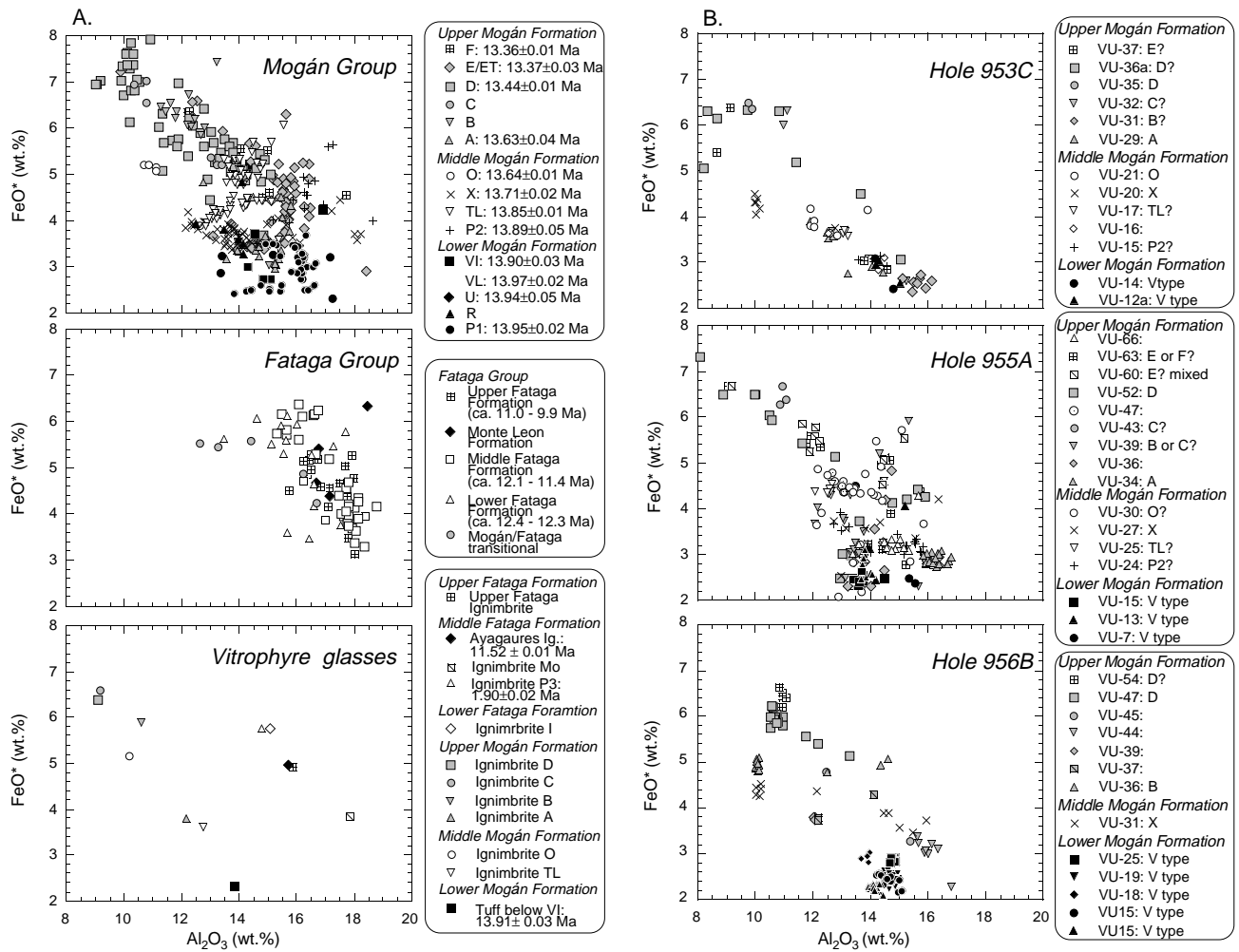


Figure 20. A. FeO* vs. Al₂O₃ for major subaerial ignimbrite cooling units of the Mogán and Fataga Groups, and vitrophyre glasses from the Mogán and Fataga Formations. B. EMP analyses of glass shards from volcaniclastic units corresponding to the Mogán Group.

bulk-rock compositions from the volcaniclastic layers correlated with the Mogán Group are dominantly peralkaline trachytic to rhyolitic, with Al₂O₃ concentrations generally <14 wt% and SiO₂ concentrations more than 65 wt%. Zr/Nb ratios are generally higher than 5. The trachyphylonitic Fataga volcaniclastic layers are richer in alumina (up to ~19 wt%), have higher alkali concentrations and lower Na/K ratios, and have Zr/Nb ratios ~4. Anorthoclase compositions are generally slightly more potassic (up to 40 mol% Or) in the Fataga, whereas very sodic anorthoclase compositions characterize volcaniclastic layers from the LMF. Phlogopite is a ubiquitous phenocryst in the volcaniclastic layers of the Fataga Group, but is present in only one of the 15 subaerial ignimbrite cooling units in the Mogán Group.

Within the lower interval of the volcaniclastic sequences (Mogán, ~50 m thick in the two southern holes and 90 m thick in the northern hole, many volcaniclastic layers have been drilled that are several decimeters thick, coarse-grained, compositionally relatively homogenous and contain abundant, angular, brown, nonvesicular, felsic glass shards, which may have formed by quench fragmentation of hot ash flows that entered the sea. About seven of these characteristic syn-ignimbritic volcaniclastic units can be correlated unequivocally between the holes, as well as to their source ignimbrites on land. The correlations are based on compositions of glass shards, presence of index minerals, and differences in compositions of feldspar, pyroxene, and am-

phibole. A major interval ~40 m thick at Hole 953C, represented by volcaniclastic units compositionally intermediate between the Mogán and Fataga rocks, is only marginally represented in the two southern drill holes. We speculate that many pyroclastic flows erupted during this time interval were drained through the northeastern outlet of the caldera basin and sedimented in the sedimentary basin north of the island, but were ponded in the southern part of the caldera basin, where they are now exposed as hydrothermally altered intra-caldera ignimbrites only.

The correlation of specific ignimbrite-related volcaniclastic layers allows to calculate sedimentation rates in the interval between 14 and 13.3 Ma fairly precisely between the holes (Figs. 21, 22). Sedimentation rates at Hole 953C are 97 m/m.y. for the interval between syn-ignimbrite D (VU-36) and A (VU-29), 142 m/m.y. from syn-ignimbrite A to X (VU-20), and 113 m/m.y. from syn-ignimbrite X to P1 (VU-1). At Holes 955A and 956B, sedimentation rates are significantly lower for all three intervals: 43 and 54 m/m.y. for the interval between syn-ignimbrite D and A, 69 and 84 m/m.y. for the interval between syn-ignimbrite A and X, and 72 and 93 m/m.y. for the interval between syn-ignimbrite X and P1. The remarkable thickness of many volcaniclastic units that formed as a direct result of ash flows entering the sea rather than by erosion of consolidated rocks, and the enormous lateral extent of these volcaniclastic layers, requires that

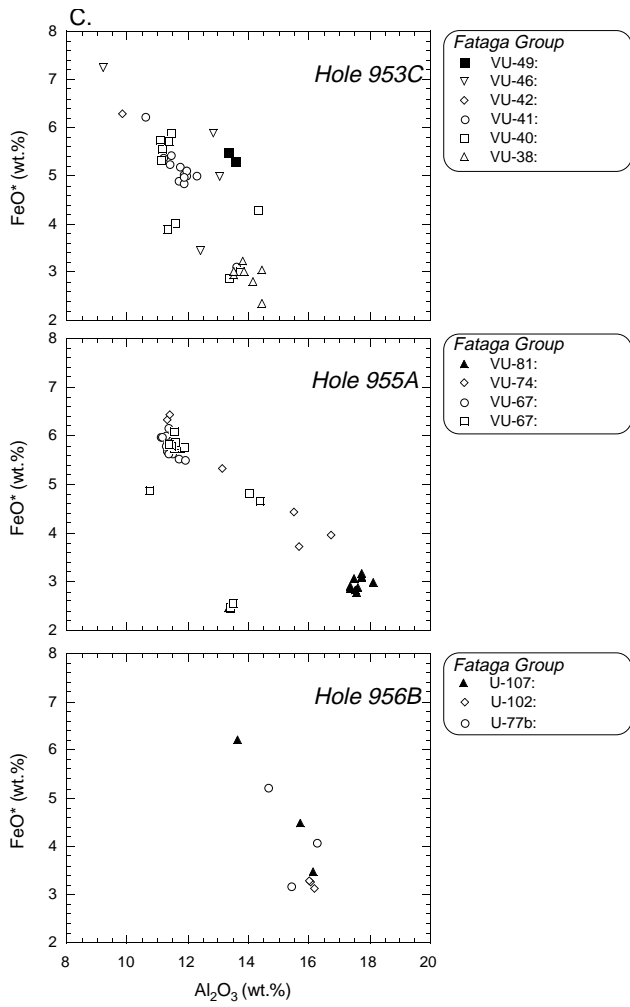


Figure 20 C. EMP analyses of glass shards from volcaniclastic units corresponding to the Fataga Group. The generally strong increase in iron and the decrease in alumina throughout the Mogán group is well shown. Rocks from the Mogán Group do not extend to extreme iron enrichment and are also characterized by high alumina concentrations, generally >15 wt%. The change from the LMF to UMF (decrease in and increase in iron and titanium), and the clear separation in Al_2O_3 concentrations between Fataga and Mogán ignimbrites is also well shown in the glass compositions. As expected, the glass compositions are generally less rich in Al_2O_3 , because of the presence of feldspar phenocrysts in the whole rocks. In general, the glass compositions from the volcaniclastic units show the same trend with time illustrated for the subaerial deposits. The broad spectrum in individual cooling units (e.g., ignimbrite X) is also mirrored in a broad spectrum of glass compositions in VU-20 (Hole 953C), VU-27 (Hole 955A), and VU-31 (Hole 956B). The fact that much fewer analyses are shown for the Fataga interval, which represents three-quarters of the entire stratigraphic interval under discussion, is mostly because of the higher degree of alteration in the more commonly zeolitized tuffs in the Fataga, the less common occurrence of thick volcaniclastic units, and our focus on the Mogán for which the subaerial equivalent ignimbrite cooling unit had been documented in detail.

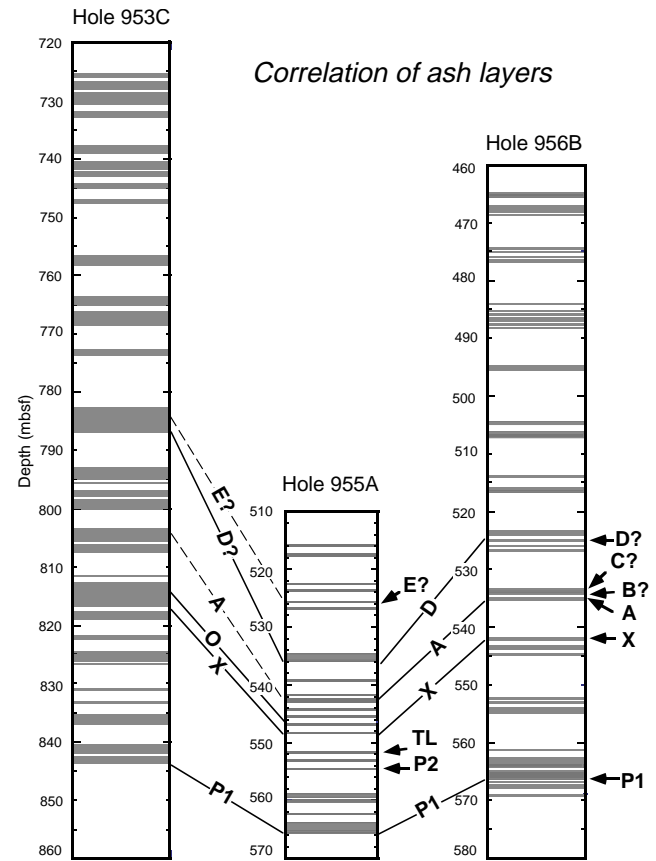


Figure 21. Correlation of volcaniclastic units between Holes 953C, 955A, and 956B.

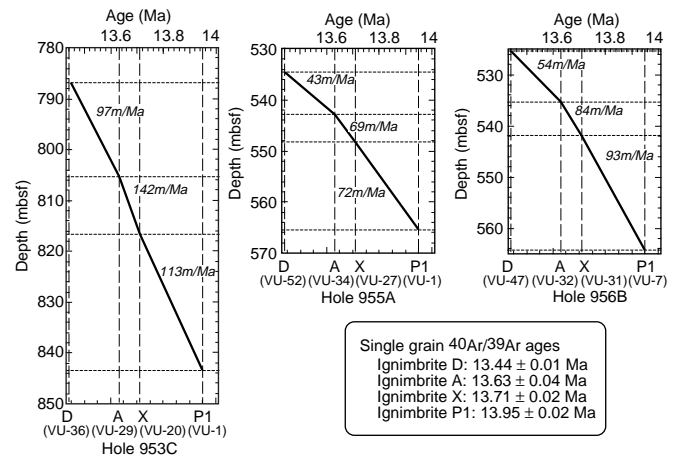


Figure 22. Sediment accumulation rates for the Mogán interval at Holes 953C, 955A, and 956B.

the volumes of ignimbrites on land, most of which ranges from 20 to 40 km³, must be approximately doubled. The following discussion of unsolved problems is meant to illustrate the point that we are aware of the limitations of the correlation of individual volcaniclastic layers for which we have provided the large database.

The problem of correlation of volcaniclastic layers would be facilitated if we could unequivocally identify volcaniclastic fallout layers that resulted from highly explosive eruptions and airborne ash clouds falling into the water and sedimented directly on to the seafloor. The fact that we have not yet clearly identified more than a few of such fallout layers can be attributed to many factors, including the general lack of large, Plinian-fall eruptions associated with low-viscosity, peralkaline ash-flow eruptions. More serious, however, is the fact that the abundant turbidites commonly show evidence of being erosional. Thin, fallout ash layers deposited shortly prior to the pyroclastic flow on land would likely be eradicated by these subsequent ash turbidites. Moreover, it is likely that ash from co-ignimbrite ash falls would be sedimented in a chaotic environment of turbulent convecting, muddy water above the moving ash turbidites following entry of ignimbrites into the sea.

Another problem is related to our poor understanding of the generation of the major volcaniclastic units (e.g., fragmentation and transport mechanisms) that led to their deposition. In the companion paper (Schmincke and Sumita, Chap. 16, this volume), we specify major criteria by which we attempted to identify volcaniclastic layers that most likely were emplaced synchronously with an eruption. However, we have not been able to specify whether individual volcaniclastic layers in each of the drill holes were deposited at exactly the same time as the subaerial eruption. Although we can be confident that some flow units of the ignimbrites on land were emplaced effectively synchronously, there may have been a significant delay in deposition of the submarine volcaniclastic units. We envision that the pyroclastic flows produced a chaotic pile-up of deposits at the land/sea interface, which grew until the last flow unit was emplaced. As this hot pile began to weld, it likely exploded as a result of wave action, and mixed with sediments present at the bottom of the shallow sea before emplacement of the first flow unit. Because we assume that this transitional zone between the land and sea effectively stopped the fast advance of the pyroclastic flows, we expect a decoupling of glass and crystal debris mass flows from the postulated pile-up zone peripheral to most of the island. The generation of glass-shard turbidites from these chaotic piles will inevitably occur at different times and, hence, it is unlikely that volcaniclastic layers drilled in the three holes will have been deposited exactly synchronously. It is one of the main goals in our ongoing study to elucidate this problem, by focusing on volcaniclastic layers that share a maximum in compositional and textural similarity in two or three holes.

During this study we have recognized volcaniclastic layers that we think can be correlated among all three holes using some textural and compositional criteria and their stratigraphic position and which therefore appear to have been deposited quasi-synchronously but which contain glass shards and minerals differing significantly in composition. We do not yet know how much of this difference results from compositional differences along the roughly concentric eruptive fissure, because not all parcels of the chemically zoned magma column are erupted in equal proportions from the caldera or is because of compositional differences as a function of time. A problem amenable to further analysis is presented by our as yet incomplete understanding of whether the compositional heterogeneity in a volcaniclastic layer reflects the compositional heterogeneity and systematic compositional zonation of the parent cooling unit, or whether it is be-

cause of erosional mixing. We have addressed this problem in a more detailed study of P1 ashes (Freundt and Schmincke, Chap. 14, this volume) and have begun similar high-resolution analyses of selected volcaniclastic units in the overlying intervals.

Because the production of volcaniclastic layers in the Mogán time interval corresponds approximately with the subaerial record, we expected to be able to correlate the eight major volcaniclastic layers in the lower part of the Fataga interval to the main interval of subaerial ignimbrite emplacement during Fataga time. But this was not the case. For example, between 11.4 and 12 Ma, when at least six major ignimbrites were emplaced on land which formed the Middle Fataga Formation, we expected to see a major pulse of volcaniclastic layer production to occur in the drill holes. The biostratigraphic dating in all three holes suggests that the period of sedimentation of the major volcaniclastic layers believed on textural evidence to be related to ignimbrite emplacement into the sea ends at ~12 Ma. Because of the fairly detailed dating of the subaerial ignimbrites by single-crystal, ⁴⁰Ar/³⁹Ar methods (Bogaard and Schmincke, Chap. 11, this volume), we suspect that the biostratigraphic dating for this interval is significantly too high. Many of the conclusions in this first report are tentative and will probably be modified as a result of our ongoing work on the Miocene felsic volcaniclastic layers drilled during Leg 157.

We are looking into the immobility of several elements in glasses from the entire compositional section because there are some clear relationships between the degree of glass alteration and its composition. Once we better understand the mobility of critical elements, additional glass shards will be analyzed to sharpen our characterization of specific volcaniclastic layers and to better understand processes that generate volcanic ash turbidites from pyroclastic flows that enter the sea.

ACKNOWLEDGMENTS

Our work on Gran Canaria, planning and participation in Leg 157, and extensive laboratory work was supported by several grants from the Deutsche Forschungsgemeinschaft, notably Schm 250/41-1, 60-1 and 60-2, Alexander von Humboldt-Stiftung and EC project MAS2-CT94-0083 (STEAM). Many colleagues and friends have helped to have all the data ready by the deadline. These include Petra Gloer and Jürgen Freitag for overseeing the microprobe laboratory, Antje Merkau and Kerstin Wolff for heading the XRF laboratory, Iris Nowak and Claudia Heller for major efforts in word processing, Sven Duggen and Nico Urbanski for analyzing some of the feldspars from subaerial ignimbrites, Simone Rast for reorganizing thousands of samples and always keeping them in order, Beate Mocek for making the database of bulk rock chemistry from subaerial rocks, and Boris Behncke for making many corrections on the volcaniclastic unit list and helping with the diagrams. Dieter Dettmar provided first-rate polished sections. We enjoyed the congenial atmosphere at the core repository in Bremen and thank especially Walter and Alex. The crew, technicians, captain, and drilling supervision aboard ship provided for a highly competent and pleasant working atmosphere, a fundamental prerequisite for getting almost 3000 m of core out of the clastic apron of Gran Canaria in a very short time. The manuscript has greatly benefited from critical comments by James Gardner, Frank Trusdell, and Wendell Duffield.

REFERENCES

- Bogaard, P., Schmincke, H.-U., Freundt, A., Hall, C., and York, D., 1988. Eruption ages and magma supply rates during the Miocene evolution of

- Gran Canaria: single crystal $^{40}\text{Ar}/^{39}\text{Ar}$ laser ages. *Naturwissenschaften*, 75:616–617.
- Freundt, A., and Schmincke, H.-U., 1992. Mixing of rhyolite, trachyte and basalt magma erupted from a vertically and laterally zoned reservoir, composite flow P1, Gran Canaria. *Contrib. Mineral. Petrol.*, 112:1–19.
- _____, 1995a. Eruption and emplacement of a basaltic welded ignimbrite during caldera formation on Gran Canaria. *Bull. Volcanol.*, 56:640–659.
- _____, 1995b. Petrogenesis of rhyolite-trachyte-basalt composite ignimbrite P1, Gran Canaria, Canary Islands. *J. Geophys. Res.*, 100:455–474.
- Jarosewich, E., Nelen, J.A., and Norberg, J.A., 1980. Reference samples for electron microprobe analysis. *Geostand. Newslett.*, 4:43–47.
- McDougall, I., and Schmincke, H.-U., 1977. Geochronology of Gran Canaria, Canary Islands: age of shield-building volcanism and other magmatic phases. *Bull. Volcanol.*, 40:1–21.
- Mosbah, M., Metrich, N., and Massiot, P., 1991. PIGME fluorine determination using a nuclear microprobe with application to glass inclusions. *Nucl. Instr. Meth. Phys. Res.*, B58:227–231.
- Schmincke, H.-U., 1969. Petrologie der phonolithischen bis rhyolitischen Vulkanite auf Gran Canaria, Kanarische Inseln [Habilitationsschrift]. Heidelberg, Ruprecht-Karls-Univ.
- _____, 1973. Magmatic evolution and tectonic regime in the Canary Islands, Madeira, and Azores. *Geol. Soc. Am. Bull.*, 84:633–648.
- _____, 1976. The geology of the Canary Islands. In Kunkel, G. (Ed.), *Biogeography and Ecology in the Canary Islands*: The Hague (W. Junk), 67–184.
- _____, 1994. *Geological Field Guide: Gran Canaria* (7th ed.): Kiel, Germany (Pluto Press).
- Schmincke, H.-U., Weaver, P.P.E., Firth, J.V., et al., 1995. *Proc. ODP Init. Repts.*, 157: College Station, TX (Ocean Drilling Program).

Date of initial receipt: 5 August 1996

Date of acceptance: 22 January 1997

Ms 157SR-114

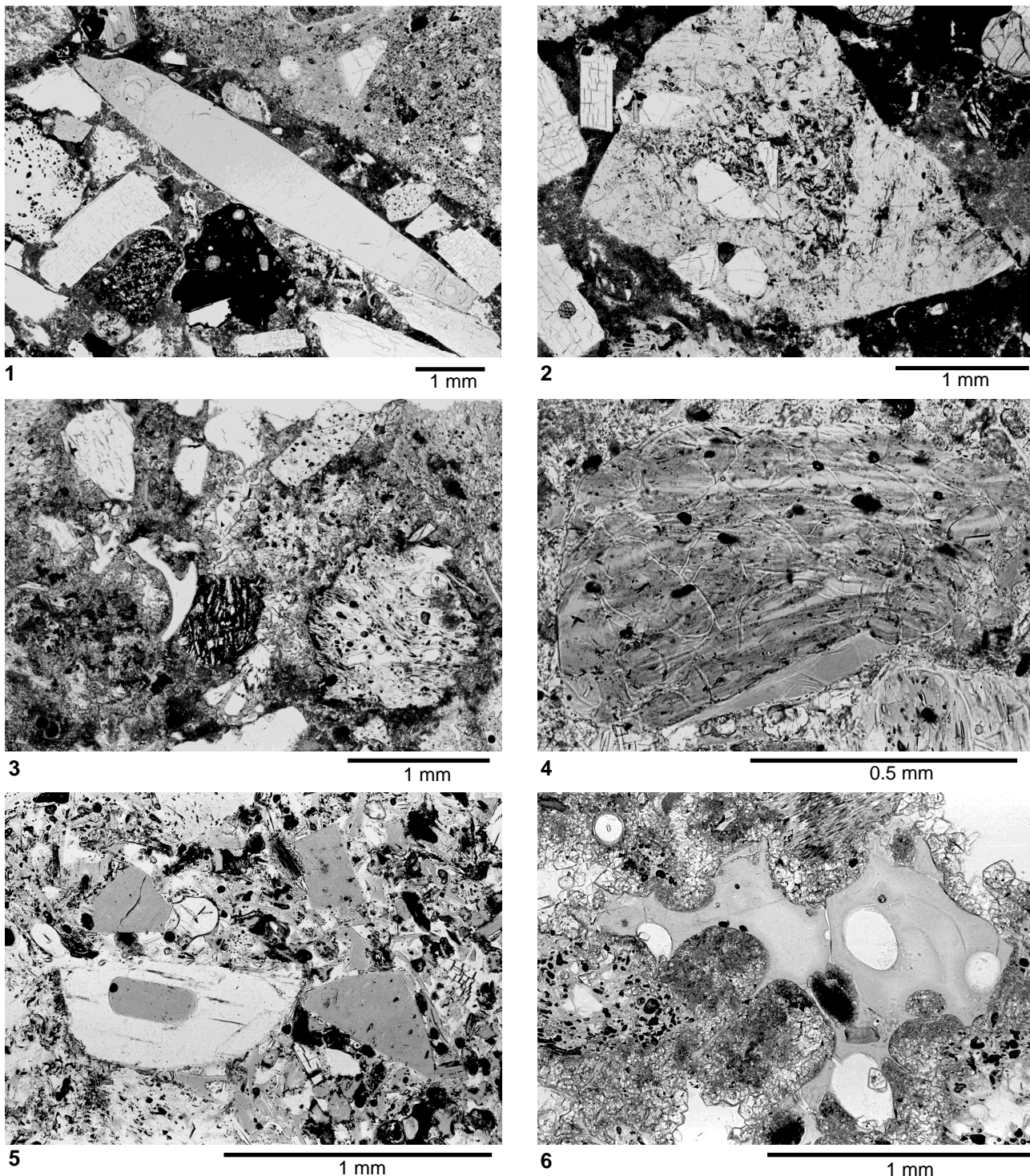


Plate 1. **1.** Large pantelleritic completely welded splintery glass shard with perlitic cracks at both ends of the shard (Sample 157-953C-64R-1, 62–74 cm). **2.** Fragment of welded tuff showing moderate welding in the central part (Sample 157-953C-64 R-4, 62–74 cm). **3.** Fragments of partially welded tuff (left), blocky shards and bubble-wall shards (Sample 157-953C-68R-4, 56–60 cm). **4.** Fragment of strongly welded tuff with visible stretched shard outlines (Sample 157-953C-62 R-2, 0–4 cm). **5.** Blocky vitric shard and feldspar with melt inclusion and bubble (Sample 157-953C-65R-2, 94–98 cm). **6.** Large single rhyolitic shard with thick glass septa (Sample 157-953C-64R-3, 72–75 cm).

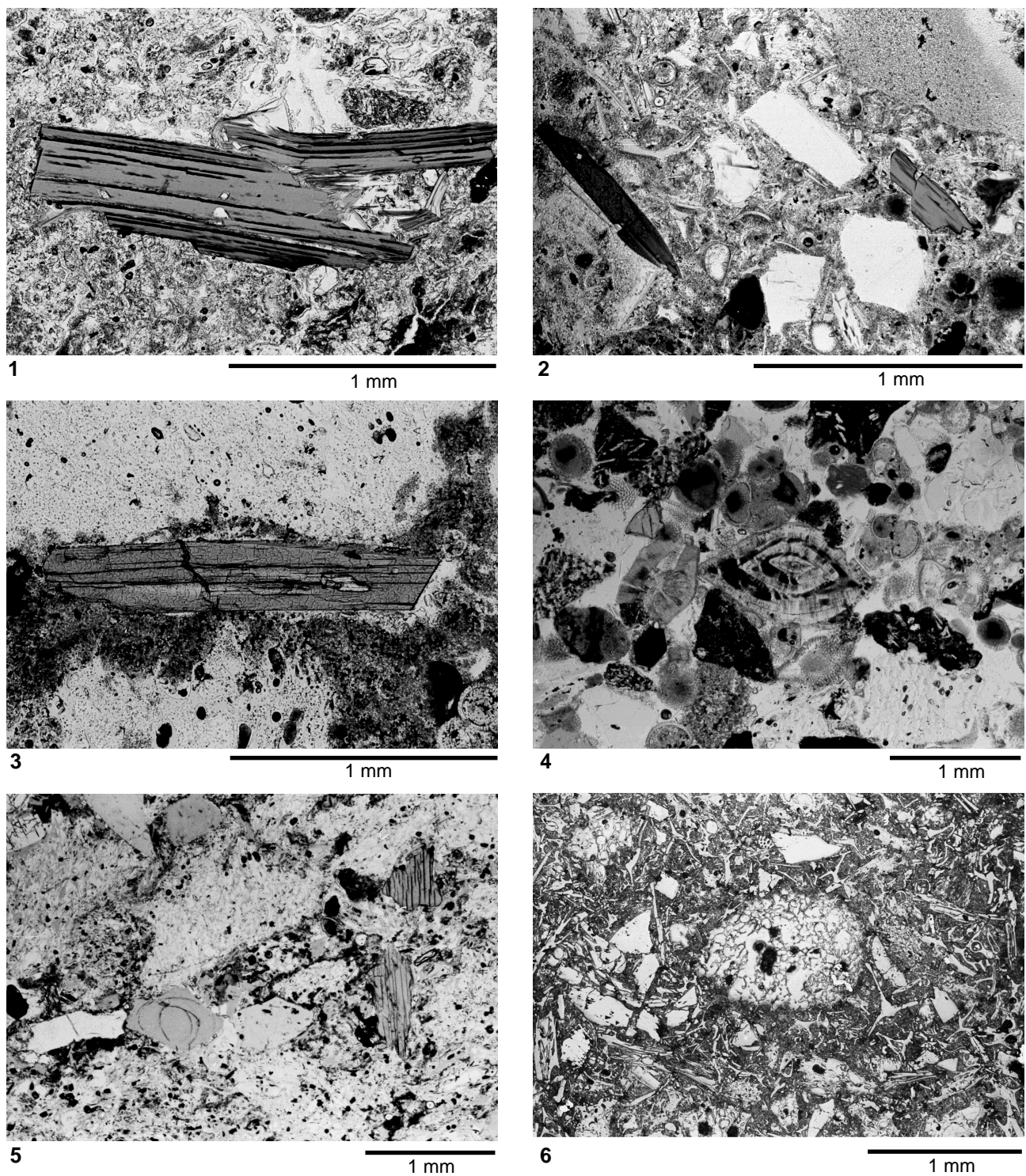


Plate 2. **1.** Large phlogopite crystal (Sample 157-953C-58R-4, 41–45 cm). **2.** Large chevkinite phenocryst, anorthoclase, amphibole (right), bubble-wall shard and foraminifers (Sample 157-953C-67R-4, 53–59 cm). **3.** Large aegirine crystals and two pumice shards. Planktonic foraminifers (left; Sample 157-953C-55R-3, 74–82 cm). **4.** Mixture of blocky and vesicular rhyolitic glass shards, tachylite fragments, and large benthic foraminifera (center; Sample 157-953C-69R-1, 0–7 cm). **5.** Vitric tuff composed mostly of pumice and minor blocky glass shard (Sample 157-953C-65R-2, 94–98 cm). **6.** Pumice shards surrounded by matrix of bubble-wall shards set in a dark nannofossil matrix (Sample 157-953C-65R-6, 100–101 cm).